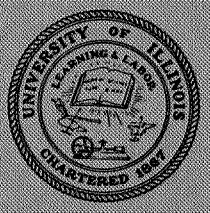

UNIVERSITY OF ILLINOIS
URBANA

AERONOMY REPORT NO. 20

STUDIES OF THE EQUATORIAL IONOSPHERE USING ROCKET TECHNIQUES

by
M. Mukunda Rao

July 1, 1967

Supported by
National Aeronautics and
Space Administration
Grant NsG-511

Aeronomy Laboratory
Department of Electrical Engineering
University of Illinois
Urbana, Illinois

CITATION POLICY

The material contained in this report is preliminary information circulated rapidly in the interest of prompt interchange of scientific information and may be later revised on publication in accepted aeronomic journals. It would therefore be appreciated if persons wishing to cite work contained herein would first contact the authors to ascertain if the relevant material is part of a paper published or in process.

A E R O N O M Y R E P O R T

N 0. 20

STUDIES OF THE EQUATORIAL IONOSPHERE USING ROCKET TECHNIQUES

by

M. Mukunda Rao

July 1, 1967

Supported by
National Aeronautics and
Space Administration
Grant NsG-511

Aeronomy Laboratory
Department of Electrical Engineering
University of Illinois
Urbana, Illinois

ABSTRACT

A rocket radio propagation experiment developed at the University of Illinois measures the differential absorption and the phase difference between the ordinary and extraordinary magnetoionic components generated at the ground and received at the rocket. From these measurements and by analyzing the standing wave pattern formed by the interference of direct and reflected waves, the electron densities and the electron collision frequencies of the ionosphere through which the rocket passes are deduced. The system was designed for use at temperate latitudes where the so-called "quasi-longitudinal" approximation of the Appleton-Hartree equation holds. During the NASA Mobile Launch Expedition during the International Quiet Sun Year (1964-65) a rocket carrying this experiment was launched from the aircraft carrier USNS Croatan, very close to the magnetic equator. This equatorial experiment necessitated certain changes in the system which are described in detail in this report.

The methods of analyzing the data obtained during the equatorial experiment are developed and the results thereby obtained are presented. The problems encountered in the use of propagation experiment at the equator are stated and ways and means of improving the existing technique are discussed, as are some of the equatorial ionospheric problems which can be studied using this technique. This report is intended to aid planning of possible further equatorial ionospheric studies utilizing the rocket radio propagation technique.

ACKNOWLEDGMENT

The author is deeply grateful to Prof, S. A. Bowhill for his inspiring guidance throughout the progress of this work. Thanks are due to Dr. J. S. Shirke and Dr. E. A. Mechtly for many useful discussions.

TABLE OF CONTENTS

		Page
1.	INTRODUCTION	1
	1.1 The D-Region and Equatorial Ionospheric Absorption	1
	1.2 The Equatorial Sporadic E	4
	1.3 The Equatorial F-Region	6
	1.4 The Current Systems and Storms	8
	1.5 Summary	10
2.	PROPAGATION EXPERIMENT AND ITS MODIFICATION FOR THE EQUATORIAL LAUNCHING	11
	2.1 Introduction	11
	2.2 System Description	11
	2.3 Rocket Antenna and Receiver	22
	2.4 Polarization Tests	26
	2.5 Data Reduction	31
	2.6 Discussion	36
3.	METHODS OF DATA ANALYSIS	38
	3.1 Introduction	38
	3.2 Appleton-Hartree Equation and the Approximations	38
	3.3 The Quasi-Transverse Approximation	44
	3.4 Electron Density from Phase Difference Measurements	49
	3.5 Electron Collision Frequency from Differential Absorption	52
	3.6 Standing Nave Analysis	53
	3.7 Summary and Discussion	56
4.	RESULTS OF AN EQUATORIAL ROCKET RADIO PROPAGATION EXPERIMENT	58
	4.1 Introduction	58
	4.2 Differential Absorption Data	58
	4.3 Phase Difference Data	64
	4.4 Standing Wave Pattern Analysis	64
	4.5 Discussion	68
	4.6 Results	72
5.	PROBLEMS IN THE APPLICATION OF PROPAGATION EXPERIMENT FOR THE STUDIES OF THE EQUATORIAL IONOSPHERE	77
	5.1 Introduction	77
	5.2 Comparison of Differential Absorption and Faraday Rotation Values Obtained under QL and QT Conditions	77
	5.3 Launching into QL Region from an Equatorial Launch Site	80
	5.4 Summary and Discussion	85

TABLE OF CONTENTS (cont'd)

		Page
6.	SOME PROBLEMS OF THE EQUATORIAL IONOSPHERE WHICH COULD BE STUDIED BY ROCKETS	86
	6.1 Introduction	86
	6.2 The D-Region and Equatorial Ionospheric Absorption Problems	86
	6.3 Electrojet and Equatorial Sporadic E Problems	90
	6.4 F-Region Problems	95
	6.5 Summary and Discussion	99
REFERENCES		101
APPENDIX		106

LIST OF ILLUSTRATIONS

Figure		Page
2.1	Block diagram of the radio propagation experimental system.	13
2.2	Schematic for obtaining linear polarizations.	15
2.3	RF attenuator drive.	16
2.4	Polarizations at the earth's equator.	19
2.5	Schematic of the rocket receiving antenna used for the equatorial launching.	20
2.6	Photograph of the rocket receiving antenna used for the equatorial launching.	21
2.7	Block diagram for adjusting the receiving antenna for circular polarization.	23
2.8	Circuitry of the hybrid junction.	24
2.9	Photograph of the rocket receiver.	25
2.10	Block diagram for polarization tests.	27
2.11	(a) Whirly output signal for 30% modulation. (b) Whirly output signal when only one mode is excited.	28
2.12	Near field radiation patterns obtained during the equatorial launching.	30
2.13	Illustration on the concept of Faraday rotation at the equator.	32
2.14	Block diagram of Faraday rotation data processor for the equatorial experiment.	35
3.1	Geometry for the computation of path difference from rocket trajectory (after Salah and Bowhill, 1966).	54
4.1	Propagation experiment data format.	59
4.2	Variation of extraordinary power with time after launch.	60
4.3	The variation of Faraday rotation with time after launch during ascent.	61
4.4	The variation of Faraday rotation with time after launch during descent.	62
4.5	Typical standfng wave pattern.	63

LIST OF ILLUSTRATIONS (cont'd)

Figure		Page
4.6	Observed and theoretical number of cycles of the standing wave pattern.	65
4.7	The electron density profile obtained from the equatorial experiment.	66
4.8	Comparison between the observed and expected values of Faraday rotation and differential absorption.	67
4.9	Ionogram corresponding to the time of rocket launching.	70
4.10	Detailed variation of electron current with altitude showing small scale structure.	71
4.11	The electron density profiles at various latitudes for the same solar zenith angle.	73
4.12	Comparison of electron density profiles near the vicinity of magnetic equator for different solar zenith angles.	74
5.1	Variation of the angle (e) between the direction of propagation and the magnetic field lines with the launch characteristics of the rocket.	79
5.2	The electron density and electron collision frequency profiles utilized for the investigation.	81
5.3	The regions wherein the quasi-longitudinal and quasi-transverse approximations hold.	82
5.4	Location of Thumba equatorial launch site with reference to the magnetic equator.	84
6.1	Anomalous absorption values observed during local summer (after Beynon and Jones, 1965).	88
6.2	Occurrence frequency of aspect sensitive spread F as seen by Alouette I, September 1962 to January 1963 (after Calvert and Schmid, 1964).	94
6.3	Comparison of topside electron density profiles obtained from Alouette I, backscatter sounding and a simultaneous rocket flight on July 2, 1963 (after Schmerling, 1966).	98

1. INTRODUCTION

The equatorial ionosphere can be characterized by various phenomena which are different for different altitude regions. Therefore its latitude range, as is usually referred to, is different for different regions of the ionosphere. The mode of propagation of radio waves is entirely different at the equator from that of other latitudes, because of the nearly horizontal magnetic field lines. Therefore close to the magnetic equator the quasi-transverse approximation holds for the Appleton-Hartree equation. Aikin (1965) characterizes the equatorial D-region by the absence of particle ionization. The equatorial E-region is confined to $\pm 5^\circ$ latitude of the magnetic equator and it is characterized by the presence of strong current system called the electrojet and a special type of sporadic E called the equatorial Es(Es-q), which is believed to be a manifestation of the electrojet. The equatorial F-region which is supposedly the region lying between $\pm 20^\circ$ of the magnetic equator has many interesting anomalies, the most interesting of them being the one detected by Appleton (1946). The incidence of spread F phenomena in the equatorial zone is considerably higher than at middle latitudes, and it occurs mostly at night. However the nature of this phenomenon at the equator is believed to be different from that occurring at other latitudes.

The various phenomena of the equatorial ionosphere have been organized into four sections in this chapter, and existing knowledge is summarized. However this summary is not meant to be exhaustive; rather, only those topics relevant for rocket studies are summarized.

1.1 The D-region and Equatorial Ionospheric Absorption

Though the lower ionosphere in the equatorial zone may be characterized by the absence of particle ionization, the boundaries of this zone are very ambiguous.

Therefore as a working definition it may be said that it is the latitude region in which the 'seasonal anomaly' in ionospheric absorption exists (Skinner, 1965). The index of absorption 'n' as deduced from the noontime absorption values obtained during various seasons is much higher than the value obtained using the diurnal variation of absorption. This is the case only at equatorial latitudes and this phenomenon is referred to as the 'seasonal anomaly' in ionospheric absorption. The cosmic ray production function reaches a minimum value at the geomagnetic equator (Aikin, 1965) and as such the main sources of ionization in the D-region are 2-8 Å x-rays and Lyman-a at 1215.6 Å. The Lyman-a energy flux is relatively constant with solar conditions. The most important loss processes in the D-region are believed to be (Aikin, 1965):

(1) three body attachment of electrons to molecular oxygen

(2) photodetachment from 0_2

(3) ion-ion recombination

(4) dissociative loss processes.

Nicolet and Aikin (1960) predicted the ion and electron density distribution for various solar conditions. However several recent measurements showed that the existing D-region theories are in need of modification. By a study of trans-equatorial and middle latitude VLF propagation, Chilton and Radicella (1965) showed that there are basic differences between those two propagation characteristics. They believe that these differences strongly suggest changes in the structure of the lower D-region with latitude. It is thought that these differences are due to latitudinal variation in the daytime electron density gradient.

Ionospheric absorption of radio waves has been studied in the equatorial zone by two main methods. The first is the vertical incidence pulse reflection technique and the second one consists in recording the level of cosmic radio noise at a frequency at about 20 MHz by a device known as a riometer. Such

studies in the equatorial zone have been made in Africa (Ibadan, Dakar), India (Waltair, Ahmedabad, Delhi, and Banaras), Ceylon (Colombo) and the Far East (Singapore). Studies have been made on the variation of absorption with wave frequency, sun's zenith angle, lunar time, and solar activity. Arising out of these studies, there are many discrepancies, the most important of them being the dependence of absorption on wave frequency and the solar zenith angle. During summer, the noontime absorption values are lower than what is expected and this phenomenon is called the 'summer anomaly'. For stations having the same latitude but belonging to different longitude zones, the variation of absorption with sunspot activity is different, giving rise to the so-called 'longitude anomaly'. Whether the absorption values measured at equatorial stations are proportional to f^{-1} or f^{-2}, f being the operating frequency, is not yet definitely known. Another major problem still to be resolved is the question of the relative contribution of the various ionospheric regions to the total absorption (Skinner, 1965).

Recently there are some reports indicating the existence of an equatorial anomaly in absorption near the equator which parallels that in the F2-layer critical frequency (F_oF2). Flügel (1962) first suggested that there is magnetic control of absorption near the equator with substantially higher absorption on either side at latitudes of about $\pm 15°$. Shirke (1966) using shipboard vertical incidence absorption measurements at varidus latitudes, confirmed the existence of an equatorial and low-latitude anomaly in ionospheric absorption. However the anomaly is noticed to be present during the afternoon hours rather than the forenoon hours. But the question remains unanswered whether the anomalies in absorption are due to changes in ionization density, collision frequency, or both.

The absorption of radio waves in the ionosphere depends on:

(1) the collision frequency of the electrons,

(2) the electron density in the absorbing region, and

(3) the gradient of ionization in the reflecting region.

Interpretation of absorption data is only possible if at least one of these can be evaluated with some accuracy (Piggott, 1965). Well planned rocket experiments could well be the answer to resolve the anomalies and discrepancies present in the ionospheric absorption at equatorial latitudes.

1.2 The Equatorial Sporadic E

Berkner and Wells (1937) first observed that a kind of sporadic E with special features occurs regularly on ionograms obtained at Huancayo, very close to the magnetic equator. Many studies since have shown (Smith, 1957) that Huancayo and other stations near the magnetic equator have a higher daytime incidence of sporadic E than any other Es zone in the world. This type of Es is now designated as Es-q and is called equatorial Es. It is mainly a daytime phenomenon, and is nonblanketing in nature. Matsushita (1951) showed that Es-q is closely related to the equatorial electrojet, a daytime current stream flowing along the magnetic equator at a height of about 100 km. Knecht and McDuffie (1962) suggested that equatorial Es occurs in a belt having a width of about 700 km, which agrees very well with the width of the equatorial electrojet as deduced from geomagnetic observations.

Using rocket-borne magnetometer measurements, Cahill (1955) observed that the horizontal current density showed two maxima at heights of 105 km and 125 km of roughly equal magnitude, indicating a bifurcation of the equatorial electrojet. From both radio sounding measurements (ionosondes) and VHF radio scattering measurements of the equatorial ionosphere (Matsushita, 1962; Cohen and Bowles, 1963), it is known that there are irregularities of ionization density associated with the electrojet. These equatorial Es irregularities are generally aligned

with the earth's magnetic field and move transversely across it, as indicated by the aspect sensitive nature of radar echoes obtained during backscatter studies. The irregularities in the electrojet constitute a layer of the order of seven km thickness centered at an altitude between 100-105 km (Bowles, et al., 1960). Bowles and Cohen (1962) have found that the field-aligned irregularities to which the Es-q is attributed are embedded in the regular E-layer.

Many attempts have been made to explain the mechanism by which the field-aligned irregularities are produced. A theory of the two-stream ion wave instability in a plasma developed by Farley (1963) takes into account both the effect of collisions of ions and electrons with neutral particles and the presence of a uniform magnetic field. Applying the results to the ionosphere, it was found that irregularities of ionization density should arise spontaneously in regions in which a sufficiently strong current is flowing normal to the magnetic field lines. These irregularities will be strongly aligned with the magnetic field and may have a wide range of wavelengths. The various predictions of the theory are in agreement with the observed characteristics of certain field-aligned irregularities found in the equatorial ionosphere that are associated with the equatorial electrojet.

During March 1965, a series of six rockets were launched in the vicinity of the magnetic equator by Blumle et al., (1965), for the purpose of measuring the electron density distribution of the equatorial ionosphere to an altitude of 200 km. Ionograms obtained at the firing showed equatorial sporadic E at 110 km but there was no evidence of a large increase in density in the altitude region of the electrojet. Even after about three decades of study, the equatorial electrojet is still an enigma and Whitehead (1966) had to conclude that it is impossible to construct a model of the equatorial electrojet current to fit the rocket measurements of this current, and other evidence concerning this region.

1.3 The Equatorial F-Region

When the F2-layer is investigated at different observatories at different times, its behavior is found to be very complicated and difficult to summarize. Any summary will oversimplify the facts and will not cover some of the more striking peculiarities. It is usual to describe the overall behavior of the F2-layer by pointing out how it differs from that of a hypothetical Chapman layer.

It is well known that the latitudinal distribution of noontime F-region critical frequency shows a dip around the magnetic equator (Appleton, 1946, 1954; Rastogi, 1959a) with peaks on either side at about ±15°-20° latitude. The region within these peaks is usually referred to as equatorial F-region. The variation is more systematic if the noontime F_oF2 data is plotted against magnetic latitude instead of geomagnetic latitude. This observation suggests that movements in the F2-region along the earth's magnetic field lines are probably important in explaining this anomaly. If f_oF2 is plotted in the same way, at different times of the day, it was shown by Rastogi (1959a) that the trough observed when noon f_oF2 is plotted, is replaced by a peak when midnight f_oF2 values are utilized. He has also established that the distribution of noontime f_oF2 is controlled by the magnetic dip, ,rather than the geomagnetic latitude, and that the peaks of f_oF2 occur at ±30° dip in low sunspot years, and at ±35° dip at high sunspot years. (Rastogi 1959b, 1959c).

If electron production and loss rates do not vary greatly with latitude in the equatorial region, it might be inferred that ionization movements are responsible for the anomaly. Mitra (1946) first suggested that ionization produced in the region of the magnetic equator would diffuse downwards along the field lines and possibly give rise to the N_mF2 maxima observed at higher latitudes. A second ionization movement proposed by Martyn (1955) and developed by Duncan (1960) is due to the presence of an electrostatic field in the F-region. This

field causes the ionization to drift in a direction perpendicular both to the magnetic field lines and to the electric fi'eld 'direction, so that an eastward electric field will cause an upward vertical motion of the ionization. Martyn (1955) envisages a "fountain effect" in which the ionization is lifted upward at low latitudes and then deposited at higher latitudes by diffusion along the field lines. The equatorial F-region has been described (Goldberg and Schmerling, 1963; Goldberg et al., 1964; Goldberg, 1965) in terms of rapid diffusion along the lines of force and an assumed Chapman-like F-layer vertical profile at the magnetic equator, but without taking explicit account of production, loss, or electromagnetic drift. By investigating the effect of a vertical electromagnetic drift of any magnitude on the equatorial ionization distribution, a quantitative treatment of the Appleton anomaly is given by Hanson and Moffett (1966).

The most important of the F-region irregularities is the spread F phenomenon. The global distribution of spread F occurrence shows two regions of high incidence, one above 60° geomagnetic and the other within ±20° of the geomagnetic equator. Spread F configurations as appearing on ionograms are generally attributed to:

(1) aspect-sensitive scattering by their magnetic field-aligned irregularities;

(2) ducting along broad irregularities; and

(3) refraction within large scale reductions in electron density

(Calvert and Schmidt, 1964). Spread F is mainly a nighttime phenomenon at equatorial latitudes and the diurnal behavior is similar in northern and southern latitudes around the geomagnetic equator. The onset of spread F takes place, generally between 2000-2100 hours. LMT and the percentage occurrence reaches its maximum shortly after midnight (Murthy, 1966).

1.4 The Current Systems and Storms

By definition the mean solar quiet day variation, S_q, is the average magnetic variation over several quiet days. It is an operational definition and it is impossible to eliminate completely the effects of disturbances in order to obtain an "ideal S_q". The term S_q should not be referred to individual days. It is generally accepted that the equatorial electrojet is part of the quiet day current system. The jet is considered as that part of the current responsible for the increased horizontal field variation in a narrow belt near the dip equator. It is supposed to be an intense eastward electrojet current set up as a result of the crowding of current lines into the narrow belt of high conductivity at the dip equator. For purposes of some analysis the measured field variations are usually separated into electrojet and world-wide parts (Ogbuhei and Osborne, 1965).

A number of studies of the electrojet using measurements of ground level magnetic fields have been reported. These confirmed that the width, intensity, and axis position of the electrojet vary considerably from day to day. Rocket observations of the equatorial electrojet over Thumba, India were made by Maynard et al., (1965). At 1000 hours local time, the total change in field between apogee (170 km) and 100 km below apogee was about 90 gamma. Recent rocket measurements of ionospheric currents near Peru (Maynard and Cahill, 1965) located a strong current at about 110 km in the electrojet region. It was suggested that there is evidence for two current layers just outside the electrojet zone. The results of 8 rocket flights into and near the equatorial electrojet just off the coast of Peru were reported by Davis et al., (1966). A noontime flight on the geographic equator penetrated a current layer with maximum current density near altitude 115 km. This layer evidently is due primarily to the Pederson current and is the same one responsible for the midlatitude S_q

magnetic variations. The other rockets were flown within 200 km of the measured magnetic equator where they penetrated the equatorial electrojet. This current, due to the sum of the Pederson current and Hal current, enhanced by polarized electric fields, has a lower boundary near 87 km altitude and maximum current density of 10 amp/km^2 near 107 km altitude.

During magnetic storms an additional disturbance (D) magnetic field is superposed on the normal field of the earth. There are many reports of enhancement of the horizontal component during the daylight hours in the magnetic equatorial zone at sudden commencements and impulses, solar daily disturbance variations (DS), and solar flares (Bhargava, et al., 1964; Matsushita, 1964; and Rastogi et al., 1965). This enhancement is supposed to be caused by the high conductivity in the magnetic equatorial zone. Matsushita (1964) reviewed the theoretical models of magnetic storms and concluded that none of them are very satisfactory.

The relationship between the ionospheric storms and magnetic storms has always been very ambiguous. Olatunji (1965) could find no relation to K_P and A_P for ionospheric storms recorded at Talara, Ibadan, and Singapore. There was some indication in his studies that ionospheric storms began from half to nine hours later than magnetic storms in 1960 and 1961. It is well known that noon f_oF2 at equatorial stations during any of the seasons increases with increasing magnetic activity. Further, the daytime values of f_oF2 are greater on disturbed than on quiet days. However Rastogi and Rajaram (1965) showed that during the IGY-IGC period the noon values of f_oF2 at Huancayo decreased with increasing K-index during the December solstice, while during the June solstice f_oF2 is positively correlated with K. The abnormal decrease of f_oF2 during the disturbed days is found only at the equatorial stations of Huancayo, Chimbote, Chiclayo, and Talara (75°W meridian) during the December solstice. For the

years 1953-1961, this decrease was only seen during maximum solar activity. Comparing the variations at different longitudes it is found that this abnormality occurs only at Huancayo.

1.5 Summary

From a study of the various equatorial phenomena as described above, it can be easily seen that many of the anomalies are far from being completely understood. It has been realized that well planned rocket experiments collaborating with ground-based experiments could be a key in understanding these anomalies. In the succeeding chapters the radio propagation experiment using rockets developed at the University of Illinois, will be described in detail and its applicability for studying the equatorial problems will be discussed.

2. PROPAGATION EXPERIMENT AND ITS MODIFICATION FOR THE EQUATORIAL LAUNCHING

2.1 Introduction

In this chapter a radio propagation technique for studying the characteristics of the lower ionosphere using rockets is briefly described. This technique has been developed by the Coordinated Sciences Laboratory of the University of Illinois (Knoebel et al., 1965). Unique features of the system include:

(1) feedback around a nullseeking technique, which increased absorption measurement accuracy, and

(2) artificial rotation of the polarization ellipse (by synthesizing the o- and x-waves) which extends the range over which Faraday rotation can be resolved.

The purpose of the experiment is to measure with improved techniques the electron density and electron collision frequency in the lower ionosphere. Thus far, more than 25 rocket launchings have been made during various ionospheric conditions and at various latitudes utilizing this system and it has proved very successful in obtaining the desired information.

All the launchings, except one, were made at high latitudes. The system originally developed for this region will be first described briefly. During the NASA Mobile Launch Expedition during the International Quiet Sun Year (1964-65) one rocket was launched from the aircraft carrier USNS Croatan, very close to the magnetic equator. This equatorial experiment necessitated some changes in the system and these will be discussed in detail in the succeeding sections of this chapter.

2.2 System Description

At high latitudes (say Wallops Island, Virginia, (Geog. Lat. 37° 50'N; Long. 75° 29'W) where most of the rockets utilizing this technique were launched) the

so-called "quasi-longitudinal" approximation of the Appleton-Hartree equation holds since the direction of propagation of the transmitted wave is very nearly in the direction of the earth's magnetic field. Under this condition the refractive index 'n' is given by

$$\eta^2 = 1 - \frac{X}{1 - jZ \pm Y_L} \tag{2.1}$$

where $X = \frac{\omega_N^2}{\omega^2} = \frac{Ne^2}{\varepsilon_o m} \cdot \frac{1}{\omega^2}$

$Y_L = \frac{\omega_L}{\omega} = \frac{eB_L}{m\omega}$

$Z = \frac{\nu}{\omega}$

ω = angular frequency of the propagating radio wave

N = electron density of the medium

e = absolute value of electron charge

m = electron mass

ε_o = permittivity of free space

B_L = component of the earth's magnetic flux density along the ray path

ν = effective collision frequency of electrons with other constituents of the medium

The wave polarization ρ, defined by the ratio of the components of the magnetic field intensity of the wave along two perpendicular directions in the plane transverse to the direction of propagation is

$$\rho = \pm j \tag{2.2}$$

for the quasi-longitudinal case. From the $\pm Y_L$ term in equation (2.1) it is seen that there are two values for the refractive index 'n' in space, giving rise to

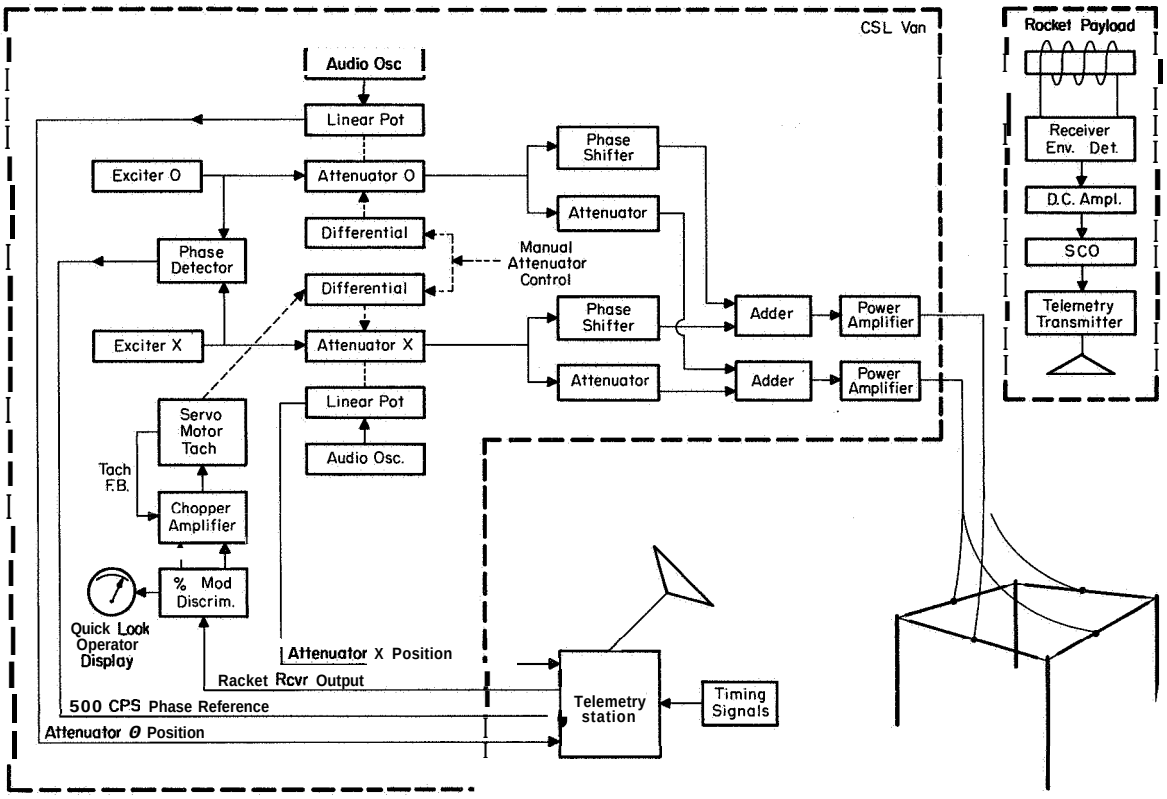

Figure 2.1 Block diagram of the Radio Propagation experimental system

two modes of propagation. From equation (2.2) it is seen that the resulting space and time quadratures cause the two modes to be oppositely circularly polarized waves, the ordinary and extraordinary.

The ground station for the quasi-longitudinal regime is therefore essentially as shown in Figure 2.1, generating two oppositely circularly polarized waves, differing in frequency by 500 Hz. A polarization ellipse is thus generated, spinning at a rate of 250 *rps*. The 500 Hz modulation produced in the output of the rocket antenna is telemetered to the ground and recorded simultaneously with the 500 Hz reference frequency which produced the polarization rotation. A constant ellipticity is maintained in the signal received in the rocket by an automatic electrical adjustment at the ground, which gives a continuous measure of the differential absorption of the ordinary and extraordinary magnetoionic components; the relative phase of the two signals giving the Faraday rotation angle. The Faraday rotation and differential absorption are thus measured up to the altitude where one of the waves is reflected, It is known that the extraordinary wave is reflected at an altitude lower than the ordinary wave. Therefore, above the extraordinary reflection height, electron densities cannot be obtained by Faraday rotation or differential absorption measurements.

By examining the receiver output trace on a telemetry chart it may be seen that a standing wave pattern is superimposed on the receiver output. This pattern is due to direct and reflected ordinary wave vectors adding at the rocket. Analysis of the standing wave thus produced yields a measure of the ordinary phase refractive index which may be used to calculate electron density.

However at the equator, the direction of the propagated radio wave will be transverse to the earth's magnetic field. For this case, the quasi-transverse approximation of the Appleton-Hartree equation is valid, and so the

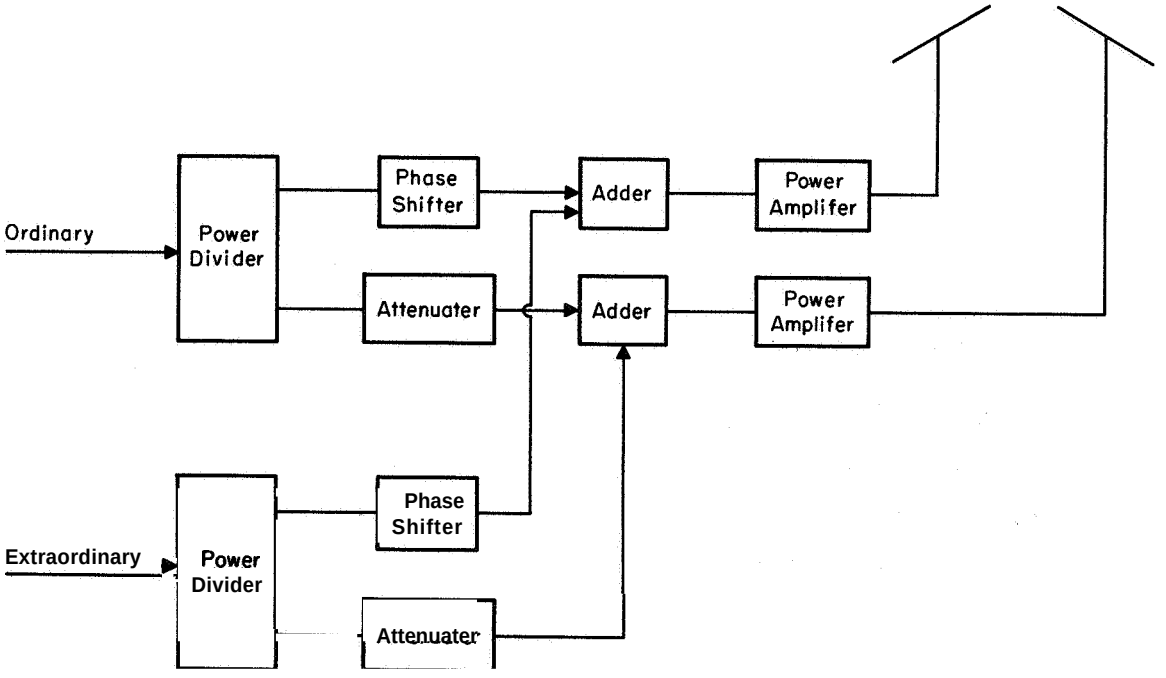

Figure 2.2 Schematic for obtaining linear polarizations

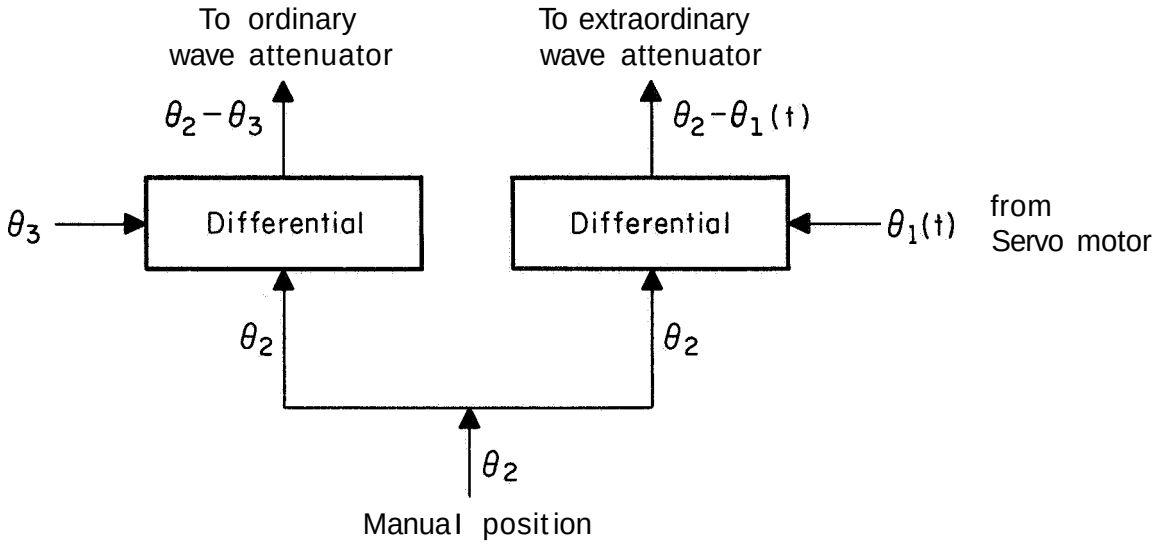

Figure **2.3** R. F. Attenuator Drive

refractive index, n is given by

$$n^2 = 1 - \frac{X}{1 - jZ} \quad \text{with} \quad \rho = 0 \tag{2.3}$$

for the ordinary wave, and

$$n^2 = 1 - \frac{X(1 - X - iZ)}{(1 - jZ)(1 - X - jZ) - Y^2} \quad \text{with } \rho = \infty \tag{2.4}$$

for the extraordinary wave,

From these equations, it can be shown that the ordinary wave is linearly polarized with its electric vector parallel to the earth's magnetic field; while the extraordinary wave is linearly polarized with the electric vector perpendicular to the earth's magnetic field. Hence, during the equatorial rocket firings, the experimental setup has been modified to transmit linearly polarized waves, with the ability to position the two linear polarizations about the axis of propagation. A scheme of this experimental setup is shown in Figure 2.2 which is nothing but the original system except for some changes in the antenna system.

Figure 2.1 is a block diagram of the entire system used during most of the launchings. All the ground-based equipment except the transmitting antennas are within a van as shown within the dotted lines at the left. The two exciters x- and o- are crystal-controlled CW oscillators differing in frequency by 500 Hz and operating 250 Hz above and below the desired center frequency. The output of each exciter is controlled by waveguide-beyond-cut-off attenuators whose range is 0-50 dB. Figure 2.3 gives the mechanical system controlling the attenuators. The output shaft of each differential controls an attenuator position.

The input to one differential (extraordinary) consists of a time dependent angle $\theta_1(t)$ coming from the servo motor via a slip clutch and speed reducer, and an angular position θ_2 (power level) set manually. The output of this differential, which controls the extraordinary wave attenuator, consists of $\theta_2 - \theta_1(t)$. The inputs to the second differential [ordinary) consists of the manually set angular position θ_2 (power level) and a fixed position θ_3, which is used only for calibration purposes. The output of this differential, which controls the ordinary wave attenuator, consists of $\theta_2 - \theta_3$. The voltage across a potentiometer connected to output shaft of each differential is used to monitor the position of each attenuator.

During the rocket flight, the extraordinary wave transmitted power is controlled by means of an attenuator activated by feedback of the received signal telemetered from the rocket, keeping the ordinary transmitted power constant. When the rocket enters the ionosphere, the extraordinary is absorbed more than the ordinary. As the differential absorption appears, the attenuation is continually reduced by a servo mechanism to maintain the modulation of the received signal at a fixed 32 percent, corresponding to a 10 dB difference in the intensity of the two received wave components. The attenuator settings are continuously recorded along with the other data, enabling subsequent determination of the differential absorption.

The scheme as shown in Figure 2.2 was developed for obtaining either circular or linear polarizations. The o- and x-waves can be independently adjusted for either circular or linear polarizations by variable attenuators and phase shifters. As seen in the figure, the signal which is to be the ordinary wave is passed through a power divider, half the power going through a variable phase shifter and half through a variable attenuator. The outputs are sent to adders which

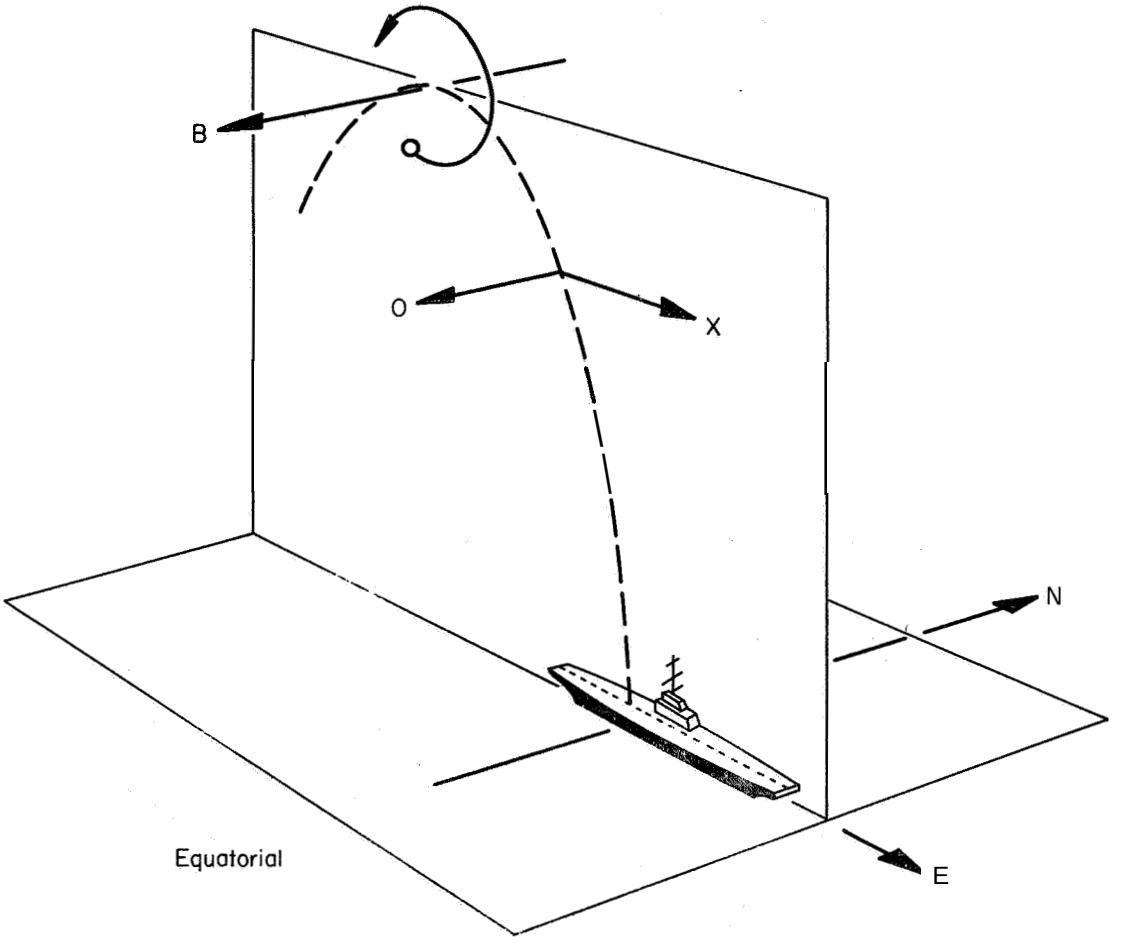

Figure 2.4 Polarizations at the earth's equator

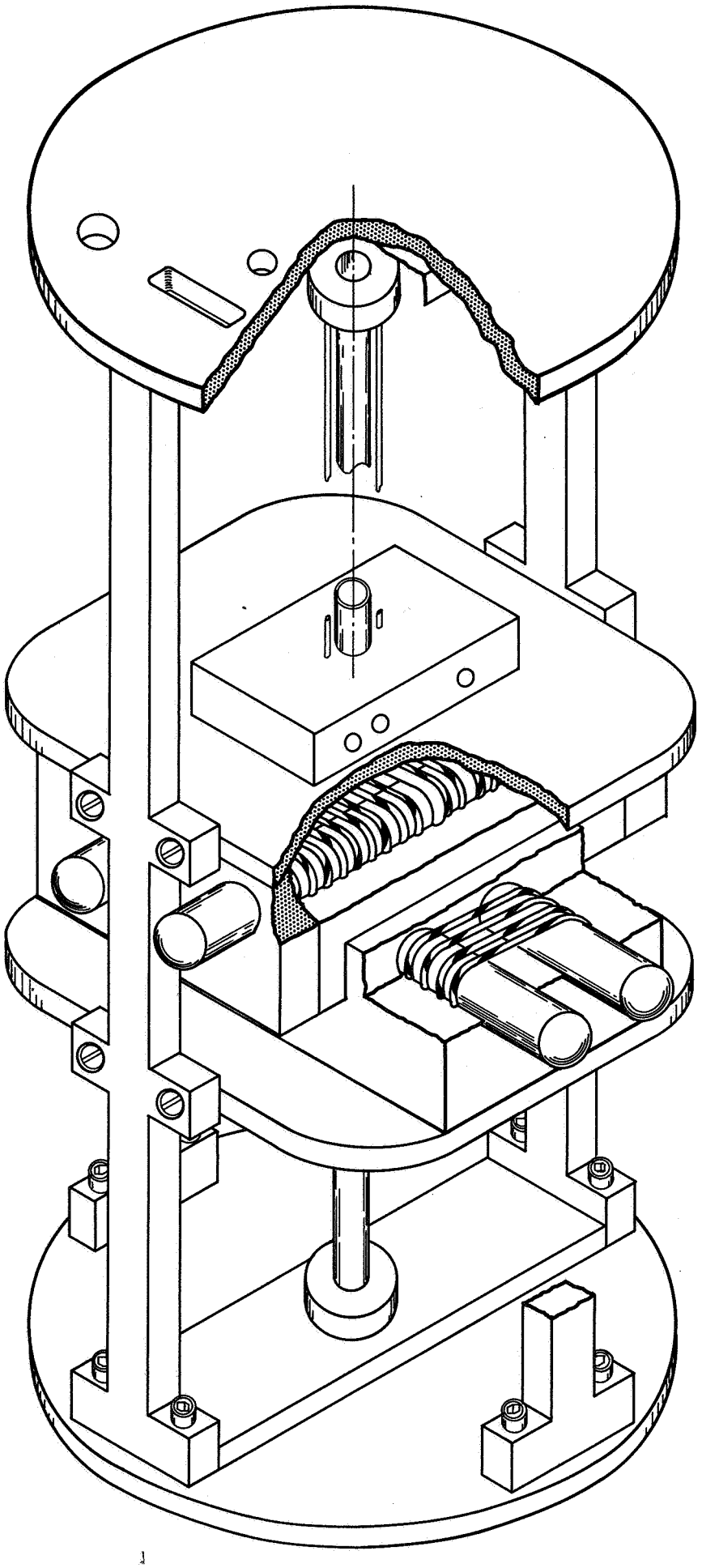

Figure 2 5 Schematic of the rocket rᵉceiving antenna usᵉd for thᵉ equatorial launching

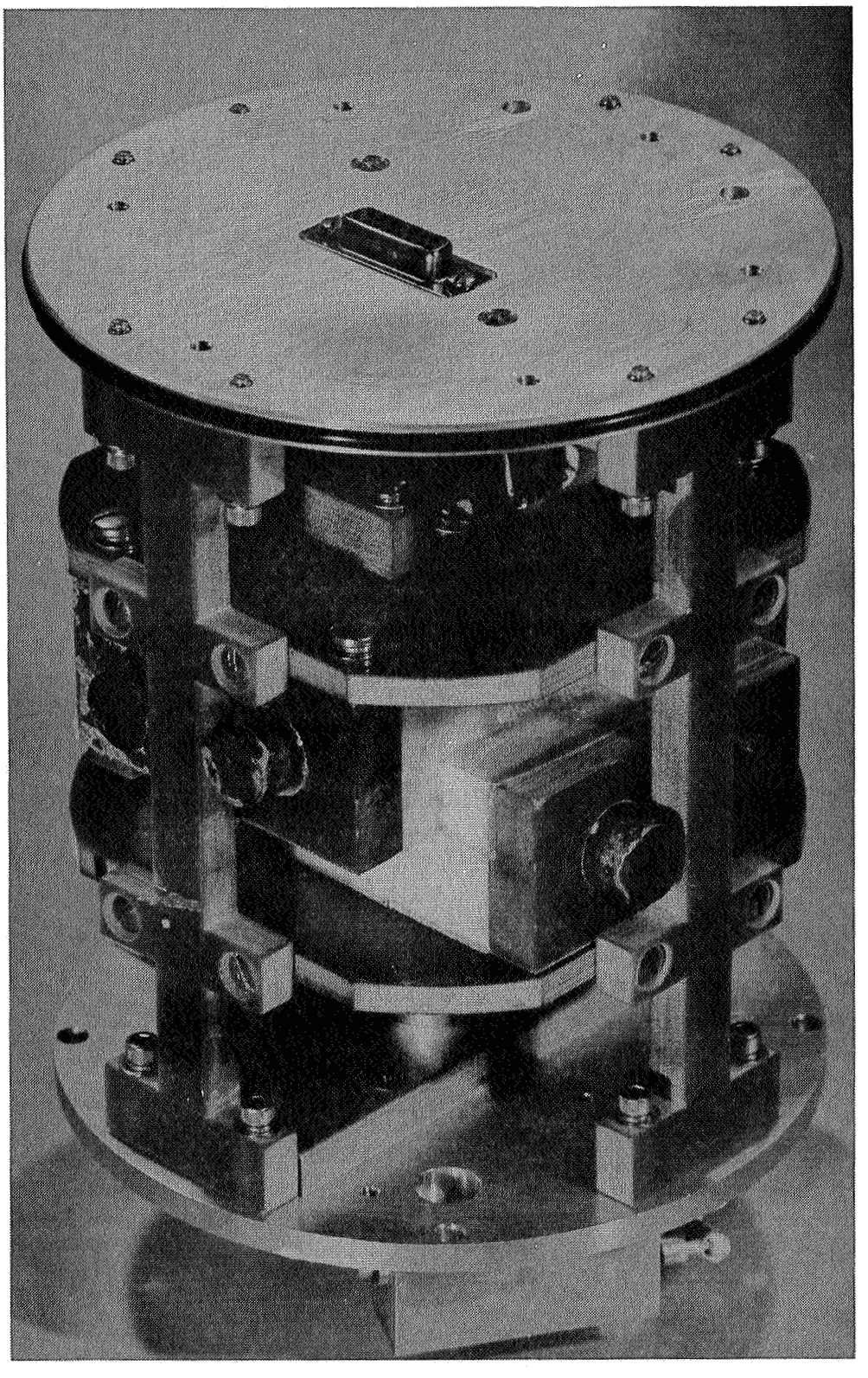

Figure 2.6 Photograph of the rocket receiving antenna used for the equatorial launching

have 30 dB isolation between adjacent channels, then are amplified and radiated. The extraordinary wave is treated identically.

The major difference in the equatorial and non-equatorial experiments comes in the transmitting and receiving antenna systems. Since for the non-equatorial shots, both the ordinary and extraordinary waves are circularly polarized, the transmitting antenna array orientation is immaterial. However, it becomes very critical for the equatorial launching. For least contamination between the two waves, the dipoles must be perpendicular to each other as accurately as possible. Moreover, one dipole (generating the ordinary wave) should be parallel to the true magnetic north-south. The dipole transmitting the extraordinary wave would therefore be in the east-west direction; that is, perpendicular to the earth's magnetic field lines. How this was done for the equatorial experiment (14.228), when the rocket was launched from the ship USNS Croatan during the NASA Mobile Launch Expedition, is shown in Figure 2.4.

2.3 Rocket Antenna and Receiver

A ferrite rod linear antenna located in the rocket gives an RF signal output which is amplitude modulated in the region of 500 Hz (the frequency difference of the o- and x-waves), plus twice the rotation of the rocket spin, plus a small contribution from Faraday rotation. The rocket spin is independently measured by a magnetic aspect sensor contained in the payload. However, for the equatorial shot, instead of a linearly polarized antenna, a circularly polarized antenna is required. So in this case, two ferrite loop antennas (linear) were mounted perpendicular to each other as shown in Figure 2.5. A photograph of the antenna used is shown in Figure 2.6. A shielded line is used for each of the antennas and the outputs of the two antennas were coupled to the receiver

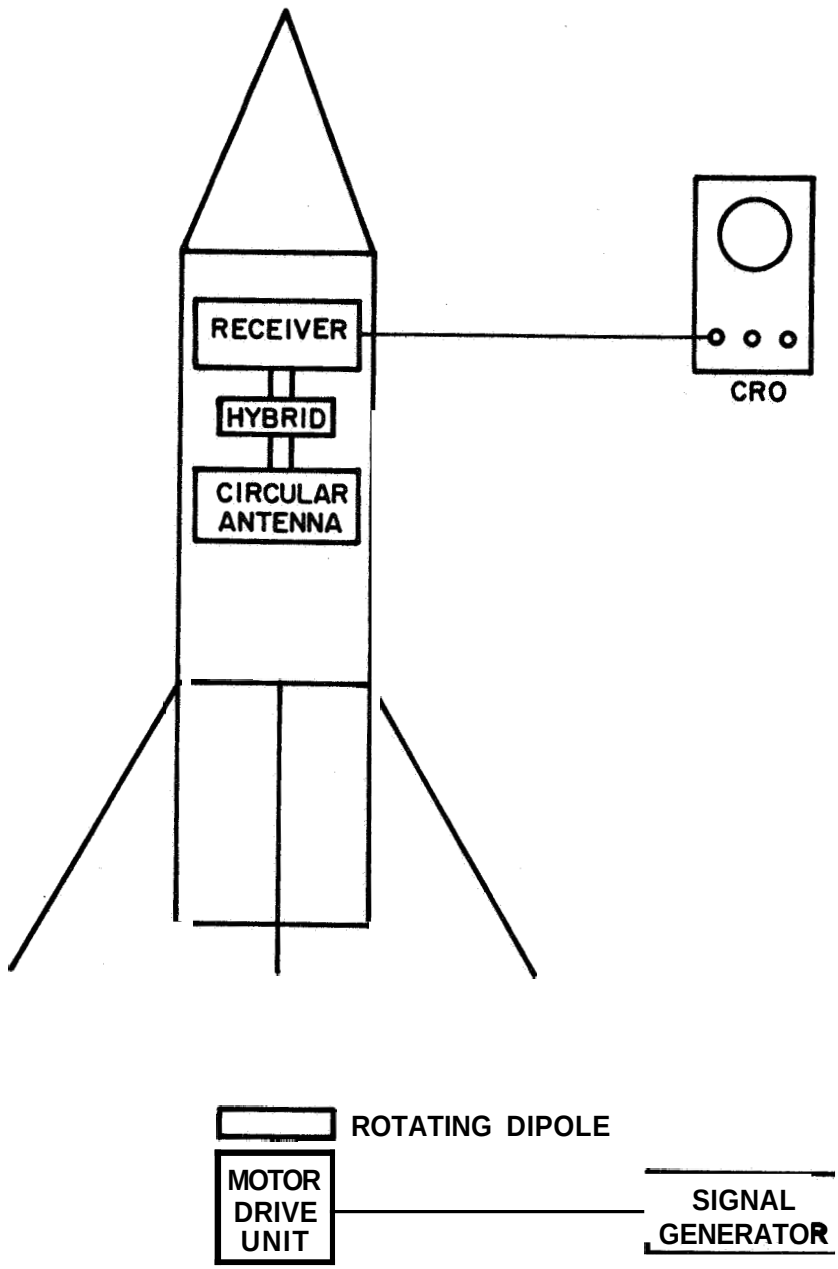

Figure 2.7 Block diagram for adjusting the receiving antenna for circular polarization

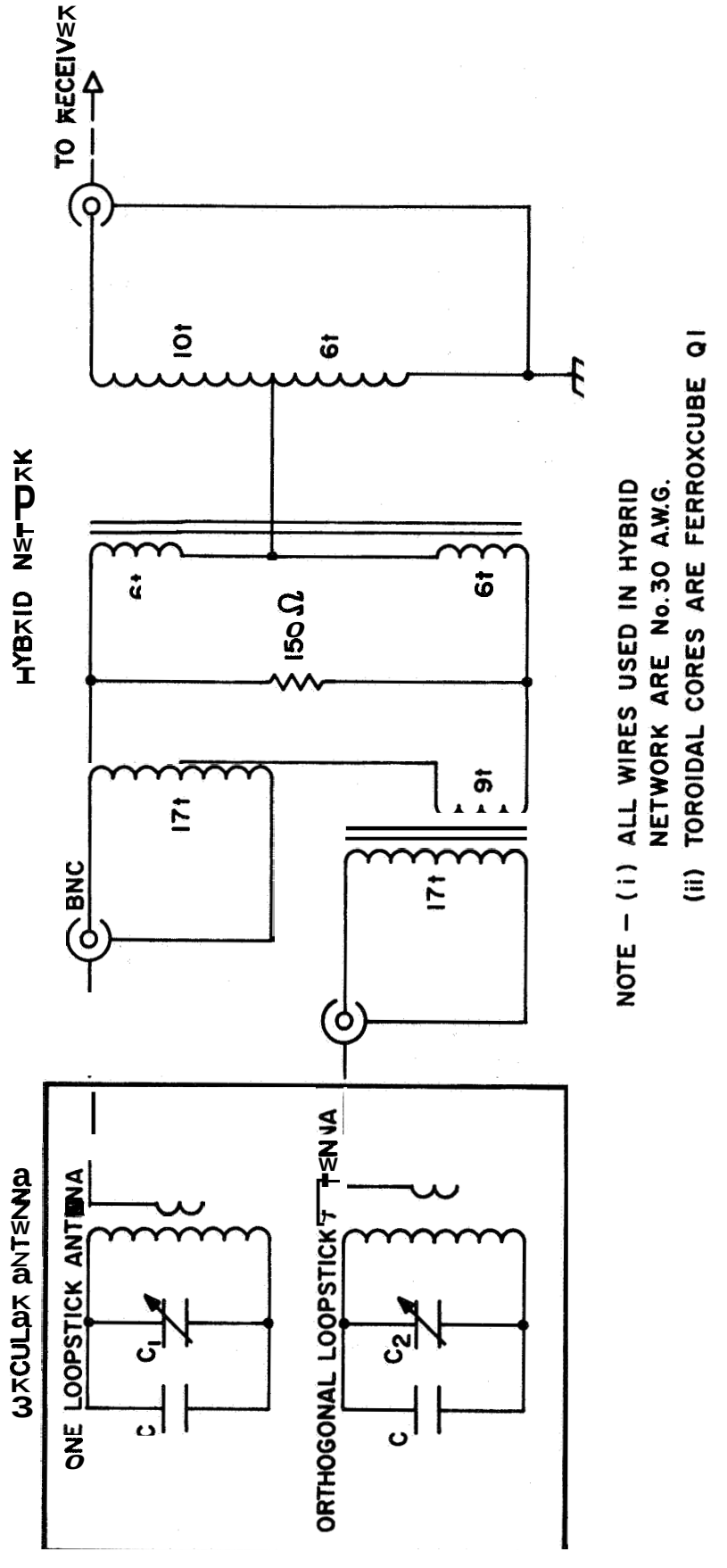

Figure 2.8 Circuitry of the hybrid junction

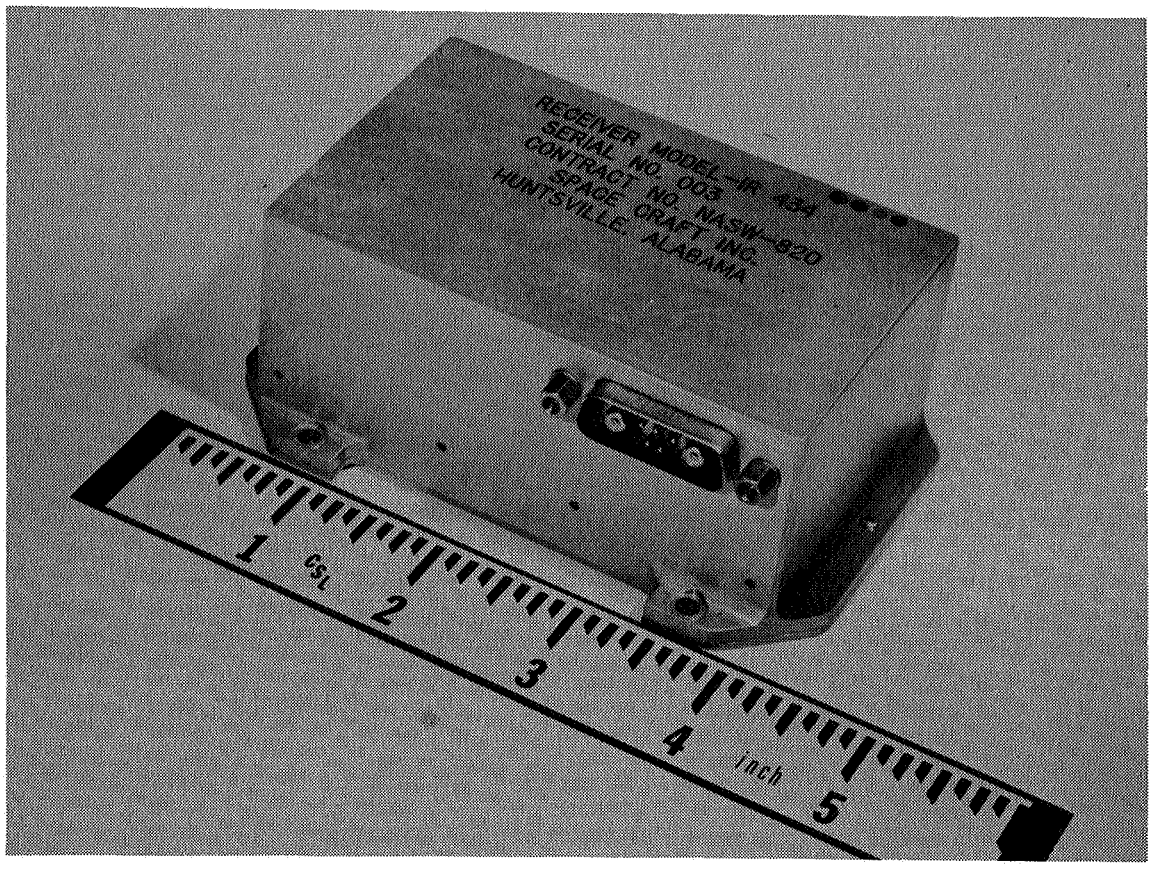

Figure **2.9** Photograph of the rocket receiver

by a hybrid junction circuit (Berg and Howland, 1962). The antennas were then tuned off resonance, one above and the other below to give a circularly polarized pattern. In Figure 2.7 the block diagram for adjusting the receiving antenna for circular polarization is given. A signal at the center frequency of the receiver is radiated by a horizontal ferrite rod antenna mounted on a motor-drive unit. The output of the receiver is observed on an oscilloscope and adjusted for minimum modulation. The detailed circuitry of the hybrid junction is shown in Figure 2.8. The trimmer capacitors C_1 and C_2 are utilized for making this adjustment. The central portion of the antenna is encapsulated in foam to provide additional support for the ferrite rods. Because of the circularly polarized antenna, the rocket spin rate will not enter the receiver output for the equatorial shot.

The output of the antenna is fed to a transistorized crystal controlled superheterodyne receiver designed and developed by Space Craft, Incorporated (see Figure 2.9). The sensitivity of the receiver for a 10 dB signal to noise ratio and a signal which is 90 percent modulated at 500 Hz is 120 dbM or better. Its dynamic range is from threshold to -60 dbM with no more than 6 dB change in output level. The receiver bandwidth is about 2 kHz and the AGC time constant for the first payload was about 100 m sec. The modulated RF signal is detected, DC coupled and amplified to a 5-volt level for feeding a standard FM-AM telemetry subcarrier oscillator and telemetry transmitter.

2.4 Polarization Tests

One method of testing the transmitting antenna array for purity of polarization at medium latitudes involves transmitting short pulses of RF with the system set up for extraordinary polarization. A sensitive receiver is tuned to the frequency transmitted with the output of the receiver displayed on an

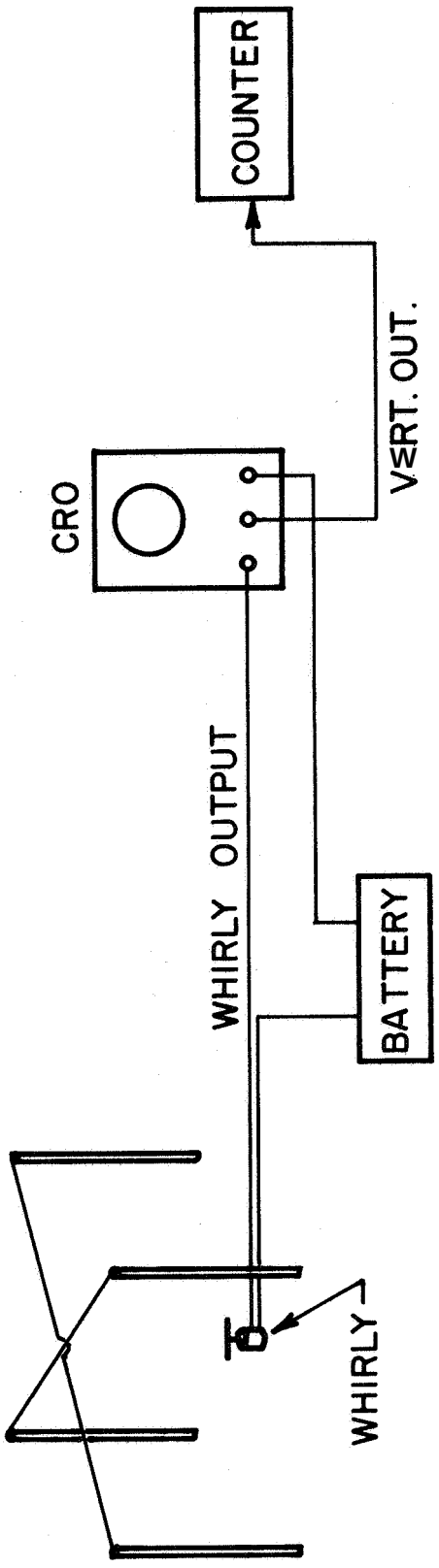

Figure 2 10 Block diagram for polarization tests

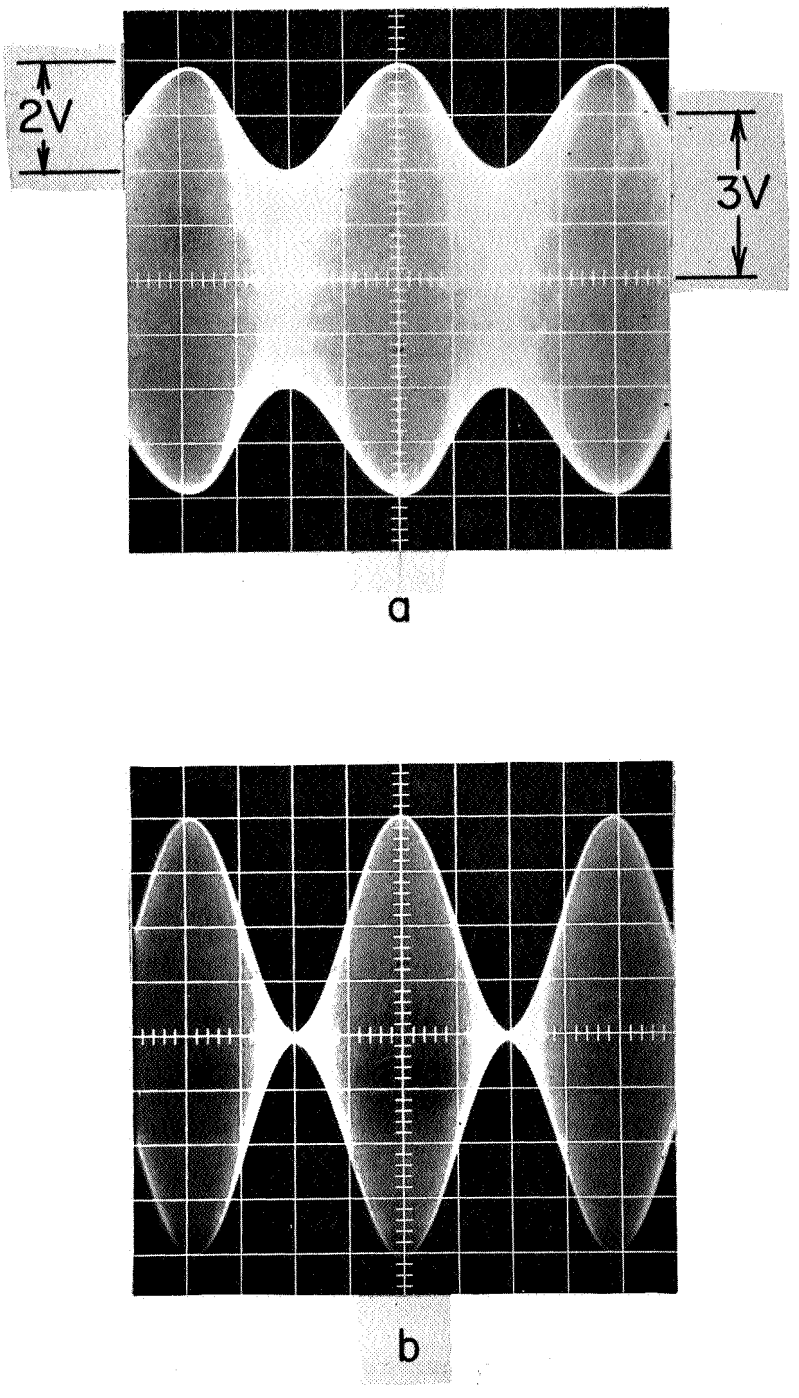

Figure 2.11 (a) Whirly output signal for 30%modulation
(b) Whirly output signal when only one mode is excited

oscilloscope. Any return pulses from the ionosphere, observed on the oscilloscope, are indications that the polarization is not purely extraordinary, as during the daylight hours, extraordinary polarization is highly attenuated by the D-layer so that any reflected energy would be too small to be detectable. Therefore, any echoes observed indicate that energy is being transmitted in other than extraordinary mode and adjustments should be made to minimize this return energy. Conversely, it is possible to transmit in the ordinary mode of polarization and adjust for maximum return echoes as the ordinary mode is less attenuated by the D-layer. However, at the equator, as will be shown in the later chapters, the differential absorption is small which means that both the ordinary and extraordinary waves are absorbed more or less equally. So this method may not be practicable at the equator.

Another method of testing the transmitting antenna array for polarization purity is by using a small rotating dipole placed at the center of the array. In Figure 2.10, the block diagram of the setup used for the polarization tests is shown. The dipole is a horizontal ferrite rod antenna mounted on a motor drive unit capable of rotating either clockwise or counterclockwise. The one-turn link output of the antenna is brought through a coaxial line to an oscilloscope in the transmitter van. The ordinary attenuator is set at 20 dB and the extraordinary at 30 dB and by varying the outputs of the ordinary and extraordinary exciters, the modulation is adjusted for 30 percent (Figure 2.11 (a)). For high latitudes, since the o- and x-waves are circularly polarized and rotate in opposite directions, the sense of rotation is checked by measuring the carrier signal frequency of the rotating dipole, which is shifted by the dipole rotation frequency. For the equatorial experiment, when only one mode is excited at a time, the output of the rotating loop must exhibit 100 percent modulation at twice the spin rate of the loop as shown in Figure 2.11 (b). So for the

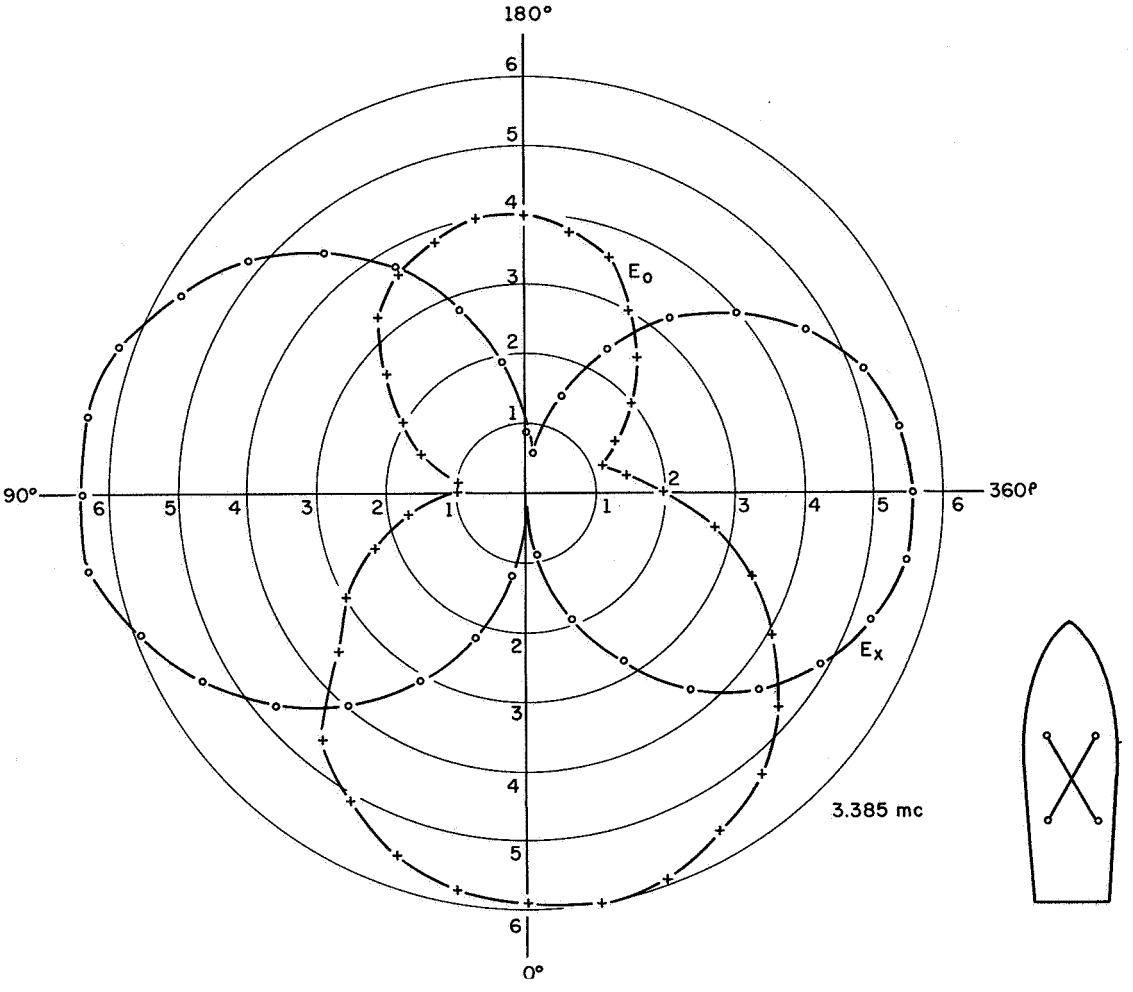

Figure 2.12 Near field radiation patterns obtained during the equatorial launching

equatorial experiment also, a linear antenna is sufficient for the polarization tests. Near-field radiation patterns for the ordinary and extraordinary are shown in Figure 2.12. These patterns were obtained during the equatorial launching (14.228) at the operating frequency of 3.385 MHz. The lack of symmetry in the patterns, as can be noticed from the figure, is attributed to the interference caused by the ship's structure and other nearby antenna elements. It is believed that much of these difficulties will not be encountered if the experiment is conducted at a ground launch site.

2.5 Data Reduction

The advantages of this system are as follows:

(1) a high sample rate of Faraday rotation and differential absorption is obtained due to the 500 cps frequency difference between the extraordinary and ordinary waves;

(2) the high sampling frequency is far removed from any spin modulation and from standing wave modulation at all altitudes, thereby enabling the signal frequency to be clearly distinguished from the standing wave pattern ; and

(3) the servo system, which maintains a constant ratio of ordinary to extraordinary power at the rocket, considerably reduces the nonlinearity of the rocket receiver for measuring relative absorption between the two waves and transfers this measurement to a set of precision RF attenuators located on the ground.

These refinements have enabled Faraday rotation and differential absorption measurements to be made to resolutions of about one degree and 0.2 dB, respectively.

The concept of Faraday rotation as is understood at high latitudes is somewhat difficult to comprehend at the equator. This is partly because the ordinary

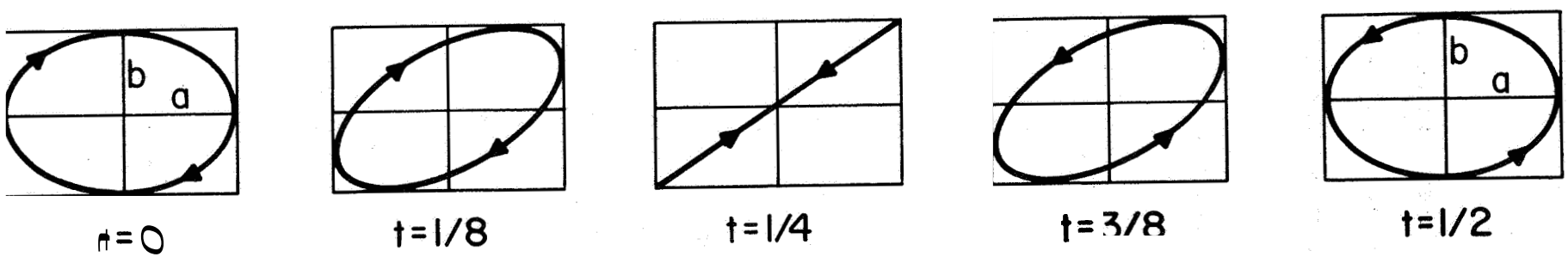

Figure 2.13 Illustration on the concept of Faraday rotation at the equator

and extraordinary waves are linearly polarized and perpendicular to each other. When two sine waves, varying about axes at right angles, are combined, the resultant figure is no longer a sine wave but varies with the relative time phase of the waves, In the present case, let us take 'a' as the amplitude of the extraordinary wave, and 'b' as the amplitude of the ordinary wave (Figure 2.13) and these are being separated by a frequency of 500 Hz, thus introducing a time phase of 2nt or 360' X t, t being the unit of time. The resultant of these two waves is a straight line when they are in time phase (or 180' out of phase) and is an ellipse for all other values of phase position. Since in the present case, $t = \frac{1}{500}$ sec the rocket receiver output is modulated by a 500 Hz signal. As these waves enter the ionosphere, since the phase velocities for the ordinary and extraordinary waves are different, an additional phase difference will be introduced which is analogous to the Faraday rotation at high latitudes. In order to avoid confusion, the term 'Faraday rotation' will be avoided as far as possible in this report hereafter and instead it will be referred to as "phase difference". However at times for convenience sake, the term Faraday rotation is used and it should be understood as the phase difference between the ordinary and extraordinary waves.

The two main parameters derived from the data are differential absorption and total relative phase versus time after launch or rocket height. The standing wavelength at the higher altitudes can also be readily obtained versus time after launch. Other parameters include the height at which the first extraordinary reflection occurs, the height at which the ordinary reflection takes place and the height at which the second extraordinary reflection (Z-trace) occurs. The manual method of extracting the differential absorption consists of subtracting the instantaneous dB readings of the RF waveguide-beyond-cut-off attenuators at given intervals of time. Immediately before each rocket firing,

as part of the countdown procedure, and again immediately after splash, a Calibration is made of each RF attenuator. The calibration consists of manually setting each attenuator by 10 dB steps and recording the audio output voltage of the coupled linear potentiometers. As a result a chart can be made of RF attenuation in dB versus audio voltage, The amplitudes of the extraordinary and ordinary attenuation can be then obtained from the data in dB readings from the calibration chart. The difference in the dB readings is the uncorrected differential absorption.

The Faraday rotation can be extracted by any of three methods. Each method uses the fact that the rocket receiver signal contains the frequency components $(500 \pm 2f_s \pm 2f_F)$ Hz; where 500 Hz represents the difference frequency of o- and x-waves, f_s is the instantaneous rocket spin rate and f_F is the instantaneous Faraday rotation rate. Also, the magnetic aspect sensor signal contains the frequency component $\pm f_s$. In the simplest method, the rocket receiver signal is multiplied with the 500 Hz reference signal to get the difference frequency $\pm 2f_s \pm f_F$. However, for the equatorial shot, since a circularly polarized antenna is used in the payload, the rocket spin rate is not included in the rocket receiver output signal. As such, in this case when the rocket receiver signal is multiplied with 500 Hz reference signal, the resultant is $\pm 2f_F$.

A second, more laborious method is to count the individual cycles of the rocket receiver signal up to a particular time T and substract the total number of cycles of the 500 Hz and twice the total number of cycles of the magnetic aspect sensor signal $\pm f_s$ (for non-equatorial shots only) which leaves $2\int_o^T f_F \, dt$.

The third method is the most laborious but gives Faraday rotation to resolutions of about one degree. This is done by a Faraday rotation data processor developed by the Coordinated Sciences Laboratory (Gooch et al., 1966) which

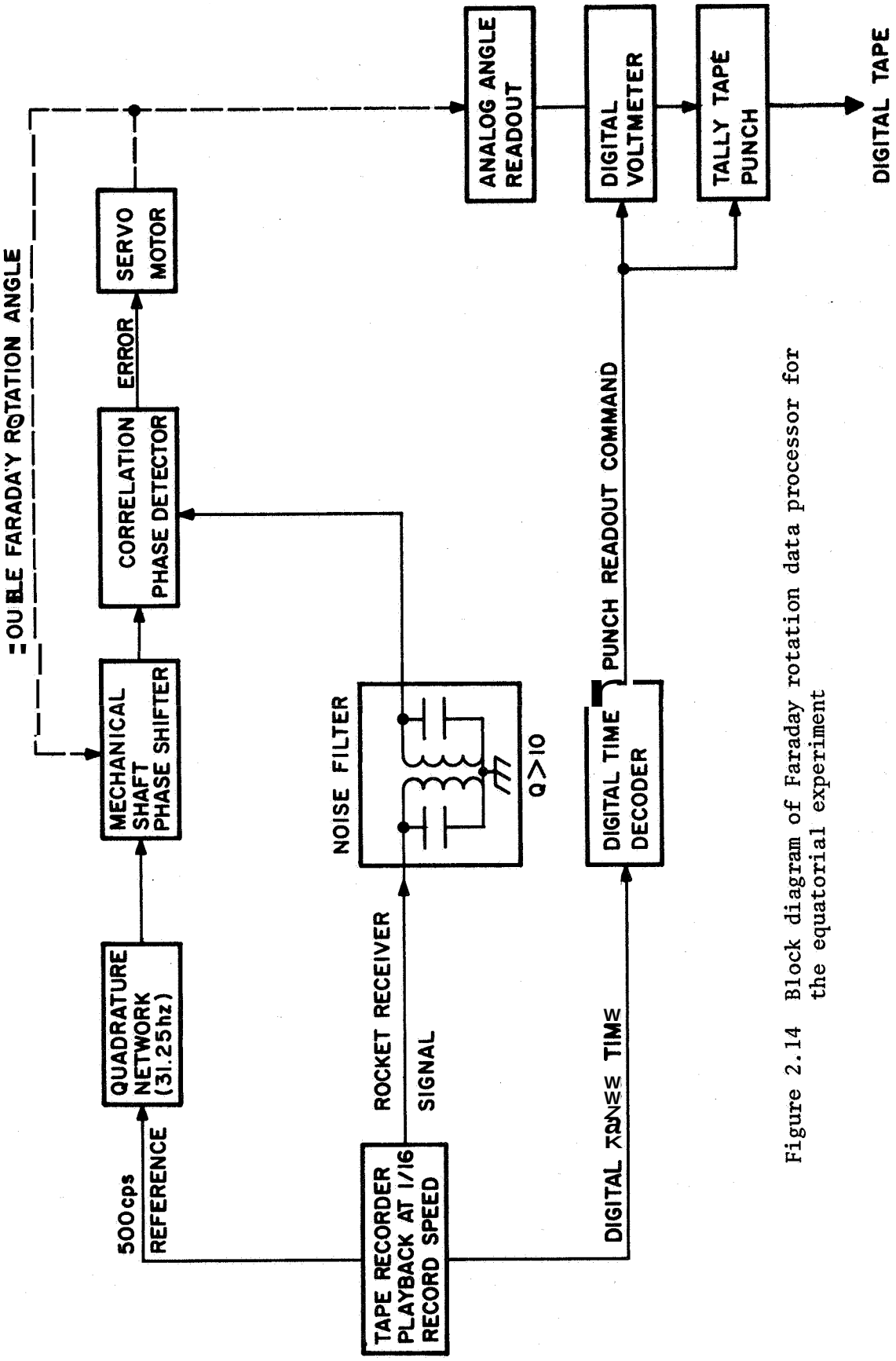

Figure 2.14 Block diagram of Faraday rotation data processor for the equatorial experiment

automatically extracts the accumulated Faraday rotation. This is done by removing the accumulated roll phase component and the accumulated phase due to the x- and o-wave difference frequency of 500 Hz from the composite rocket receiver signal. However, for the equatorial shot, the desired accumulated Faraday rotation is obtained by simply removing the 500 Hz difference frequency of the o- and x-waves from the composite rocket receiver signal. The block diagram of such a simplified system as was used for the equatorial shot (14.228) is given in Figure 2.14. The x- and o-wave difference frequency signal is fed to a mechanical phase shifter which has a servo driven shaft input corresponding to Faraday rotation angle. In the event of Faraday rotation, the rocket receiver signal phase changes with respect to the reference phase, producing a polarized output from the correlation phase detector. This output is a servo error signal which causes the servo to turn the mechanical phase shifter by an amount necessary to bring the rocket receiver and reference phase again to the original 90° difference. The servo shaft position indicates Faraday rotation and is read by a helipot. A detailed description of the processor may be found in the CSL report by Gooch et al. (1966).

2.6 Discussion

The propagation experimental setup, as originally developed is designed for considerable flexibility in operation. However, if a decision is made that it will be used only for equatorial launchings, the experimental setup might be simplified considerably. For example, the power divider and phase shifter networks, which were originally used for obtaining circular polarizations, can be altogether avoided. The only essential item is that the transmitting antennas should be along the magnetic N-S and E-W directions. Moreover, emphasis should be given for adjusting the receiving antenna for circular polarization as accurately as possible. Otherwise some complications will come in, while

reducing the Faraday rotation data. As will be shown in the later chapters, the observed differential absorption and Faraday rotation are small at the equator when compared to high latitudes, Therefore, some thought should be given to improve the present setup so that these parameters could be measured more accurately.

3. METHODS OF DATA ANALYSIS

3.1 Introduction

In this chapter the Appleton-Hartree equation for the complex index of refraction for the propagation of an electromagnetic wave in a magnetoionic medium will be presented. Then a particular case which is known as quasi-transverse approximation to the general equation will be discussed. Following this, equations will be derived for obtaining electron densities and collision frequencies from the measured differential absorption and Faraday rotation values at the equator. Equations for analyzing the standing wave pattern are also derived.

3.2 Appleton-Hartree Equation and the Approximations

The Appleton-Hartree equations, which give the complex index of refraction and the polarization for a (weak) plane electromagnetic wave propagating in a homogeneous, absorbing, ionized gas in the presence of a constant, external magnetic field is

$$n^2 = 1 - \frac{X}{(1 - jZ) - \frac{Y_T^2}{2(1-X-jZ)} \pm \left[\frac{Y_T^4}{4(1-X-jZ)^2} + Y_L^2 \right]^{1/2}} \qquad (3.1)$$

and

$$R = -\frac{j}{Y_L} \left\{ \frac{\frac{1}{2} Y_T^2}{1-X-jZ} \mp \left(\frac{\frac{1}{4} Y_T^4}{(1-X-jZ)^2} + Y_L^2 \right)^{1/2} \right\} \qquad (3.2)$$

where

$$X = \omega_N^2/\omega^2 = \frac{Ne^2}{\varepsilon_o m} \frac{1}{w^2}$$

$$Y = \omega_H/\omega = \frac{eB}{mw}$$

$$Y_L = \omega_L/\omega = \frac{eB_L}{m\omega}$$

$$Y_T = \omega_T/\omega = \frac{eB_T}{m\omega}$$

$Z = v/w$

ω = angular frequency of the propagating radio wave

N = electron density of the medium

e = absolute value of electron charge

m = electron mass

ε_0 = permittivity of free space

B = earth'smagnetic flux density

B_L = component of the earth's magnetic flux density along the ray path

B_T = component of the earth's magnetic flux density perpendicular to the ray path

v = effective collision frequency of electron with other constituents of the medium.

These equations include the effects of the electrons only and do not take into account the presence of heavy particles except through collisions of neutral particles with the electrons. Although the Appleton-Hartree equation is strictly valid only for a homogeneous medium, it is also sufficiently correct for application to slowly varying media, that is where the change of refractive index as given here is small in a distance of one vacuum wavelength (of the incident radiation) divided by 2π.

In applying these equations to problems of propagation through the ionosphere it is convenient to make use of two approximations, one of which applies where waves are propagated sufficiently nearly along the direction of the imposed

field and the other when they are propagated sufficiently nearly perpendicular to it. They are called the quasi-longitudinal (QL) and the quasi-transverse (QT) approximations, and the conditions for which they hold are:

$$[QL] \quad Y_T^4/4Y_L^2 << |(1 - X - jZ)^2| \tag{3.3}$$

$$[QT] \quad Y_T^4/4Y_L^2 >> |(1 - X - jZ)^2| \quad . \tag{3.4}$$

In this section the circumstances under which these approximations are valid will be discussed with special emphasis on the quasi-transverse approximation.

Under these two conditions Equations (3.1) and (3.2) assume the following approximate forms

QL:

$$n_{QL}^2 \doteq 1 - X/(1 - jZ \pm Y_L) \tag{3.5}$$

$$R_{QL} \doteq \pm j \tag{3.6}$$

QT (upper sign):

$$n_{QT(u)}^2 \doteq 1 - X/\left\{1 - jZ + (1 - X - jZ)\cos^2\theta\right\} \tag{3.7}$$

$$R_{QT(u)} \doteq 0 \tag{3.8}$$

QT (lower sign):

$$n_{QT(l)}^2 \doteq 1 - X/\left\{1 - jZ - Y_T^2/(1 - X - jZ)\right\} \tag{3.9}$$

$$R_{QT(l)} \doteq \infty \tag{3.10}$$

The quasi-transverse expression where the upper sign is used is derived as follows. From Equation (3.1)

$$n^2_{(u)} = 1 - X/\left\{ 1 - jZ - \tfrac{1}{2} Y_T^2/(1 - X - jZ) + [\tfrac{1}{4} Y_T^4/(1 - X - jZ)^2 + Y_L^2]^{1/2} \right\} \quad (3.11)$$

$$= 1 - X/ \left[1 - jZ - \left\{ \tfrac{1}{2} Y_T^2/(1 - X - jZ) \right\} x \left\{ 1 - [1 + 4Y_L^2 (1 - X - jZ)/Y_T^4]^{1/2} \right\} \right] \quad (3.12)$$

which with the conditions of the quasi-transverse approximation, gives

$$n^2_{(u)} = 1 - X/[1 - jZ - \left\{ \tfrac{1}{2} Y_T^2/(1 - X - jZ) \right\} \left\{ - 2Y_L^2 (1 - X - jZ)^2/Y_T^4 \right\}$$

$$= 1 - X/[1 - jZ + (1 - X - jZ) (Y_L^2/Y_T^2)]$$

$$= 1 - X/[1 - jZ + (1 - X - jZ) \cot 2\theta] \quad (3.13)$$

where θ is the angle between the wave normal and the imposed magnetic field. The expression for R show that when the quasi-longitudinal approximation is valid the two characteristic waves are circularly polarized and when the quasi-transverse approximation is valid they are linearly polarized along the principal directions.

The conditions for the two approximations

$$Y_T^4/4Y_L^2 \ll \gg (1 - X - jZ)^2 \quad (3.14)$$

may be written as

$$\frac{\omega_c^2}{\omega^2} \ll\gg (1 - X)^2 + Z^2 \qquad (3.15)$$

since

$$\frac{Y_T^2}{2Y_L} = Y \cdot (\frac{1}{2} \sin^2 \theta/\cos \theta) = \frac{\omega_H}{\omega} \cdot f(\theta)$$

where

$$f_\theta = \frac{1}{2} \sin^2\theta/\cos \theta \ .$$

Now denoting $\omega_H . f(\theta)$ as ω_c we have equation (3.15). It will be seen that the conditions depend not only on the gyrofrequency (ω_H) and the angle (θ) of propagation, but also on the magnitudes of X and Z. The question of whether a given wave can be discussed in terms of the quasi-longitudinal approximation is not, therefore, simply a question of how nearly the direction of propagation coincides with the direction of the applied field, but depends also on the electron density and the collision frequency. These approximations have been discussed in detail by Ratcliffe (1962).

If Z is taken as constant, and X is allowed to vary, the condition for the quasi-longitudinal approximation is most likely to break down when X = 1, and if it is to hold even then we must have

$$\omega_c^2/\omega^2 \ll Z^2 \ll \nu^2/\omega^2 \qquad (3.16)$$

or

$$\omega_c^2 \ll \nu^2 \ .$$

If this condition applies at X = 1 then the quasi-longitudinal approximation can be used for all values of X. Since ω_c depends only on the strength of the imposed field and the direction of propagation the condition is very simple.

When numerical cases are considered it is a reasonably good approximation to assume that the inequalities in Equation (3.16) are satisfied if the larger quantity is nine times the smaller, so that the two approximations require:

$$\nu > 3|\omega_c| \quad \text{or} \quad Z > 3Y|f(\theta)| \quad \text{for QL at } X = 1 \tag{3.17}$$

and

$$\nu < \tfrac{1}{3}|\omega_c| \quad \text{or} \quad Z < \tfrac{1}{3}Y|f(\theta)| \quad \text{for QT at } X = 1 \ . \tag{3.18}$$

If $\nu < \frac{1}{3}|\omega_c|$ the quasi-transverse approximation is appropriate when X = 1; it is now necessary to investigate the range of X, near X = 1, for which it also holds. When $\nu < \frac{1}{3}|\omega_c|$, Equation (3.15) for the quasi-transverse approximation can be written

$$\frac{\omega_c^2}{\omega^2} >> (1 - X)^2 \tag{3.19}$$

which is equivalent to

$$Y|f(\theta)| > 3|(1 - X)| \ . \tag{3.20}$$

This expression then determines the range of values of X, near X = 1, for which the quasi-transverse approximation is appropraite when $\nu < \frac{1}{3}|\omega_c|$.

Even if $\nu < \frac{1}{3}|\omega_c|$, so that the quasi-transverse approximation holds near X = 1, the quasi-longitudinal approximation may hold for other values of X.

The latter will hold, whatever the value of **v**, provided

$$Y|f(\theta)| < \tfrac{1}{3}|(1 - X)| \quad . \tag{3.21}$$

It is important to find the condition which makes the quasi-longitudinal approximation hold when $X = 1 \pm Y_L$. Then the above equation, with $\frac{1}{2} \sin^2\theta/\cos\theta$ written for $f(\theta)$, becomes

$$\tfrac{1}{2} Y \sin^2 \theta/\cos\theta < \tfrac{1}{3} Y \cos\theta \tag{3.22}$$

or

$$\tan^2 \theta < \frac{2}{3}$$

or

$$\theta < 40" \quad . \tag{3.23}$$

Provided $\theta < 40°$ it is thus always safe to assume that the quasi-longitudinal approximation is valid when $X = 1 \pm Y_L$.

If the quasi-transverse approximation were to be valid when $X = 1 \pm Y_L$, would require $\tan^2 \theta > 6$ **or** $\theta > 68°$. However at low altitudes, where X is small and Z is significant, the region in which the quasi-transverse approximation holds, is considerably less. This aspect will be taken up in detail in a later chapter.

3.3 The Quasi-Transverse Approximation

As long as the direction of the propagating wave does not deviate from the normal to the magnetic field by more than a few degrees i.e. $0 \approx 90°$, not only the quasi-transverse approximation is valid but also the term containing $\cos^2 \theta$ in Equation (3.7) may be neglected. The equations for the refractive index

of ordinary wave are then given as:

$$n_o^2 = 1 - \frac{X}{1-jZ} \quad . \tag{3.24}$$

The refractive index for the extraordinary wave is given as:

$$n_X^2 = 1 - \frac{X}{1-jZ-\frac{Y_T^2}{1-X-jZ}} \quad . \tag{3.25}$$

To investigate the absorption and phase variation, the complex refractive index is written as

$$n = \mu - j\,\chi \quad . \tag{3.26}$$

Therefore Equation **(3.24)** may be written as

$$n_o^2 = (\mu_o - j\chi_o)^2 = 1 - \frac{X}{1-jZ} \quad . \tag{3.27}$$

To obtain separate eauations for μ_o and χ_o, the real and imaginary parts must be separated in the right hand side of the above equation and must be equated to those on the left hand side.

Now

$$\begin{aligned}(\mu_o - j\chi_o)^2 &= 1 - \frac{X(1+jZ)}{(1-jZ)(1+jZ)} \\ &= 1 - \frac{X(1+jZ)}{1+Z^2} \\ &= 1 - \frac{X}{1+z^2} - j\,\frac{XZ}{1+Z^2} \\ &= a - jb \text{ say}\end{aligned} \tag{3.28}$$

where

$$\left.\begin{aligned} a &= 1 - \frac{X}{1+Z^2} \\ b &= \frac{XZ}{1+Z^2} \end{aligned}\right| \qquad (3.29)$$

From Equation (3.28) we have

$$\mu_o^2 - \chi_o^2 - j\ 2\mu\chi = a - jb \quad .$$

Equating the real and imaginary parts of both sides of the above equation we have

$$\left.\begin{aligned} \mu_o^2 - \chi_o^2 &= a \\ 2\mu_o\chi_o &= b \quad . \end{aligned}\right\} \qquad (3.30)$$

From this, it can be written that

$$\mu_o = \left\{ \frac{\sqrt{a^2 + b^2} + a}{2} \right\}^{1/2} \qquad (3.31)$$

$$\chi_o = \left\{ \frac{\sqrt{a^2 + b^2} - a}{2} \right\}^{1/2} \quad . \qquad (3.32)$$

Equation (3.31) can further be simplified in the following manner

$$\mu_o = \left\{ \frac{1}{2} \left[a \left(1 + \frac{b^2}{a^2} \right)^{1/2} + a \right] \right\}^{1/2} \quad . \qquad (3.33)$$

Since b contains XZ in the numerator, b < a; so the above equation may be

simplified as

$$\mu_o = \left\{\frac{1}{2}\left[a\left(1 + \frac{1}{2}\frac{b^2}{a^2}\right) + a\right]\right\}^{1/2}$$

$$\doteq \left\{a\left(1 + \frac{1}{4}\frac{b^2}{a^2}\right)\right\}^{1/2}$$

$$\doteq a^{1/2}\left(1 + \frac{1}{4}\frac{b^2}{a^2}\right)^{1/2}$$

$$\mu_o \doteq a^{1/2}\left(I + \frac{1}{8}\frac{b^2}{a^2}\right) \quad . \tag{3.34}$$

In the above equation the term $(1 + \frac{1}{8}\frac{b^2}{a^2})$ may be called the correction factor which if at all is effective, it is only close to X = 1. So for all practical purposes the above equation may be written as

$$\mu_o = a^{1/2} = \left\{1 - \frac{X}{1+Z^2}\right\}^{1/2} \quad . \tag{3.35}$$

From Equation (3.32) we have

$$\chi_o = \left\{\frac{a\left(1 + \frac{b^2}{a^2}\right)^{1/2} - a}{2}\right\}^{1/2} = \left\{\frac{a\left(1 + \frac{1}{2}\frac{b^2}{a^2}\right) - a}{2}\right\}^{1/2}$$

$$= \frac{1}{2}\frac{b}{\sqrt{a}} = \frac{1}{2}\frac{XZ}{1+Z^2}\frac{(1+Z^2)^{1/2}}{(1-X+Z^2)}\,1/2$$

$$\chi_o = \frac{1}{2}\frac{XZ}{[(1+Z^2)(1-X+Z^2)]}1/2 \quad . \tag{3.36}$$

Now for the extraordinary wave using Equation (3.25) we have

$$n_X^2 = (\mu_x - j\chi_x)^2 = 1 - \frac{X}{1 - jZ - \frac{Y_T^2}{1-X-jZ}}$$

$$(\mu_x - j\chi_x)^2 = 1 - \frac{X\ (1-X-jZ)}{(1-jZ)(1-X-jZ) - Y_T^2}$$

$$= 1 - \frac{X\ (1-X-jZ)}{(1-X-Z^2-Y_T^2) - jZ\ (2-X)}$$

$$= I - \frac{X\ (1-X-jZ)\ [(1-X-Y_T^2-Z^2) + jZ\ (2-X)]}{(1-X-Y_T^2-Z^2)^2 * Z^2\ (2-X)^2}$$

$$(\mu_x - j\chi_x)^2 = 1 - \frac{X\ (1-X)\ (1-X-Z^2-Y_T^2) + XZ^2\ (2-X)}{(1-X-Z^2-Y_T^2)^2 + Z2\ (2-X)2}$$

$$- \frac{jXZ\ \left\{(1-X)^2 + Z^2 + Y_T^2\right\}}{(1-X-Z^2-Y_T^2)^2 + Z^2\ (2-X)^2}$$

$$= a^1 - j\ b^1 \text{ say} \qquad (3.37)$$

when

$$a^1 = 1 - \frac{X\ (1-X)\ (1-X-Z^2-Y_T^2) + XZ^2\ (2-X)}{(1-X-Z2-YZ)2 + Z^2\ (2-X)^2}$$

and

$$b^1 = \frac{XZ\ \left\{(1-X)^2 + Z^2 + Y^2\right\}}{(1-x-z-Y_T^2) + Z^2\ (2-X)^2} \qquad (3.38)$$

Now

$$\mu_x^2 - \chi_x^2 - j\ 2\mu_x\chi_x = a1 - j\ b1 \ . \qquad (3.39)$$

From this it can be written that

$$\left.\begin{aligned} \mu_x^2 - \chi_x^2 &= a^1 \\ \text{and} \qquad 2\mu_x \chi_x &= b^1 \quad . \end{aligned}\right\} \tag{3.40}$$

Therefore

$$\mu_x = \left\{\frac{\sqrt{a^{12} + b^{12}} + a^1}{2}\right\}^{1/2} = (a^1)^{1/2}\left(1 + \frac{1}{8}\,\frac{b^{12}}{a^{12}}\right)$$

$$\simeq (a^1)^{1/2}$$

$$\mu_x \simeq \left\{1 - \frac{X\,(1-X)\,(1-X-Y_T^2-Z2) + XZ2\,(2-X)}{(1-X-Y_T^2-Z^2)^2 + Z2\,(2-X)^2}\right\}^{1/2} \tag{3.41}$$

and

$$\chi_x = \left\{\frac{\sqrt{a^{12} + b^{12}} - a^1}{2}\right\}^{1/2} \simeq \frac{1}{2}\frac{b^1}{\sqrt{a^1}}$$

$$\chi_x = \left\{1 - \frac{X\,(1-X)\,(1-x-z2-Y_T^2) + XZ2\,(2-X) + \frac{1}{2}XZ\left\{(1-X)^2 + Z^2 + Y_T^2\right\}}{(1-X-Z^2-Y_T^2)^2 + Z2\,(2-X)^2}\right\}^{1/2} \tag{3.42}$$

3.4 Electron Density from Phase Difference Measurements

If the two modes of propagation, viz. ordinary (o-wave) and extraordinary (x-wave) travel along the same ray path, the phase difference, $\Delta\phi$, between the two modes in traveling a distance ΔS, is given by the equation

$$\Delta\phi = \frac{\omega}{c}\,(\mu_o - \mu_x)\,\Delta S \quad . \tag{3.43}$$

So the rate of change of phase difference may be expressed as

$$\frac{d\phi}{dt} = \frac{2\pi}{\lambda_o} (\mu_o - \mu_x) \frac{dS}{dt} \qquad (3.44)$$

where λ_o is the propagation wavelength in free space.

Using Equation (3.34) and (3.41) from the previous section we have

$$\mu_o - \mu_x = \left\{1 - \frac{X}{1+z2}\right\}^{1/2} - \left\{1 - \frac{X\,(1-X)\,(1-X-Y_T^2-Z^2) + XZ^2\,(2-X)}{(1-X-Y_T^2-Z^2)^2 + Z2\,(2-X)2}\right\}^{1/2} . \qquad (3.45)$$

For altitudes above 75 km, where $\nu << \omega$ or $Z << 1$, the terms containing Z^2 may be neglected. This simplifies the above equation to

$$\mu_o - \mu_x = (1-X)^{1/2} \left\{1 - \frac{X\,(1-X)}{(1-X-Y_T^2)}\right\}^{1/2} \quad \text{say} . \qquad (3.46)$$

This may be rewritten as

$$\left\{1 - \frac{X\,(1-X)}{(1-X-Y_T^2)}\right\}^{1/2} = (1-X)^{1/2} - \nabla . \qquad (3.47)$$

Squaring on both sides we have

$$1 - \frac{X\,(X-X)}{1-X-Y_T^2} = 1 - X + \nabla^2 - 2\nabla(1-X)^{1/2}$$

i.e.

$$2\nabla(1-X)^{1/2} = \frac{X\,(1-X)}{1-X-Y_T^2} = X + \nabla^2$$

Again by squaring both sides

$$4v^2(1-X) = \frac{X^2 Y_T^4}{(1-x-Y,)^2\ 2} + \nabla^2 + \frac{2\nabla^2 + Y_T^2}{1 - X - Y_T^2} \tag{3.48}$$

Since $Y_T < 1$, the term containing Y_T^4 may be neglected

$$\therefore\ 4\nabla^2(1-X)\ (1-X-Y_T^2) = V^4(1-X-Y_T^2) + 2v^2\ XY_T^2 \tag{3.49}$$

By simplification, this can be written as a quadratic function in X

$$4X^2 - X(8-2Y_T^2-\nabla^2) + (1-Y_T^2)\ (4-\nabla^2) = 0 \quad . \tag{3.50}$$

Therefore

$$X = \frac{(8-2Y_T^2-\nabla^2) \pm \sqrt{(8-2Y_T^2-\nabla^2)^2 - 16\ (1-Y_T^2)\ (4-V2)}}{8}$$

$$X = (1 - \tfrac{1}{4} Y_T^2 - \tfrac{1}{8} \nabla^2) \left\{ 1 \pm \left[1 - \frac{16\ (1-Y_T^2)\ (4-V2)}{(8-2Y_T^2-\nabla^2)^2} \right] \right\}^{1/2} . \tag{3.51}$$

From Equation (3.44) we have

$$\nabla = (\mu_o - \mu_x) = \frac{\lambda_o}{\pi} \cdot \frac{d\phi}{dt} / \frac{ds}{dt} \quad . \tag{3.52}$$

From the rocket trajectory, $\frac{ds}{dt}$ may be expressed as

$$\frac{ds}{dt} = V_Z \text{ cosec } \theta \tag{3.53}$$

where V_Z is the velocity of the rocket in the Z-direction and θ is the elevation angle. Therefore

$$\nabla = (\mu_o - \mu_x) = \frac{\lambda_o}{\pi V_Z \operatorname{cosec} \theta} \cdot \frac{d\phi}{dt} \quad . \tag{3.54}$$

So using this value of V in Equation (3.51) and since X is defined as equal to $\frac{Ne^2}{\varepsilon_o m\omega^2}$, the electron density N can be computed as a function of altitude.

3.5 Electron Collision Frequency from Differential Absorption

Differential absorption has been defined as the difference in absorption between the two propagated waves, namely the ordinary and extraordinary, and is expressed in nepers by,

$$\ln A = \frac{2\pi}{\lambda_o} \int_o^Z (\chi_x - \chi_o)\, dS \tag{3.55}$$

where χ_x and χ_o are given by Equation (3.42) and (3.36). The rate of change of differential absorption is thus given as

$$\frac{d(DA)}{dt} = \frac{2\pi}{\lambda_o} \cdot (\chi_x - \chi_o) \frac{ds}{dt}$$

$$\frac{d(DA)}{dt} = \frac{2\pi V_Z \operatorname{cosec} \theta}{\lambda_o} \cdot (\chi_x - \chi_o) \quad . \tag{3.56}$$

From Equations (3.42) and (3.36) it can be written that

$$X_x - X_o = \frac{\frac{1}{2} XZ \left\{(1 - X)^2 + Z^2 + Y_T^2\right\}}{(1 - X - Z^2 - Y_T^2)^2 + Z^2 (2 - X)^2} \Bigg/ \left\{1 - \frac{X(1 - X)(1 - X - Z^2 - Y_T^2) + XZ2 (2 - X)}{(1 - X - Z2 - Y_T^2)^2 + Z2 (2 - Y)^2}\right\}^{1/2} - \frac{\frac{1}{2} XZ}{\left[(1 + Z^2)(1 - X + Z^2)\right]^{1/2}} . \tag{3.57}$$

Since above 75 km, $Z << 1$, the terms containing Z^2 may be neglected, so that the above equation becomes

$$X_x - X_o = \frac{1}{2} XZ \left\{ \frac{\left\{(1 - X)^2 + Y_T^2\right\}}{(1 - X - Y_T^2)^2} \Bigg/ \left[1 - \frac{X (1 - X)}{(1 - X - Y_T^2}\right]^{1/2} - \frac{1}{(1 - X)^{1/2}} \right\} . \tag{3.58}$$

Now X which is a function of the electron density (N) is obtained from the phase difference measurements and the rate of differential absorption can be computed from the obtained differential absorption data as a function of altitude. So using these values in Equation (3.58), Z, which is a function of collision frequency, $\nu(Z = \frac{\nu}{\omega})$, is obtained at different altitudes,

3.6 Standing Wave Analysis

The phase difference and differential absorption measurements can only be obtained below the extraordinary reflection height. Thus these methods are only useful in obtaining the electron densities up to this point, though usually the rocket goes much further than this altitude. The ordinary wave which is reflected above the extraordinary reflection point at X = 1, interferes with the oncoming ordinary wave and forms a standing wave pattern. From a careful analysis of this standing wave pattern, it is possible to obtain the ordinary phase refractive

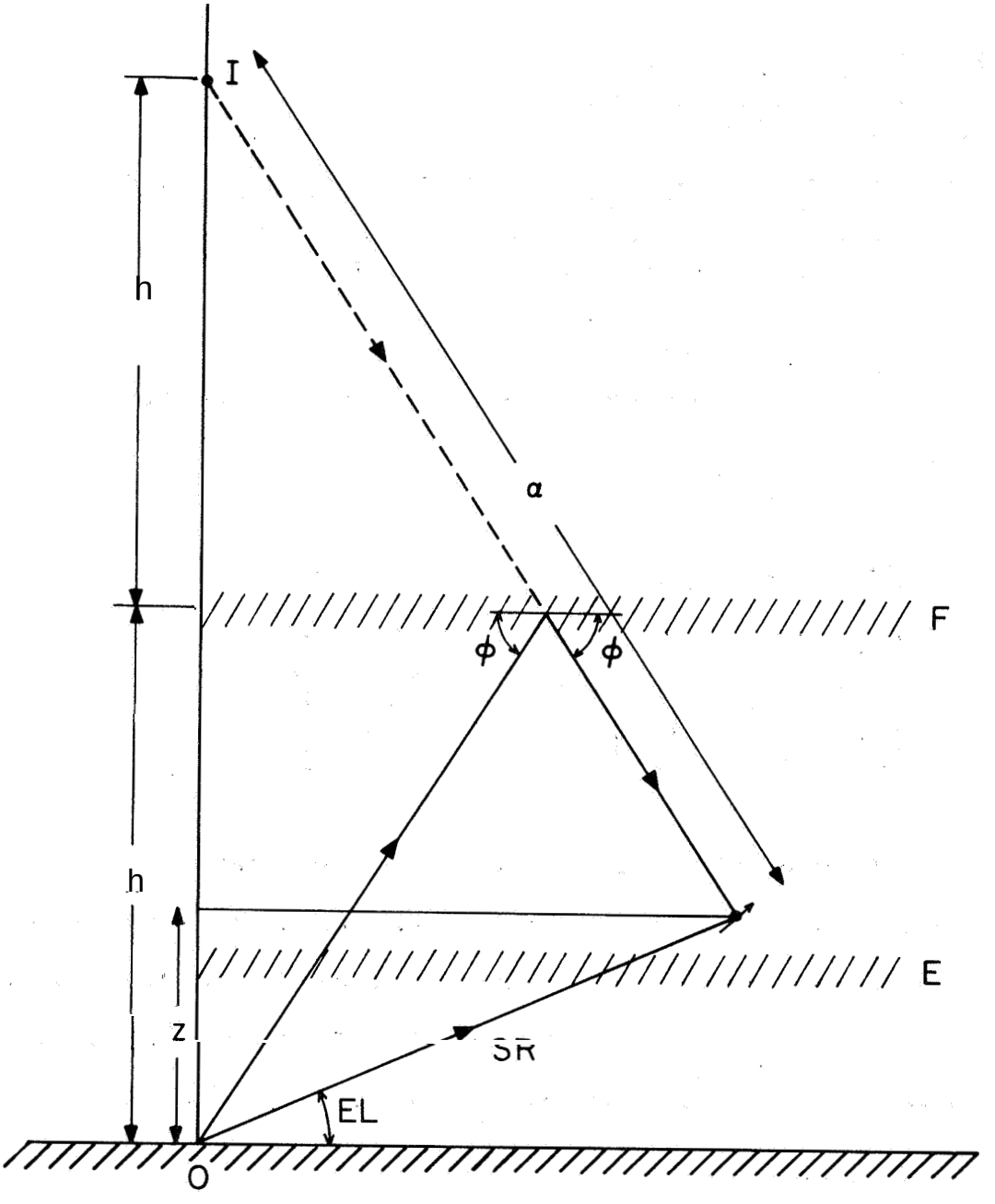

Figure 3.1 Geometry for the computation of path difference from rocket trajectory (after Salah and Bowhill, 1966).

index, and therefore the electron density, Firstly an isotropic, horizontally stratified medium is assumed and the effect of the curvature of the earth is neglected. Figure 3.1 shows the geometry of the direct and reflected waves interfering at the rocket. The ordinary reflection height depends on the operating frequency and the ionospheric conditions. For most of the shots this reflection height was in the F-region.

Since the wave is reflected at an angle equal to the incidence angle, the reflected wave may be assumed to have originated at a mirror point I at an altitude of 2h. Then by cosine law,

$$\alpha^2 = 4h^2 + (SR)^2 - 4h(SR)\ \mathrm{Sin}\ (EL) \tag{3.59}$$

where SR and EL are the slant range and elevation angle of the rocket respectively and are given by the radar trajectory. Now the rate of change of path difference between the direct and reflected waves is given as

$$\frac{d(\text{path difference})}{dt} = \frac{d(SR) - d\alpha}{dt} \tag{3.60}$$

By differentiating Equation (3.59) with respect to time it may be written

$$\frac{d(SR) - d\alpha}{dt} = \left[\left\{ 1 + \frac{2h}{\alpha} \sin (EL) \right\} - \frac{SR}{\alpha} \right] \frac{dSR}{dt} , \tag{3.61}$$

So the number of cycles per second of the standing wave pattern is given as

$$\text{No. of cycles per second} = \frac{d(\text{path difference})}{dt} \Big/ \lambda_o \tag{3.62}$$

where λ_o is the wavelength of the radio wave, Now the ratio of actual to geometric (calculated from the above equation) cycles per second gives the ordinary phase refractive index μ_o. However μ_o is a function of X as given by equation (3.35) as

$$\mu_o = \left\{ 1 - \frac{X}{1 + Z^2} \right\}^{1/2} . \tag{3.63}$$

Since $Z << 1$, Z^2 can be neglected in the above equation and can be written as

$$X = (1 - \mu_o^2) = \frac{Ne^2}{\varepsilon_o m} \cdot \frac{1}{\omega} \tag{3.64}$$

$$N = 1.24 \times 10\text{-}8 \; f2 \; (1 - \mu_o^2) \tag{3.65}$$

where f is the operating frequency given in MHz so by counting the number of cycles per second of the standing wave pattern, it is possible to obtain the electron densities.

3.7 Summary and Discussion

Out of the three methods of obtaining the electron densities as described earlier, the Faraday rotation method is the most accurate and unambiguous. This is because it is possible to measure Faraday rotation to an accuracy of 1° and the Faraday rotation is proportional to the electron density. By utilizing both the Faraday rotation and differential absorption measurements, the collision frequency model can be obtained. The accuracy of the collision frequency measurements thus depends on the accuracy of the differential absorption measurements. Above the extraordinary reflection point, the standing wave analysis is the only way of obtaining the electron densities. The accuracy of measurement of electron

densities by this method depends on how accurately one can measure the wavelength of the standing wave pattern.

The fine structure of the electron density profiles is usually provided by the DC probe measurements of electron current. Although the radio propagation measurements of electron densities possess absolute accuracy, yet they lack the good height resolution characteristic of the DC probe. Therefore, by combining both these measurements, a final electron density profile can be obtained which possesses the accuracy of the radio propagation technique and the good height resolution of the DC probe.

4. RESULTS OF AN EQUATORIAL ROCKET RADIO PROPAGATION EXPERIMENT

4.1 Introduction

As part of the United States' program for the International Quiet Sun Years, University of Illinois in cooperation with the GCA Corporation participated in the National Aeronautics and Space Administration Mobile Launch Expedition which was initiated to study the latitude behavior of the lower ionosphere during the IQSY. Five rockets were launched in March and April 1965 from the aircraft carrier USNS Croatan in a latitude zone ranging from the equator to 60°S along the west coast of South America. This was the first of the rocket series, launched close to magnetic equator (Lat. 12' 00'S; 78° 00'W) on March 20, 1965 at 0820:09 EST, which corresponds to a solar zenith angle of 59'. The payload carried various experiments, two of which measured the electron density: a radio propagation experiment from the University of Illinois and a DC probe instrumented by GCA Corporation. The operating frequency of the propagation experiment was 3.385 MHz. The rocket reached an apogee of 174 km and good data was obtained from all experiments,

The major problem in analyzing this shot was that the receiver output channel was swamped with noise. It has been found that this was due to interference of a broadcasting station which might be operating at the same frequency close to the launch site. The receiver output was very noisy upto T_o + 78 seconds, T_o being the launch time and improved abruptly from that time due to some unknown reason as shown in Figure 4.1.

4.2 Differential Absorption Data

Figure 4.2 shows the variation of extraordinary power with time after launch. The variation is rather erratic, which is understandable in view of the fact that the receiver output is noisy, However, some regular increase is noticed starting

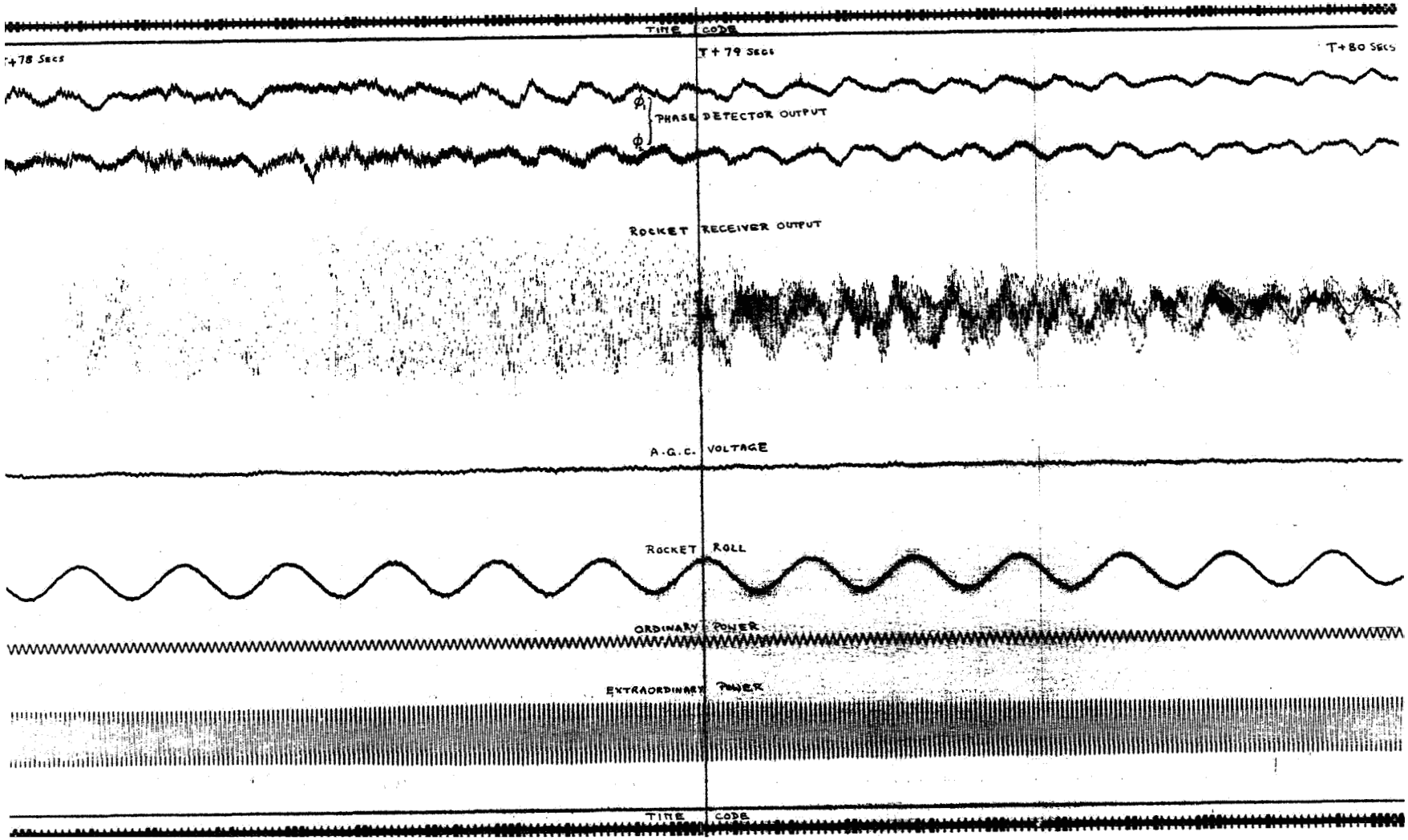

Figure 4.1 Propagation experiment data format

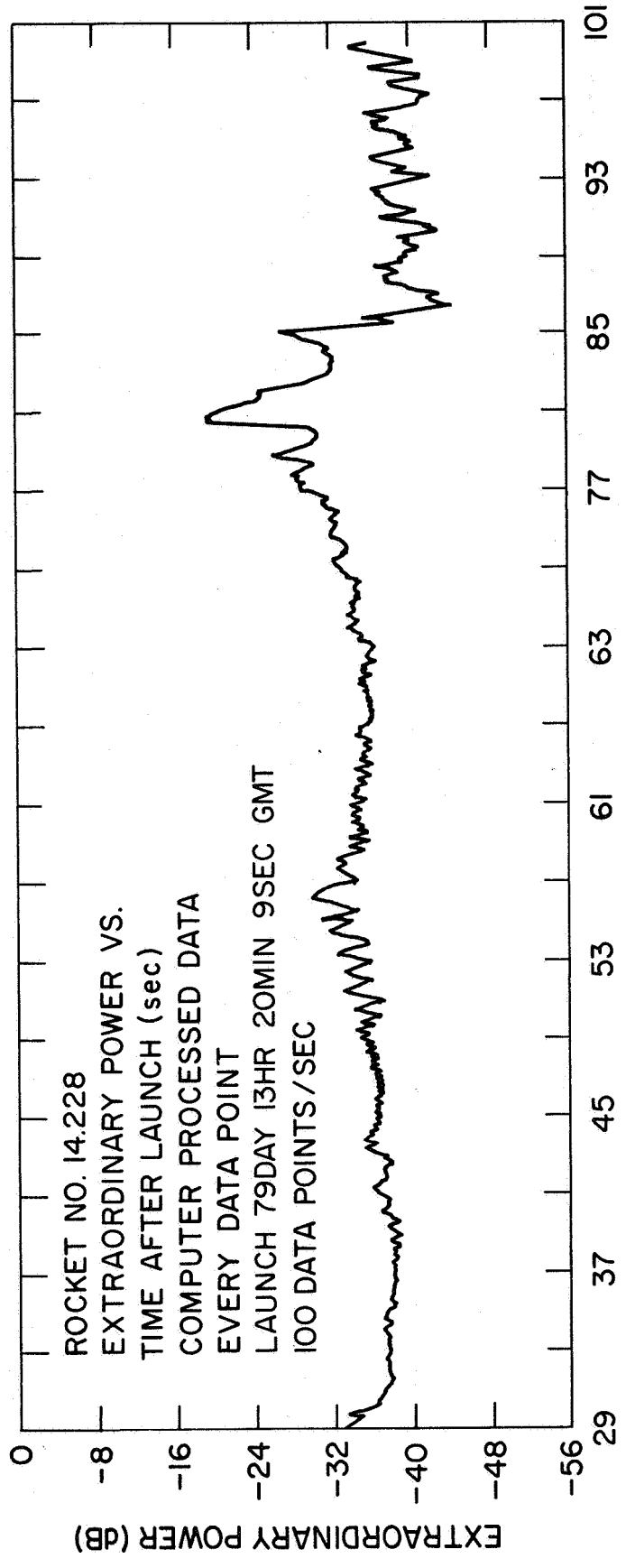

Figure 4.2 Variation of extraordinary power with time after launch

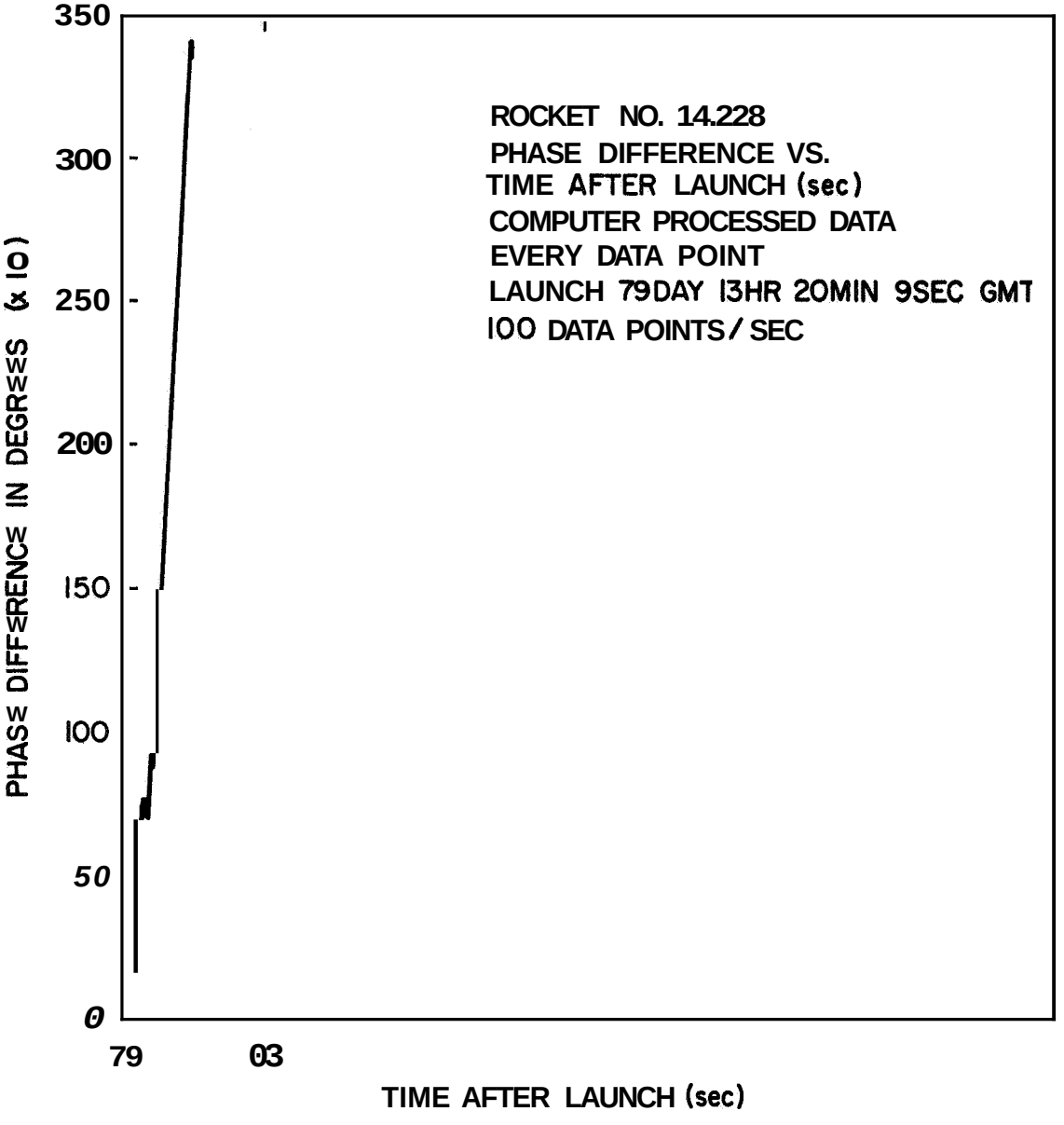

Figure 4.3 The variation of Faraday rotation with time after launch during ascent

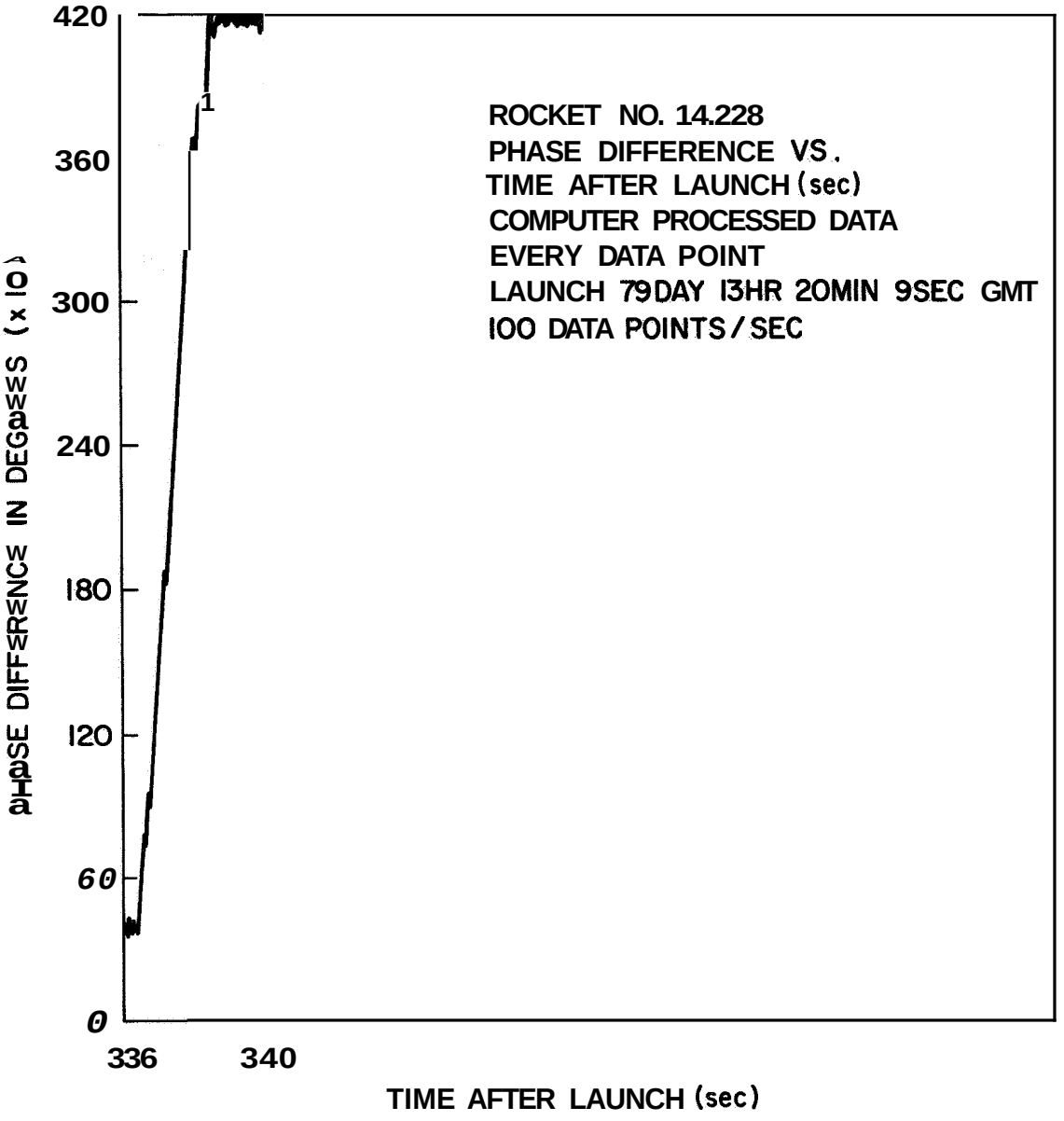

Figure 4.4 The variation of Faraday rotation with time after launch during descent

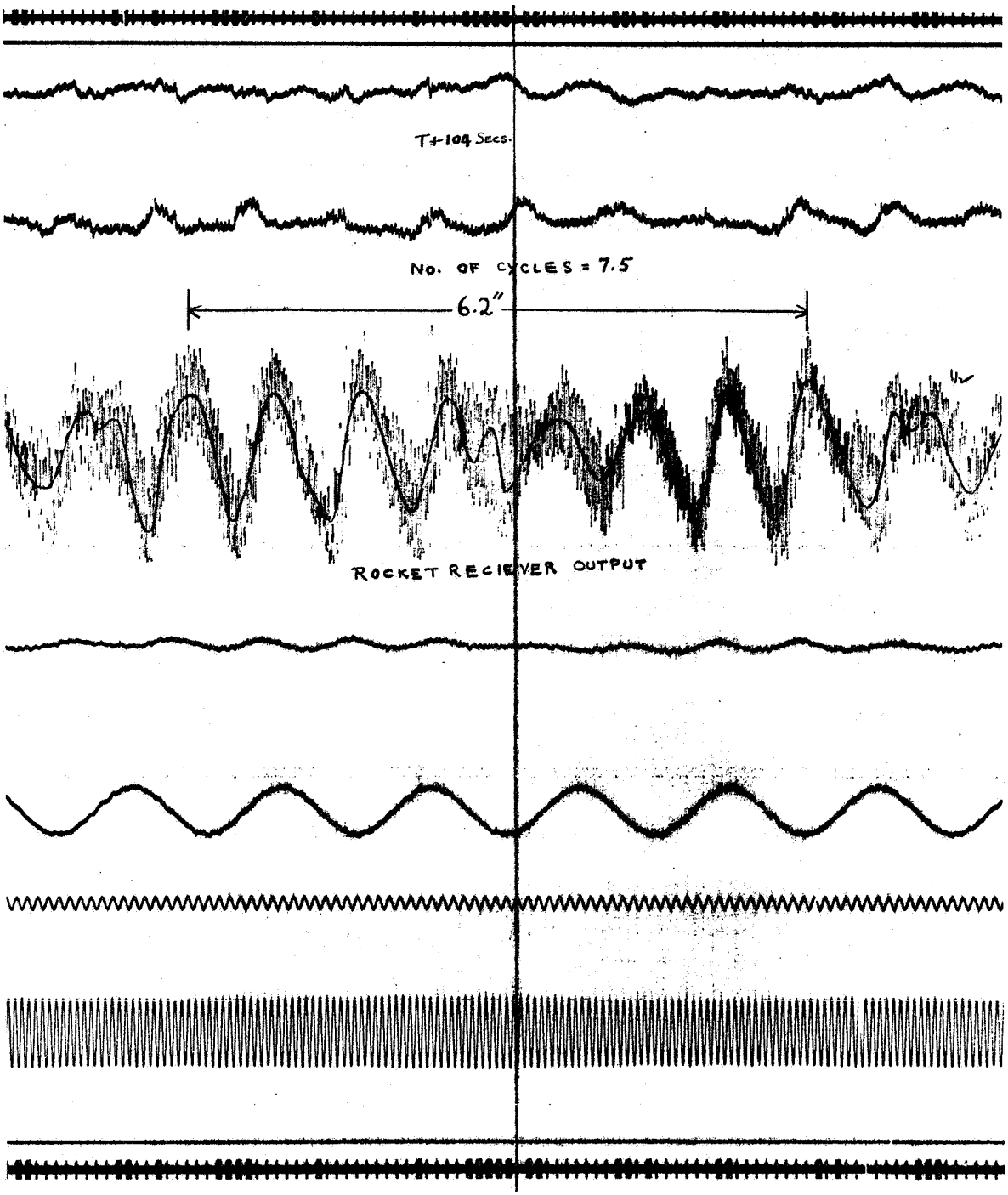

Figure **4.5** Typical standing wave pattern

from 65 sec after launch. The abrupt increase in extraordinary power between 81 and 81.5 sec after launch is due to corresponding increase in the ordinary power and as such it does not denote genuine differential absorption. Since, as already mentioned, the receiver output is noisy, the differential absorption data should be used rather cautiously.

4.3 Phase Difference Data

Due to broadcast interference and the imperfect circularity of the rocket receiving antenna, some difficulty has been encountered in the extraction of the phase difference (P.D.) data from the rocket receiver output. A number of runs have been made with heavy filtering in the receiver output channel and it has been consistently observed that the phase difference did not change much up to 70 sec after launch and then increased suddenly by 2975° in an altitude range of 1.7 km as shown in Figure 4.3. Such an unusually large phase difference within a short time cannot be accounted for by normal ionization. So if this phase difference were to be genuine, some agency other than the normal ionization should have been responsible for this. Now, if the presence of such an agency is assumed to be present at this altitude range, it is reasonable to expect a similar effect during descent also. The rocket data during descent was also processed for phase difference and as shown in Figure 4.4, it is clearly noticed that starting at a height of 95.8 km a rotation of 4320° has taken place within an altitude range of 3.6 km. So it is obvious that this data cannot be used for deducing the electron density profile and the probable reasons for the observed large Faraday rotation will be discussed in a later section.

4.4 Standing Wave Pattern Analysis

A typical standing wave pattern obtained for this shot is shown in Figure 4.5. By measuring the wavelengths of these standing waves, the observed numbers

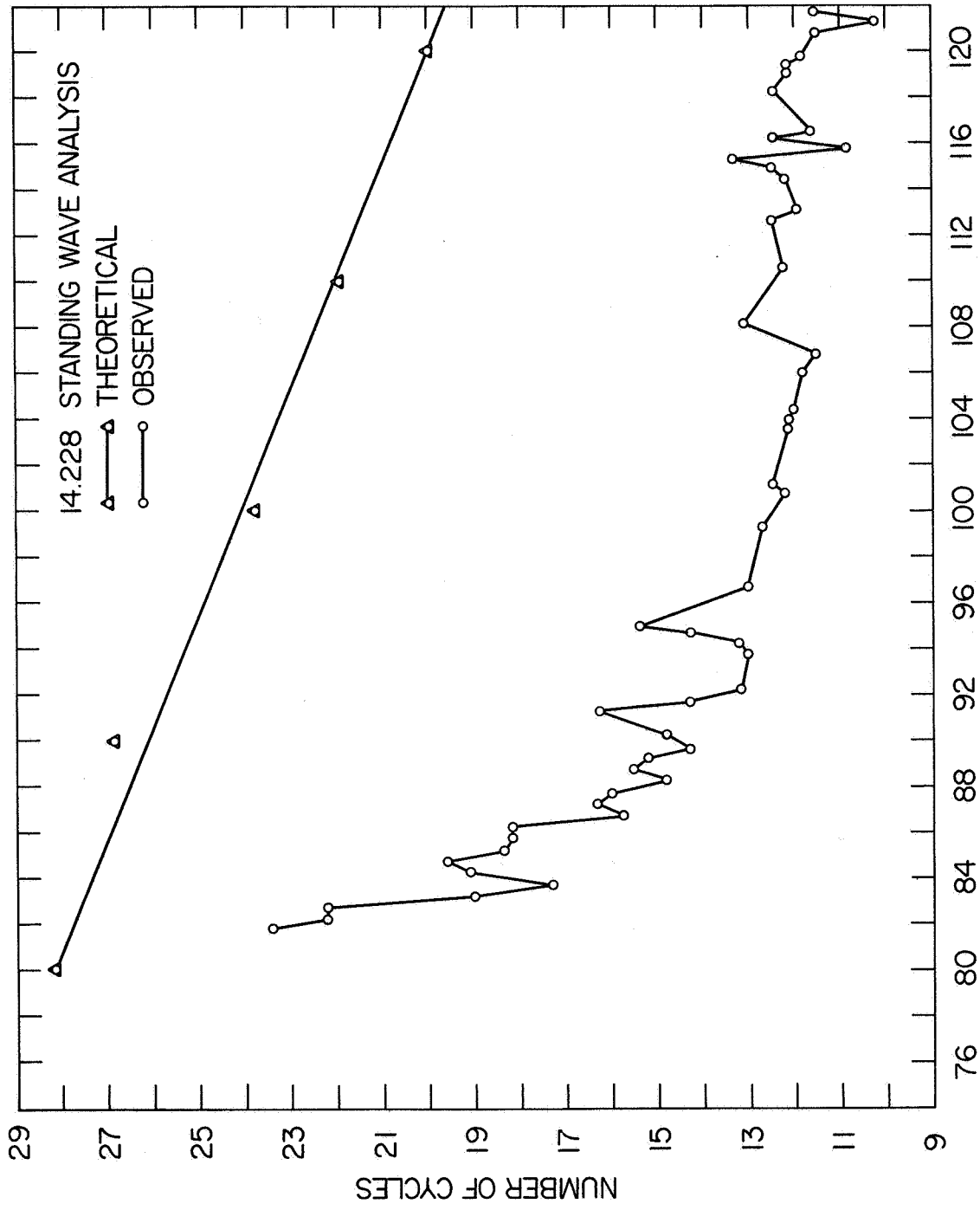

Figure 4.6 Observed and theoretical number of cycles of the standing wave pattern

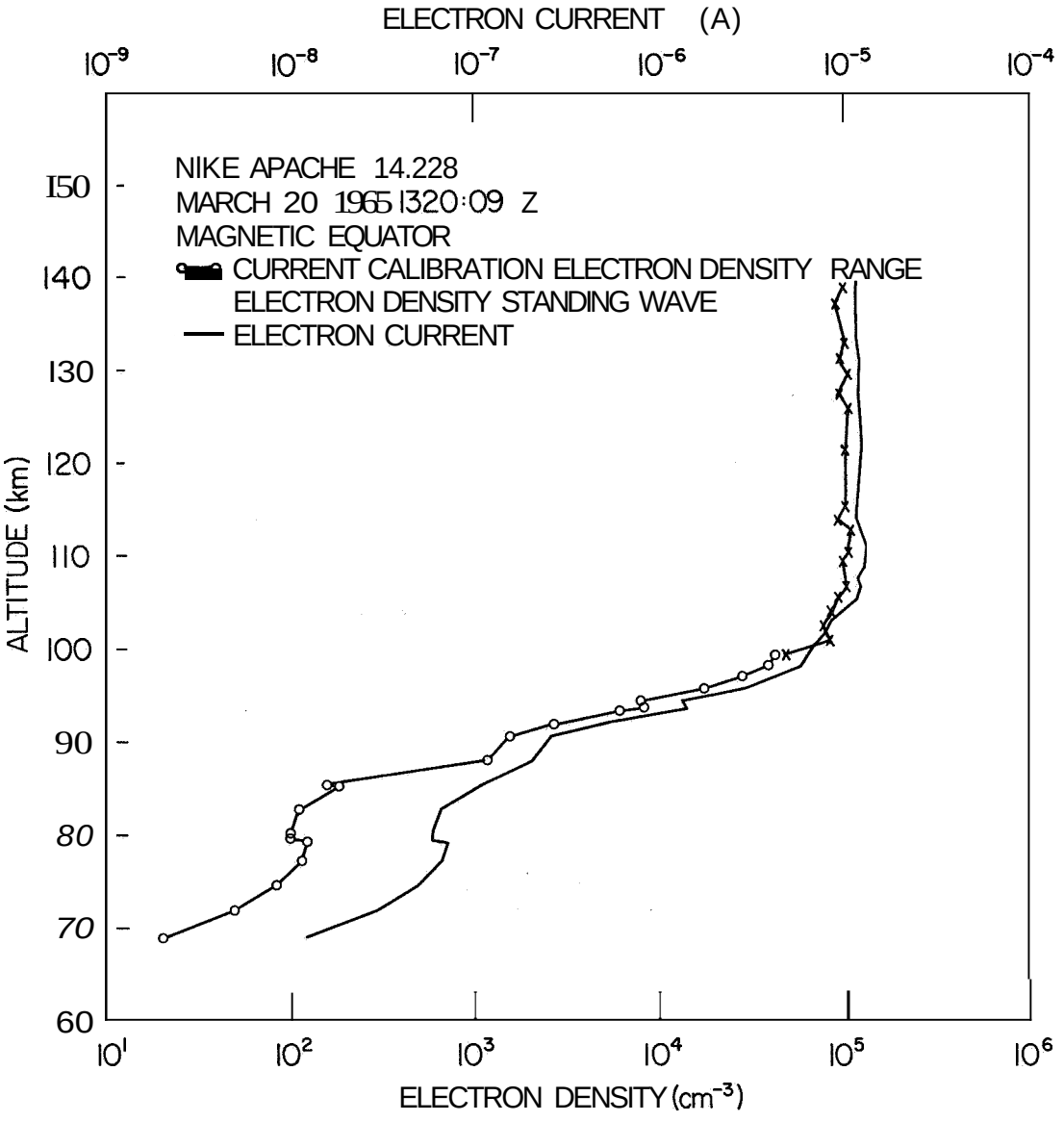

Figure 4.7 The electron density profile obtained from the equatorial experiment

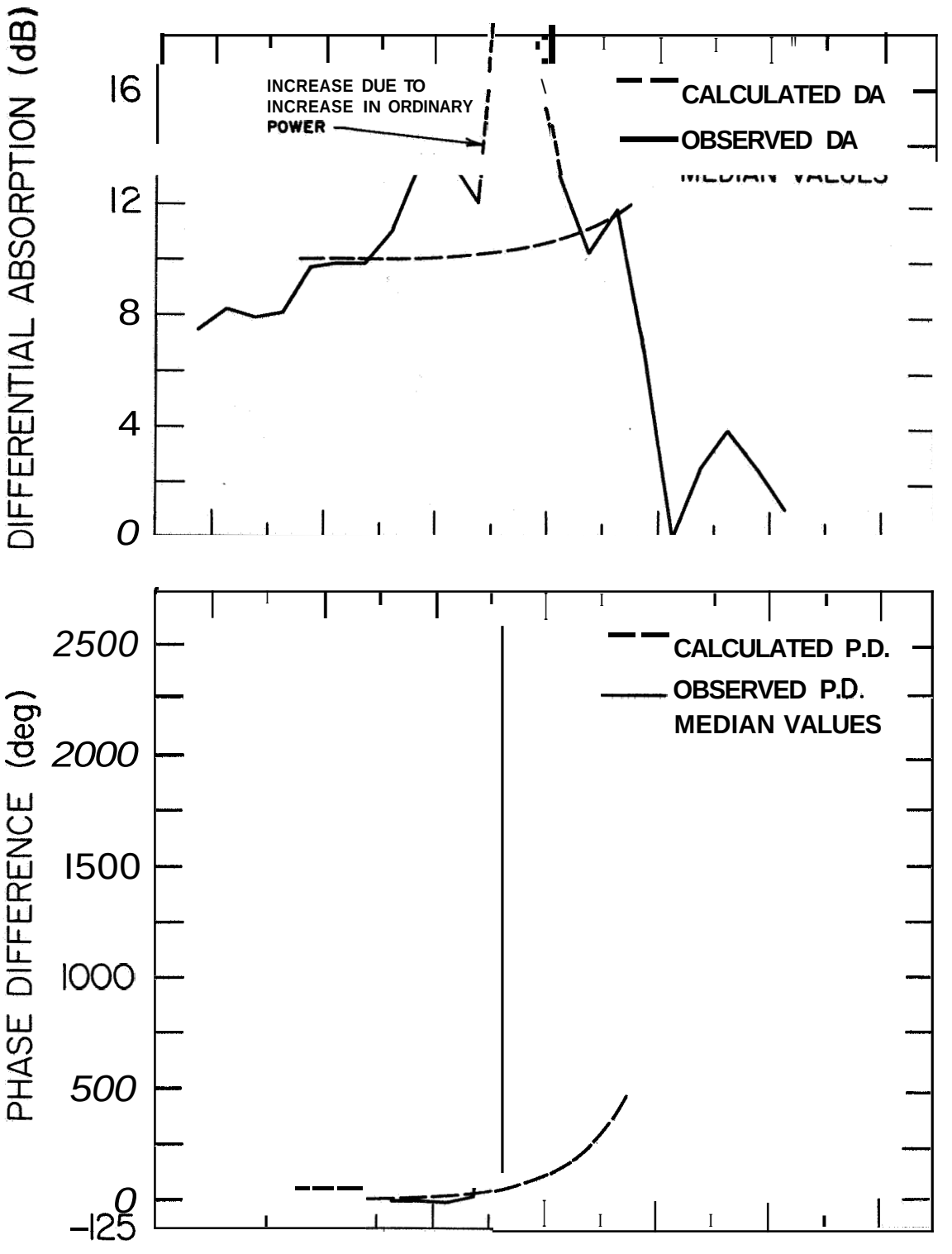

Figure 4.8 Comparison between the observed and expected values of Faraday rotation and differential absorption

of cycles per second are computed for different times. Using the trajectory data and Equation (3.62) of the previous chapter, the number of cycles that should be observed at different time intervals are calculated theoretically. In Figure 4.6 are plotted the observed number of cycles and the number calculated theoretically on the basis of free space propagation. The ratio between these parameters gives the refractive index μ; from which the electron density can be calculated using the equation

$$N = 1.24 \times 10^{-8} f^2 (1 - \mu^2) \qquad (4.1)$$

where f is the operating frequency in Hz. From this method the electron density profile is obtained in the region 98-138 km. It has been noticed from other shots where good differential absorption and Faraday rotation data were obtained, that the ratio N/I of the electron density to the electron current does not change considerably from one shot to another. As such the N/I profile from another shot (14.230) which was launched at about 16° magnetic latitude from the Carrier is used and using the probe current obtained by the DC probe for the equatorial shot, the electron density profile has been extended below 98 km (Figure 4.7).

4.5 Discussion

To explore the reason for the anomalous phase difference and absorption data observed, the electron density profile of Figure 4.7 was used, assuming a standard collision frequency model, to determine the differential absorption and phase difference values, using the Sen-Wyller (1960) theory. In Figure 4.8 these are compared with the observed values and the most striking discrepancy is noticed in the case of Faraday rotation data. So if this Faraday rotation was to be

genuine, some agency other than the normal ionization should have been responsible for this, Now it is a well known fact that close to the magnetic equator, there is a strong current system present at E-region heights which is usually referred to as "electrojet". The fact that similar large phase difference is also observed during descent in approximately the same altitude region, seems to substantiate the point that the "electrojet" might have been responsible for the observed large Faraday rotation values.

There are two possible ways of conceiving how the electrojet could possibly cause a large rate of change of phase difference:

(1) Kerr Effect: electromagnetic waves passing through a medium normal to the electric lines of force are split into two linearly polarized waves traveling with the velocities $\frac{C}{n_o}$ and $\frac{C}{n_e}$ respectively, where c is the velocity of light and with the electric vector vibrating perpendicular and parallel to the lines of force. The difference in propagation velocity causes a phase difference δ between the two waves which, for a radiation of wavelength λ_o, is $\delta = (n_e - n_o)X/\lambda_o$ where X is the length of the radiation path in the medium, Kerr found empirically that $(n_e - n_o) = \lambda_o BE^2$ where E is the electric field strength and B a constant characteristic of the material called the "Kerr constant".

(2) It is well known that the Faraday rotation of radio signals passing through an ionized medium is proportional to $B_L \times N_T$ where B_L is the magnetic field in the direction of propagation and N_T is the electron content in the medium. So changes in the magnitude or direction of magnetic field (B_L) could cause changes in the relative phase,

However by approximate calculations, it is realized that the observed large phase variations could not have been caused by either of these two processes

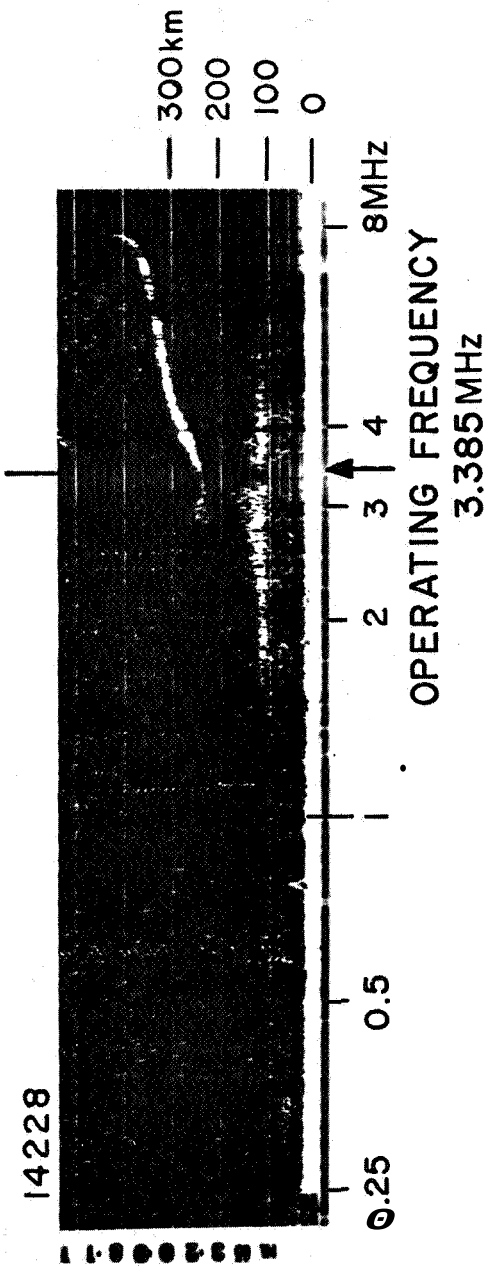

Figure 4.9 Ionogram corresponding to the time of rocket launching

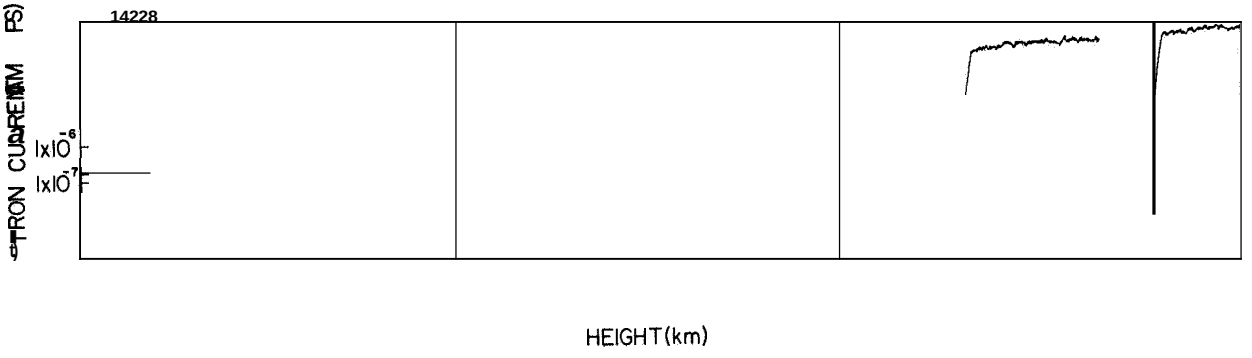

Figure 4.10 Detailed variation of electron current with altitude showing small scale structure

mentioned above. Therefore this phase difference might be either due to changes in the modes of propagation at these altitudes or might be due to imperfect polarization adjustments.

4.6 Results

In Figure 4.9 the ionogram taken close to the launch time for this shot is presented. In this ionogram, the presence of equatorial Es is clearly seen and this is usually classified as q-type Es denoted by Es-q. According to Piggott and Rawer (1961), Es-q is defined as an Es trace which is diffuse and non-blanketing over'a wide frequency range. The spread is most pronounced at the upper edge of the trace. (This type is common in daytime in the vicinity of the magnetic equator). The top frequency of the Es trace (fEs-q) is about 4.7 MHz which should correspond to an ionization of $N = 1.24 \times (fEs\text{-}q)^2 \times 10^4$ i.e. 2.74×10^5 electrons/cm^3; but no such extra ionization is seen in the electron density profile in the height range around 110 km where the Es-q is observed in the ionogram. This indicates that the equatorial Es might be only a manifestation of the electrojet, which is present at these heights. The ionization in this profile at 110 km corresponds very well to the critical frequency of the normal E-region (2.8 MHz).

It has been suggested and there is reason to believe that (Bowhill, 1966) the diffuse nonblanketing Es might be due *to* scattering of radio waves from small scale irregularities present at E-region altitudes. For this reason, the DC probe current is recorded on an expanded scale as shown in Figure 4.10 in order to investigate the presence of any irregularities. Indeed the existence of such irregularities is clearly noticed in the altitude region of 90-100 km. They have a spatial period of 80 meters and an amplitude of about 10%of the local plasma density.

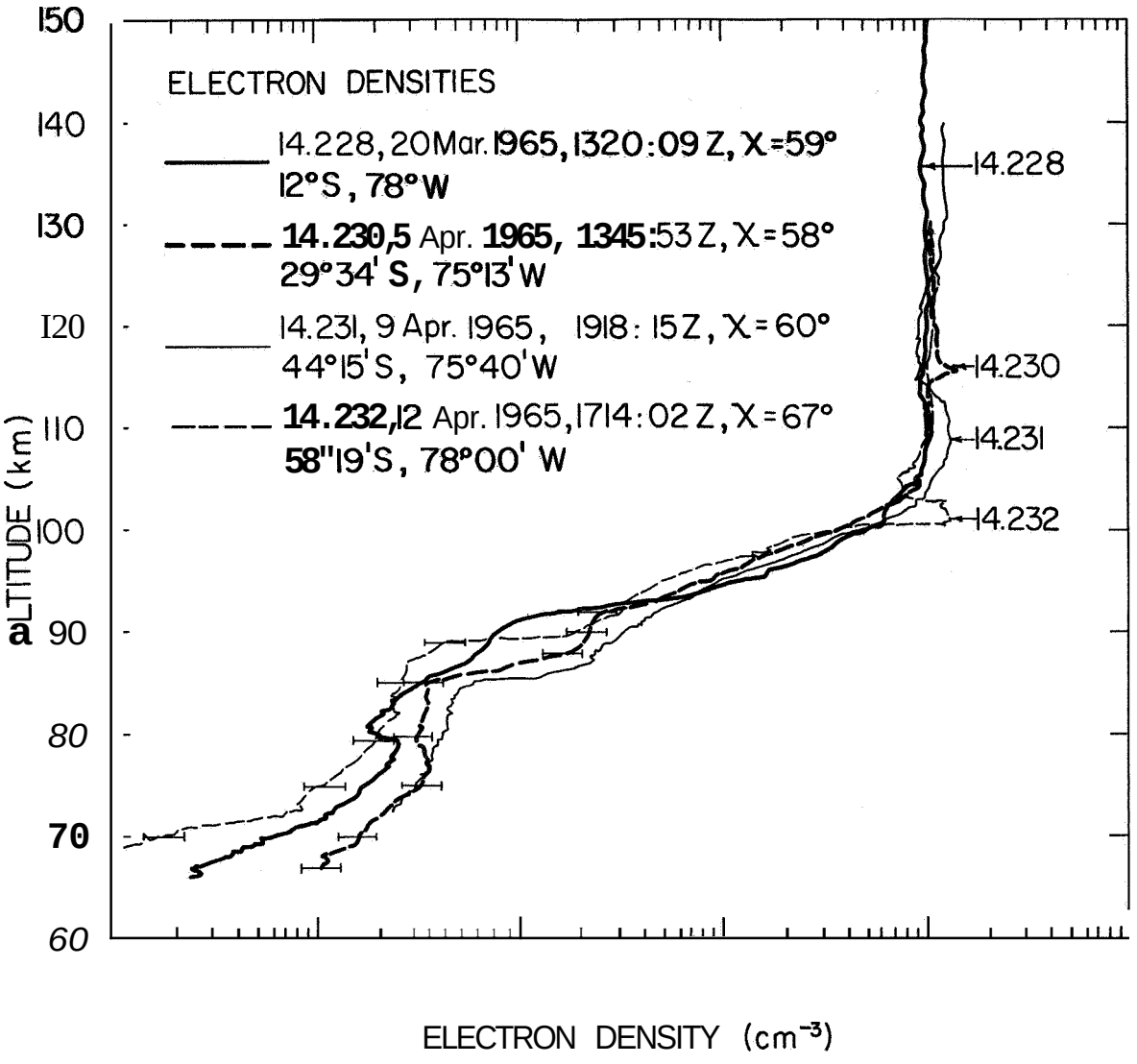

Figure 4.11 The electron density profiles at various latitudes for the same solar zenith angle

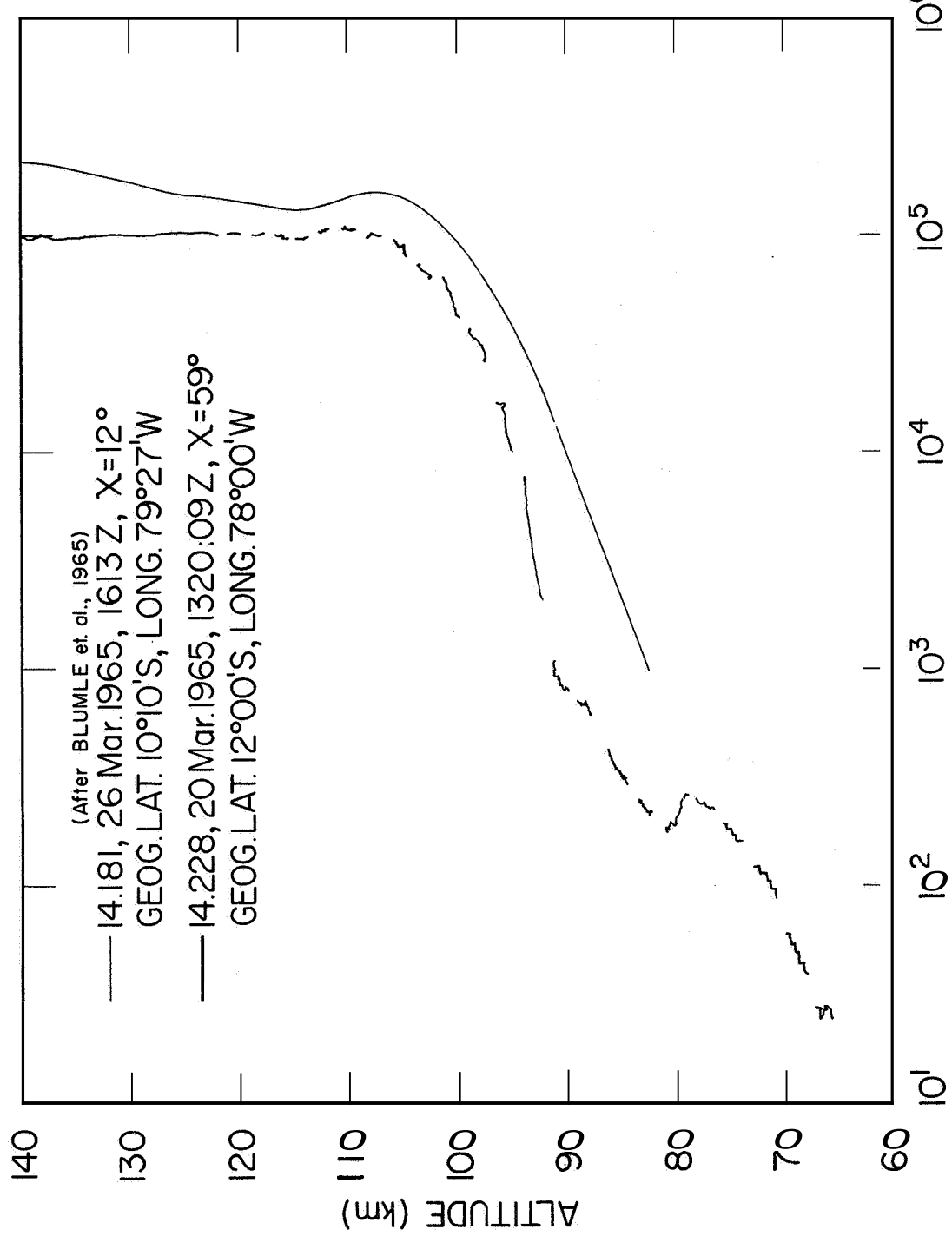

Figure 4 12 Comparison of electron density profiles near the vicinity of magnetic equator for different solar zenith angles

This launching close to the magnetic equator (14.228) has been one of the series of launchings from an aircraft carrier USNS Croatan as a part of the NASA Mobile Launch Expedition. These rockets were launched at every 16° latitude starting from the magnetic equator. All the rockets were launched at the same solar zenith angle of 60° in order to eliminate diurnal changes so that the latitude variation of the lower ionosphere can be studied. The operating frequency of the propagation experiment was 3.385 MHz for all the launchings. In Figure 4.11, the electron density profiles obtained during the carrier shots (including the equatorial launching) are presented for comparison, At a first glance, it is interesting to note the remarkable similarity between the profile obtained at various latitudes for the same solar zenith angle of 60". A further examination reveals that there is some latitude variation in the D-region rather than in the E-region. Chilton and Radicella (1965) have shown that there are basic differences between transequatorial and middle latitude VLF propagation characteristics. They suggest that these might be due to latitudinal variation in the daytime electron density gradient. From Figure 4.11 it can be easily noticed that the electron density gradient in the 90-100 km region is greater for the equatorial shot when compared to other profiles.

Blumle, et al., (1965) using a two frequency radio propagation experiment have obtained the electron density profile of the lower ionosphere in the vicinity of the magnetic equator at a solar zenith angle of 12°. This is compared in Figure 4.12 with the profile obtained from the equatorial shot (14.228) at the solar zenith angle of 60°. It is well known that electron density at a given altitude in the D- and E-regions is a function of $(\cos \chi)^n$ where n is a constant and χ is the solar zenith angle. From the simple Chapman theory, n is 0.5 at the altitude of maximum electron density in the E-region. However in the case of total nondeviative absorption, which is proportional to $\int N\nu dh$, n has a value

of 0.75. From a study of the diurnal variation of absorption, using ground-based experimental measurements in the equatorial zone (Skinner, 1965), n is found to vary between 0.62 and 0.90. This indicates that n might be different for different altitudes. To investigate the variation of n with altitude, the two profiles (Figure 4.12) obtained at approximately the same geographic location for different solar zenith angles of 60° and 12° are utilized. Using the equation $N_1/N_2 = (\cos \chi_1/\cos \chi_2)^n$, n is computed for various altitudes. χ_1 and χ_2 are the solar zenith angles as given above and N_1 and N_2 are the corresponding electron densities. From this it is noticed that n has a value of about 3 at 80 km and decreases steadily with increase of altitude, stabilizing to a value of 0.7 in the E-region, Since the ground-based absorption measurements give a value close to 0.7, it tends to suggest that major part of the absorption takes place close to the E-region.

5. PROBLEMS IN THE APPLICATION OF PROPAGATION EXPERIMENT FOR THE STUDIES OF THE EQUATORIAL IONOSPHERE

5.1 Introduction

The propagation experiment was originally developed for the studies of ionospheric phenomena at middle latitudes such as Wallops Island, Virginia, So before using this technique for the studies of the equatorial ionosphere, it is desirable to examine its applicability in that region. At the equator, since the magnetic field lines are horizontal, the direction of vertical propagation is perpendicular to it and therefore the so-called quasi-transverse (QT) approximation for the Appleton-Hartree equation applies instead of the quasi-longitudinal (QL) approximation; the equations for the Faraday rotation (FR) and differential absorption (DA) are therefore basically different. The expected Faraday rotation and differential absorption values are estimated and compared with middle latitude values for the same ionospheric conditions.

5.2 Comparison of Differential Absorption and Faraday Rotation Values Obtained Under QL and QT Conditions

Starting from the classical Appleton-Hartree formula for the complex refractive index, applying the quasi-longitudinal approximation (see Ratcliffe, 1962) and using certain simplifying assumptions that X and Z are less than 1 and small, the following equations for the differential absorption and Faraday rotation can be obtained.

$$\left.\begin{aligned} &\text{Differential Absorption} \ldots\ldots\ldots \chi_x - \chi_o = \frac{2XZY_L}{(1-Y_L^2)^2} \\ &\text{Faraday Rotation} \ldots\ldots\ldots\ldots\ldots \mu_x - \mu_o = \frac{XY_L}{(1-Y_L^2)} \end{aligned}\right\} \quad \text{QL} \qquad (5.1)$$

Now applying the same simplifying assumptions as before (viz. X and Z << 1) to the equations for the differential absorption and Faraday rotation deduced using the quasi-transverse approximation as in Chapter 3, it can be shown that

$$\left.\begin{aligned} &\text{Differential Absorption} \ldots\ldots \chi_x - \chi_o = \frac{1}{2} XZ \left[\frac{Y^2 (3-Y^2)}{(1-Y^2)^2}\right] \\ &\text{Faraday Rotation} \ldots\ldots\ldots \mu_x - \mu_o = \frac{\frac{1}{2} XY^2}{(1-Y^2)} \end{aligned}\right\} \text{QT} \qquad (5.2)$$

By taking the ratios and putting $Y_L = 0.44$ and $Y = 0.23$, typical values for an operating frequency of 3.385 MHz, it can be shown that

$$\frac{\text{D.A. for Q.L.}}{\text{D.A. for Q.T.}} = \frac{4Y_L (1-Y^2)^2}{(1-Y_L^2)^2 Y^2 (3-Y^2)} \simeq 15.60 \quad , \qquad (5.3)$$

Similarly,

$$\frac{\text{F.R. for Q.L.}}{\text{F.R. for Q.T.}} = \frac{2Y_L (1-Y^2)}{(1-Y_L^2) Y^2} \simeq 19.63 \quad . \qquad (5.4)$$

Equations (5.3) and (5.4) show that with the same ionospheric conditions and with the same operating frequency, the differential absorption and Faraday rotation values observed near the equator (where the quasi-transverse approximation holds) are much smaller than those observed at high latitudes (where the quasi-longitudinal approximation holds).

One way to increase the differential absorption and Faraday rotation at the magnetic equator is to decrease the operating frequency. However this introduces additional problems such as:

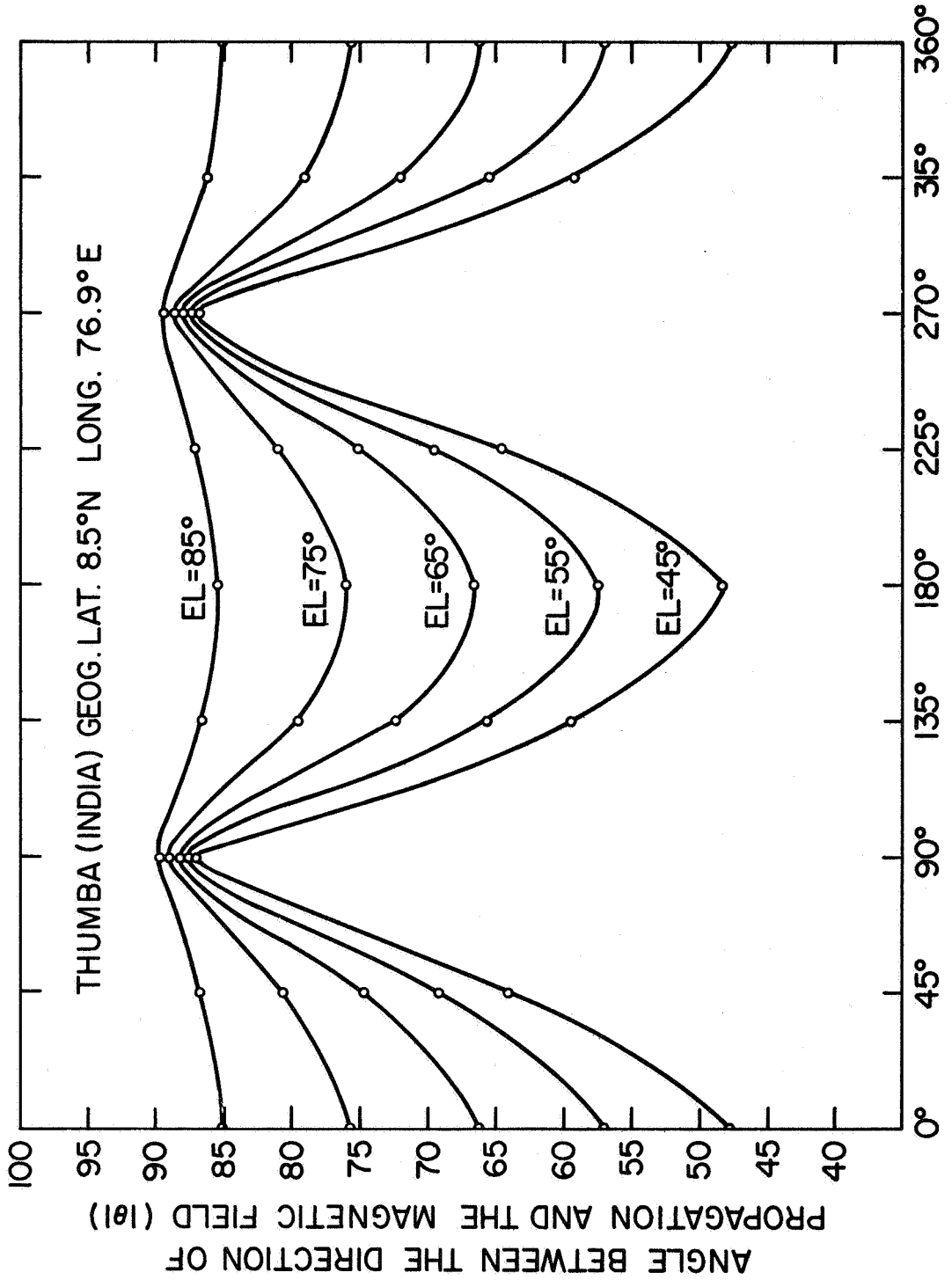

Figure 5.1 Variation of the angle (θ) between the direction of propagation and the magnetic field lines with the launch characteristics of the rocket

(1) If the operating frequency is lower than the normal E-region critical frequency, it will only be possible to obtain the electron density profile up to E-region heights,

(2) If the extraordinary reflection point is below the electrojet region, there will be no way of studying the equatorial Es which is one of the major problems at these latitudes; so the D- and E-region measurements become mutually exclusive.

Another possibility is to launch the rocket such that the angle the ray path makes with the magnetic field is sufficient for the quasi-longitudinal approximations to be applied.

5.3 Launching into QL Region from an Equatorial Launch Site

The location of the equatorial launch site at Thumba, India (Geog. Lat. 8.5°N; Long, 76.9°E) is about 35 km south of the magnetic equator. Since the angle (θ) between the direction of propagation and the magnetic field lines determines which approximation holds, θ is computed for various elevation and azimuth angles. All these computations pertain to an altitude of 100 km and the variation of θ with azimuth angle for various elevation angles ranging from 45° to 85° is shown in Figure 5.1. It can be noticed from this figure that θ varies from about 45° to 88° depending on the launch characteristics.

As discussed earlier in Chapter 3, the conditions for the two approximations can be written as:

$$Y^2 f^2(\theta) \lll (1-X)^2 + Z^2 \qquad (5.5)$$

where

$$f(\theta) = \frac{1}{2} \sin^2\theta/\cos\theta \qquad (5.6)$$

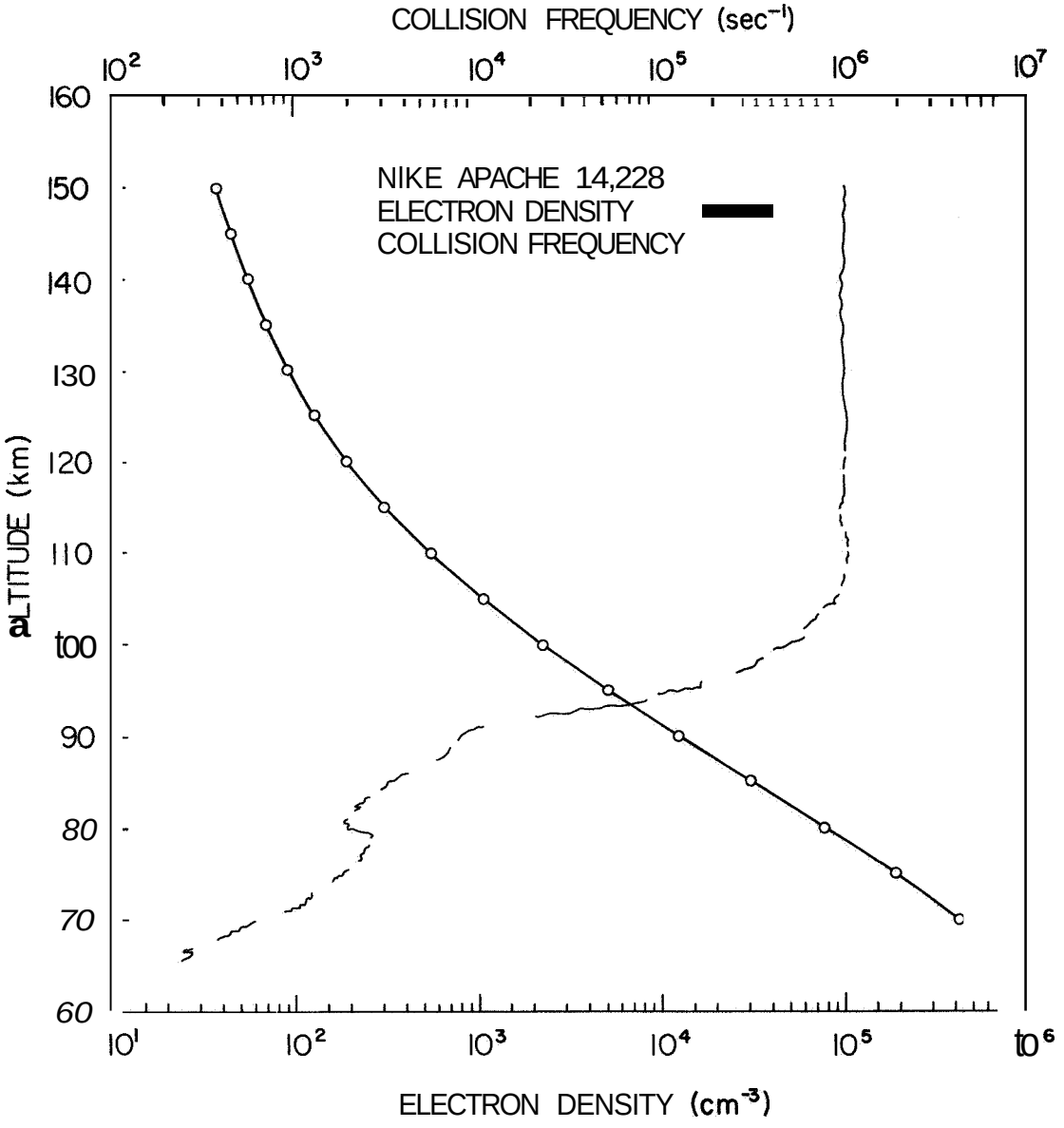

Figure 5.2 The electron density and electron collision frequency profiles utilized for the investigation

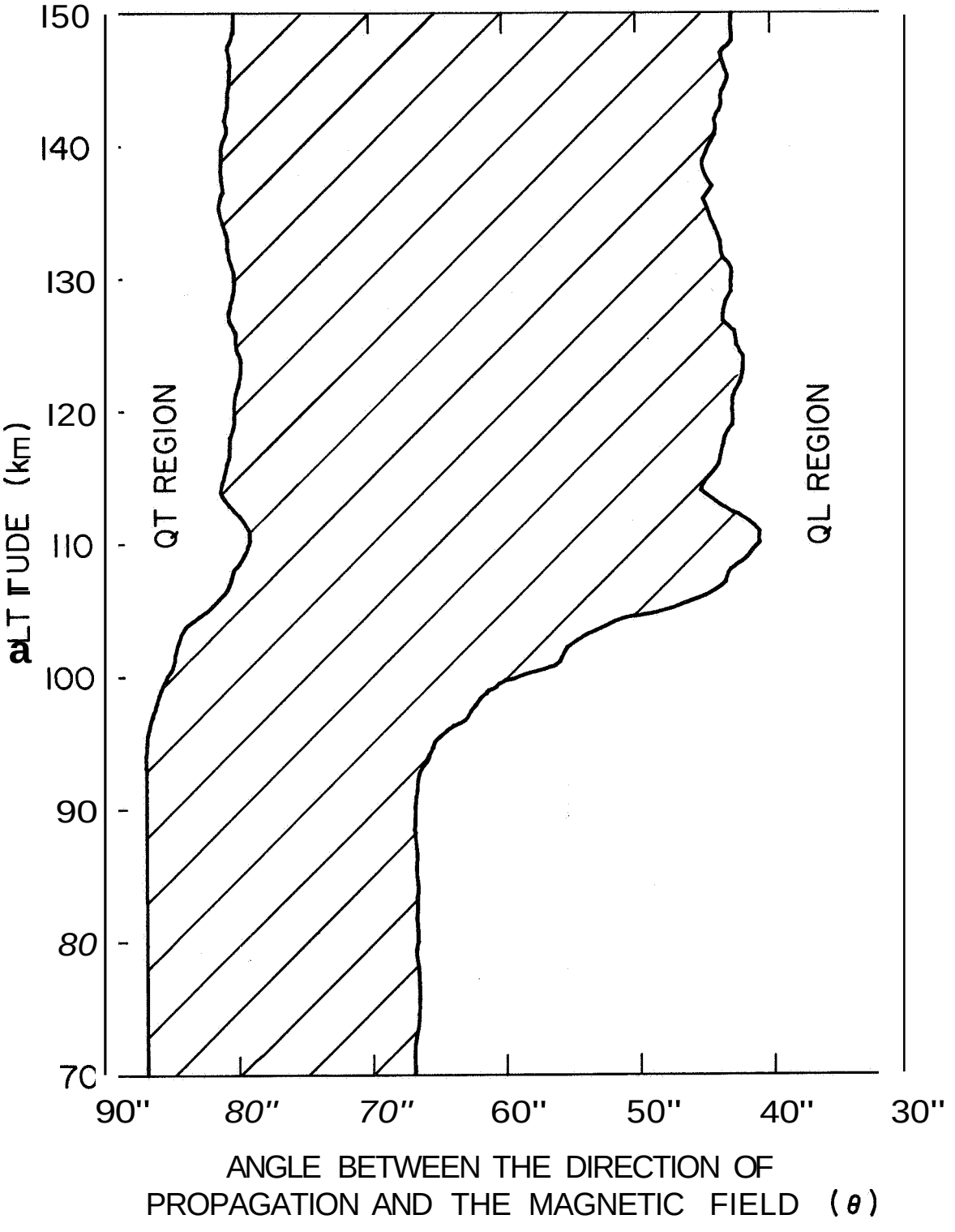

Figure 5.3 The regions wherein the quasi-longitudinal and quasi-transverse approximations hold

when numerical cases are considered it is a reasonably good approximation to assume that the inequality is satisfied, if the large quantity is nine times the smaller so that

$$\left.\begin{aligned} f(\theta) &> \tfrac{3}{4}\,(1-X)^2 + Z^2 \qquad \text{for QT} \\ f(\theta) &< \tfrac{3}{4}\,(1-X)^2 + Z^2 \qquad \text{for QL} \end{aligned}\right\} \tag{5.7}$$

From Equation (5.7), in the altitude range where Z is small such that Z^2 can be neglected and when $X = 1 \pm Y_L$, it can be shown that whenever $\theta<40°$ it is safe to assume the quasi-longitudinal approximation and whenever $\theta>68°$ it is safe to assume the quasi-transverse approximation, However at low altitudes, where X is small and Z is significant, the region in which the quasi-transverse approximation holds is considerably less.

So since the regions in which the quasi-longitudinal and quasi-transverse approximations hold vary with altitude, it is necessary to investigate its variation assuming a standard ionosphere. The electron density profile obtained close to the magnetic equator corresponding to a solar zenith angle of 60° and a typical electron collision frequency model ($\nu=1.01 \times 10^8 p$; p being the pressure in mm, Hg according to U.S. Standard Atmosphere, 1962) as shown in Figure 5.2 are assumed for this investigation. For an operating frequency of 3.385 MHz, the quasi-longitudinal and quasi-transverse regions are demarcated as shown in Figure 5.3. Therefore by consulting Figures 5.1 and 5.3 and depending on the experimental requirements, it should be possible to select optimum launch characteristics. The computer program (Fastran language) for this investigation is given in the Appendix, Using this program, it should be possible to carry out this investigation for various ionospheric conditions and for different operating frequencies.

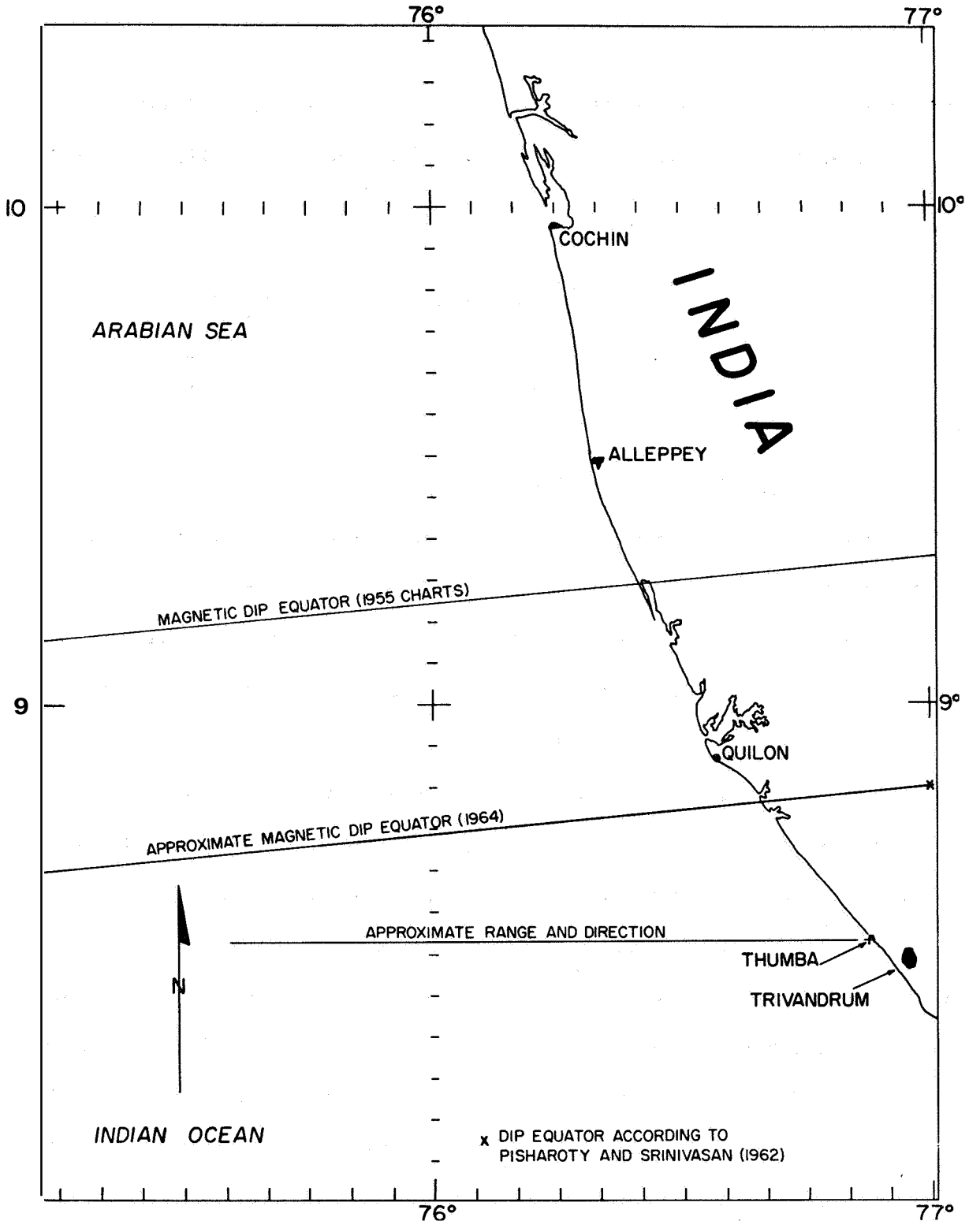

Figure **5.4** Location of Thumba Equatorial Launch site with reference to the magnetic equator

Though by launching the rocket into the quasi-longitudinal region, there will be considerable increase in the DA and FR values, some additional problems would be created by launching the rocket at an oblique angle. In Figure 5.4 is given the Thumba launch site with reference to the magnetic equator. As discussed earlier, for the quasi-longitudinal approximation to hold it is necessary to launch the rocket at an oblique angle in the magnetic meridian (i.e. in the N-S direction). However due to range safety requirements, it is possible only to launch towards south which means that the rocket will be moving away from the center of the electrojet (as it is, the launch site is about 35 km south of the magnetic equator). Moreover since the rocket is moving continuously away from the transmitting antennas, errors would be introduced in the polarization settings of the ordinary and extraordinary waves. Besides, the geometry of the radio wave propagation path from ground to the rocket would be complicated.

5.4 Summary and Discussion

So in view of the above mentioned problems which are quite complicated, it appears better to launch the rocket in the E-W direction (perpendicular to the magnetic meridian) such that the quasi-transverse approximation will hold. For daytime experiments, it may not be possible to decrease the operating frequency from 3.385 MHz without sacrificing the study of the E-region. Therefore, since the order of the differential absorption is known, the piston attenuator controlling the extraordinary transmitter power may be redesigned so that its total range is about 5 dB. Then it might be possible to record small changes in it more accurately. Though the differential absorption is small at the equator, the ordinary wave absorption is almost twice that observed at high latitudes. Using the AGC of the rocket receiver, it should also prove possible to obtain the desired information.

6. SOME PROBLEMS OF THE EQUATORIAL IONOSPHERE WHICH COULD BE STUDIED BY ROCKETS

6.1 Introduction

Inasmuch as charged particles interact with the earth's magnetic lines of force, the geometry of the equatorial magnetic field leads to many interesting ionospheric and magnetic phenomena. Many workers all over the world have been studying the equatorial ionosphere for sometime. Growing interest in the problems of the equatorial ionosphere is indicated by the two international symposia on Equatorial Aeronomy held in Peru and Brazil during the years 1962 and 1965 respectively, The symposia strongly recommended that combined ionospheric and magnetic studies be made by means of rockets in the equatorial D-, E- and F-regions and stressed that such studies should always be made in association with similar intensive observations from the ground. It is obvious that well planned rocket experiments are indispensable in not only filling gaps in the present knowledge about equatorial aeronomy but also in solving some of the outstanding problems. In the following sections some of the equatorial ionospheric problems which can be studied by rocket experiments will be discussed.

6.2 The D-Region and Equatorial Ionospheric Absorption Problems

During nighttime due to the incidence of cosmic rays

$$\frac{dN}{dt} - q - L = O \qquad (6.1)$$

where **q** is the production term due to cosmic rays and L is the loss term due to attachment. For this reason the electrons produced by incident cosmic rays must disappear by attaching themselves to the neutral molecules. These electrons detach themselves from the neutral by the first appearance of solar radiation

during the early morning hours and thereby the D-region cosmic ray **layer** is formed

$$O_2^- + h\nu \rightarrow O_2 + e$$
$$X^- + h\nu \rightarrow X + e \quad . \tag{6.2}$$

X is usually believed to be O_3. However due to some reason this layer is formed only on certain days as indicated by oblique VLF absorption starting from the solar zenith angle (χ) of 98°. So the criterion for launching the rocket, in order to investigate the cosmic ray layer should be that the VLF waves indicate absorption starting from $\chi = 98°$. The cosmic ray production function varies by a factor of ten with latitude reaching a minimum value of 23 ion pairs/cm^2/ atmosphere at the geomagnetic equator (Aikin, 1965). So by comparing the results obtained at the equator with those obtained at higher latitudes, it will be possible to ascertain whether the cosmic rays are of primary importance in the formation of this layer, as is expected,

Chilton and Radicella (1965) showed that there are basic differences in transequatorial and middle latitude VLF propagation characteristics. These differences strongly suggest that the structure of the lower D-region changes with latitude. It is thought that these differences are due to a latitudinal variation on the daytime electron density gradient. Direct evidence to this fact was obtained during the NASA Mobile Launch Expedition during IQSY (1964-65) wherein four rockets were launched at various latitudes including one at the magnetic equator, in order to study the latitudinal variation of the lower ionosphere. The results of these experiments (Figure 4.11 of Chapter 4 of this report) showed clearly that the D-region electron density gradient is larger at the

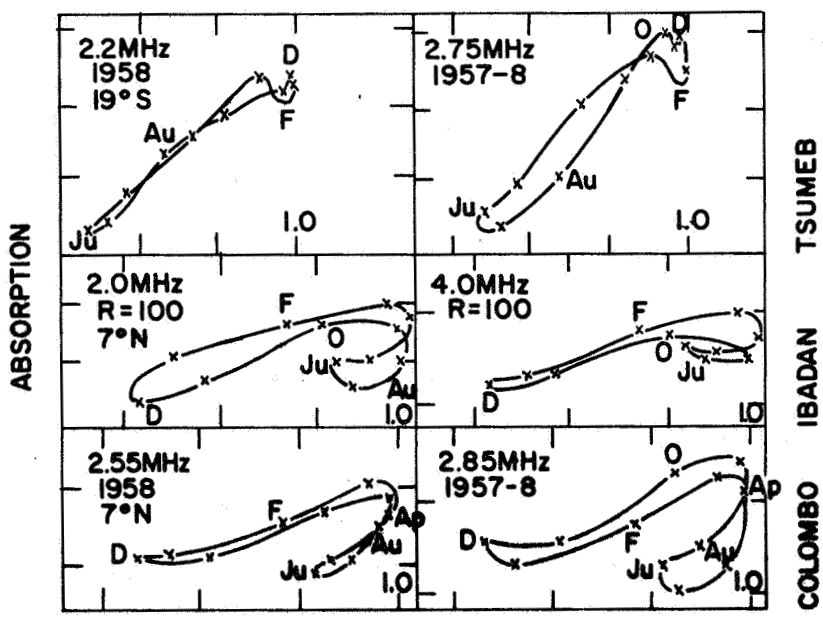

Figure 6.1 Anomalous absorption values observed during local summer (after Beynon and Jones, 1965)

equator than at other latitudes. Therefore the variation of the electron density gradient with the time of the day has to be investigated by launching rockets for different solar zenith angles during a normal quiet day.

Skinner and Wright (1956) found that the nondeviative absorption at Ibadan varied as $(\cos \chi)^{0.6}/f^{1.2}$ whereas the Appleton-Hartree theory would predict a variation of the form $(\cos \chi)^{3/2}/f^2$, f being the effective operating frequency. Whether the absorption values measured at equatorial stations are proportional to $\frac{1}{f}$ or $\frac{1}{f^2}$ is not yet definitely known. This can be investigated by conducting the propagation experiment at two frequencies simultaneously. By generating either ordinary or extraordinary wave from the ground and by'monitoring the AGC voltage of the rocket-borne receivers, the variation of absorption with altitude as a function of frequency can be studied. During this experiment, the question of the relative contribution of the various ionospheric regions to the total absorption can also be resolved.

It is well known that the measured ionospheric absorption is proportional to $(\cos \chi)^n$ where n is called the index of absorption, The value of n as deduced from the diurnal variation of absorption is lower than the one obtained using seasonal variation (Skinner, 1965). This is the seasonal anomaly in ionospheric absorption. Besides, for low latitude stations, Beynon and Jones (1965) reported that the local summer absorption values appear to behave in an anomalous way in the sense that they are smaller than expected as shown in Figure 6.1, Recently Shirke (1966) using shipboard absorption measurements at various latitudes, showed that the absorption values are low at the equator when compared to other latitudes for the same solar zenith angle (χ). This is the geomagnetic anomaly in ionospheric absorption and it is present during the afternoon hours rather than the forenoon hours, So by measuring the electron density and collision frequencies under different ionospheric conditions, the above mentioned D-region

problems and the anomalies in ionospheric absorption can be investigated as planned in Table 1. At the equatorial latitudes, during equinox months the solar zenith angle (χ) reaches very low values close to noon, thereby offers wide choice in the selection of χ angles for diurnal variation studies.

6.3 Electrojet and Equatorial Sporadic E Problems

Berkner and Wells (1937) first drew attention to the special features of sporadic E in the ionograms obtained at Huancayo, very close to the magnetic equator. During most of the sunlit hours, f_oEs at Huancayo is seen to exceed 5 MHz for more than 90 percent of the time. This was first called 'fringe E' or 'Huancayo type Es'. Now this type of Es is internationally designated as Es-q and is called equatorial Es. Usually it is readily distinguishable from the other types of Es seen on ionograms by several characteristics.

(1) It is always largely transparent to probing radio waves, that is, it never blankets reflections from higher layers.

(2) It usually shows a well defined lower edge lying between 100-110 km with scattered and diffuse echoes above the principal echo.

(3) In well developed cases, the diffuse echoes are continued below a sharp upper boundary that starts at about f_oE and increase in height with increasing frequency.

(4) Multiple echoes are not observed.

Matsushita (1951) by plotting the noon values of f_oEs of a number of stations against their magnetic dips, found that high Es-q critical frequencies during midday were restricted to a narrow zone within $\pm 10^\circ$ magnetic dip. It has been well known for many years that the daily amplitude of the geomagnetic horizontal variation field, at Huancayo is unusually large (Chapman and Bartles, 1940). A similar enhancement has been observed at other equatorial stations. It has been shown that this enhancement occurs in a narrow zone centered on the magnetic

TABLE 1

SEASON	TIME OF LAUNCH	NO. OF ROCKETS	PURPOSE
Any season	χ 98"	1	To investigate the D-region cosmic ray layer formed during the early morning hours.
Equinoxes	χ=0°, 40° & 80°	3	(i) To study the D-region electron density gradient variation with time of the day.
			(ii) To compute 'n' the index of absorption.
Summer	χ=40°; Forenoon and afternoon	2	To investigate the geomagnetic anomaly in ionospheric absorption.
			(i) To investigate the seasonal anomaly in ionospheric absorption.
Winter	χ=40°; Forenoon and afternoon	2	(ii) To investigate the geomagnetic anomaly in ionospheric absorption.
			(iii) The absorption index n can be computed using seasonal values and compared with 'n' obtained from diurnal variation.

equator (Matsushita, 1953) and it results from a strong eastward electric current during daylight hours which has been called the equatorial electrojet (Chapman, 1951).

The equatorial electrojet has been extensively studied during the IGY and its cause is thought to be a high value of Cowling conductivity in the magnetic equatorial zone at about 100 km height combined with an electrojet field caused by solar dynamo effects (Matsushita, 1962). The daily amplitude of H is a good indication of the intensity of the equatorial electrojet. It has been shown by Matsushita (1953) that the equatorial Es appears in the same narrow zone as that in which equatorial electrojet flows and that there is an obvious correlation between f_oEs-q and the daily amplitude of H, observed at the same station.

Kotadia (1962) has plotted the values of AH for Kodaikanal, Huancayo and Ibadan (equatorial stations) over a number of years and found that they exhibit a pronounced seasonal variation showing equinoxial maxima. Since it has already been proven that there is a close correlation between Es-q and H, one can expect that Es-q also exhibits *a* similar seasonal variation with equinoctial maxima. However studies of the seasonal variation of f_oEs-q for Ibadan (Mag. dip 6°S) show that it exhibited the features of an electrojet station (with equinoctial maxima) during some years and the features of a non-electrojet station (with summer maxima) during some other years (Rao and Rao, 1963). This indicates that the width of the electrojet is variable with time. Studies of the long term variations in equatorial sporadic E for the stations Huancayo and Ibadan showed that contrary to expectations the f_oEs-q values are not maximum during sunspot maximum years (Rao and Rao, 1966). This has been attributed to the decrease in the width of the electrojet during sunspot maximum years though its strength increased at the center.

From both radio sounding measurements (ionosondes) and VHF radio scattering measurements of the equatorial ionosphere (Matsushita, 1962; Cohen and Bowles, 1963), it is known that there are irregularities of ionization density associated with the electrojet. A theory of the two-stream ion wave instability in a plasma developed by Farley (1963) takes into account both the effect of collisions of ions and electrons with neutral particles and the presence of a uniform magnetic field. Applying the results to the ionosphere, it was found that irregularities of ionization density should arise spontaneously in regions in which a sufficiently strong current is flowing normal to the magnetic field lines. It is supposed that the Es-q appearing on the ionograms obtained close to the magnetic equator, is due to radio waves being scattered by these irregularities and not due to actual increases in electron density at these levels. Evidence to support this fact was first obtained by Blumle et al., (1965) by the electron density distribution measurements of the equatorial ionosphere during daytime. This was further substantiated by the equatorial rocket launch (14.228) results presented earlier in this report. Moreover the presence of irregularities was clearly noticed by the DC probe flown in this rocket, in the altitude region 90-100 km (Fig. 4.10 of Chapter 4 of this report). The spatial period of these irregularities is 80 m and their amplitude is about 12 percent of the plasma density at these altitudes.

At this stage, it is not hard to conceive some experiments to further the understanding of equatorial Es and electrojet phenomena:

(1) The variation of the characteristics of the irregularities, which are believed to be responsible for the Es-q appearance on ionograms, with the time of the day. This study can be made by launching rockets for different solar zenith angles (χ) during a normal quiet day, These investigations can be carried out simultaneously with the D-region experiment.

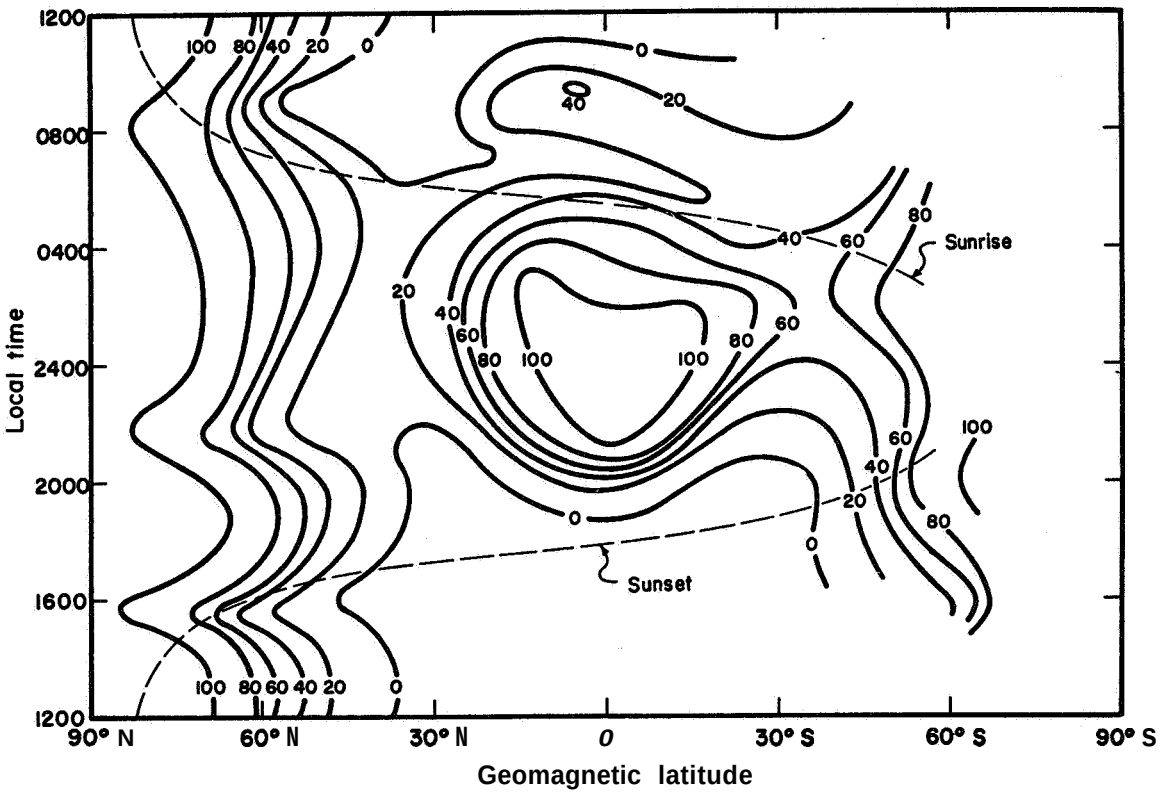

Figure 6.2 Occurrence frequency of aspect sensitive spread F as seen by Alouette I, September 1962 to January 1963 (after Calvert and Schmid, 1964)

(2) The variation of the characteristics of the irregularities with distance from the center of the electrojet. This study can be made by launching the rocket at an oblique angle in the N-S direction such that the rocket passes through the electrojet region at different distances from the center during ascent and descent.

(3) Using rocket-borne magnetometer measurements, Cahill (1959) observed that the horizontal current density showed two maxima at heights of 105 km and 125 km of roughly equal magnitude which indicated a bifurcation of the equatorial electrojet. This phenomenon needs further investigation.

(4) The seasonal variation of the width of the electrojet can be investigated by rocket experiments during different seasons for the same solar zenith angle. These experiments can also be coupled with the D-region experiments.

6.4 F-Region Problems

The equatorial F-region exhibits many anomalies and peculiarities, one of the most important of them being the spread F phenomena. The name spread F is derived from the visual appearance of the traces on ionograms where the echoes lose their sharply defined structure; they become very diffuse and broad. Therefore it is extremely difficult to measure the electron density distribution when this phenomenon occurs. The predominant feature in the geographic distribution of spread F occurrence is the existence of two areas of maximum. One is found at equatorial regions, invariably on the nighttime side of the earth, whereas the other is confined to polar latitudes, mostly in the dark hemisphere but often observed during daytime (Figure *6.2)*.

A theory of spread F irregularity production which has gained considerable attention, particularly in regard to equatorial spread F, is that due to Martyn (1959). Martyn considers that the F-layer as a whole will drift vertically under the action of large scale electric fields which interact with the earth's magnetic field. He shows that during such a process, small perturbations in the F-region may become appreciably enhanced. Where the layer is drifting upward it is the undersurface of the layer which is unstable in this respect. It is shown for an upward drifting layer that an isolated region of reduced electron density low in the layer, moves upward through the region, thus moving into regions of greater electron density where the inhomogeneity becomes more pronounced. Similarly a region of enhanced ionization moves downward into regions where the surrounding density is lower and is thus also enhanced. However, downward motion of the layer causes its upper surface to become unstable and *so* Martyn suggests that, of the two possibilities, upward drift should be more important in the production of spread F.

While Martyn's theory explains the amplification of irregularities once produced, it gives no clue as to the origin of the irregularities. Dagg (1957) suggested that irregularities in the F-layer arise from electromechanical coupling of turbulent motions in the lower ionosphere into the F-layer. Axford and Hines (1961) have suggested a similar coupling with the turbulent motions associated with the convective motion of the magnetosphere. Bowhill (1964) proposed that the field-aligned irregularities may be an effect of an increased electron temperature in the F2-layer. Thermal conduction perpendicular to the magnetic field of the earth is sufficiently small that these inhomogeneities of electron temperature could be expected to maintain themselves for a considerable period.

In order to shed some light on the mechanism of spread F, it is necessary to get the electron density when spread F phenomenon occurs. As we have seen earlier the ionosonde fails to give this information under these conditions and therefore rockets have to be used for this purpose. However the ionosonde has to be used for deciding on the criterion to launch the rocket. High altitude rockets like the Javelin and Nike-Tomahawk have to be used for this experiment.

In the D- and lower E-regions, collisions of electrons with neutral particles predominate. This is not necessarily the case in the F-region, where electron-ion collisions increase in importance, but there is little experimental evidence to tell us which type of collisions predominate, nor in fact, what the collision frequency is (Belrose, 1965). Chapman (1956) has given the following theoretical formulas for the electron-ion collision frequency.

$$\nu_{ei} = [34 + 4.18 \log_{10}(T_e^3/N_e)] N_e T_e^{-3/2} \qquad (6.4)$$

where T_e is the electron temperature, N is the electron density measured in units of cm^{-3} and ν_{ei} is the collision frequency in sec^{-1}. Since ν_{ei} is proportional to $T_e^{-3/2}$, if electron collisions are mainly with ions, when temperature increases during the day their collision frequency will decrease. Abdu et al., by galactic radio noise measurements at 25 MHz reported that at middle latitudes electron-positive ion collisions are mainly responsible for the short-wave absorption in the F-region. Measurement of electron collision frequencies in the F-region is therefore necessary to investigate the contribution of electron-ion collisions to the radio wave absorption in this region. By the rocket radio propagation experiment and by using high altitude rockets, it is possible to make the desired measurements.

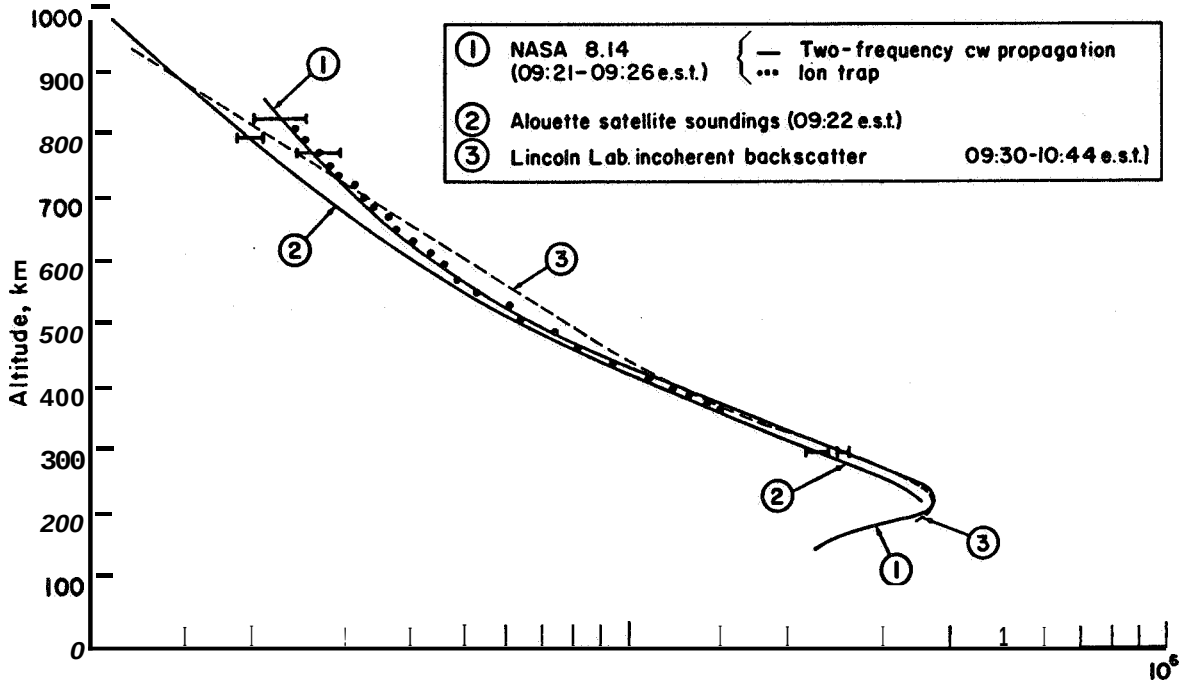

Figure 6.3 Comparison of topside electron density profiles obtained from Alouette I, backscatter sounding and a simultaneous rocket flight on July 2, 1963 (after Schmerling, 1966).

There are still some unsolved problems in deducing electron density profiles from ionograms, as on a number of occasions it has been found that the bottomside and topside profiles do not match properly. However using simultaneous rocket and Thomson scatter measurements, no serious discrepancies have emerged (Bauer and Jackson, 1964). Figure 6.3 shows such a comparison of topside electron density profiles deduced from each of the following: Alouette I, a Thomson scatter sounder, and a rocket probe launched close to the satellite that contained two independent experiments. On this occasion, it is seen that quite good agreement was obtained, but further work is needed in this direction to account for the discrepancies observed at other times between top and bottomside soundings. (Schmerling, 1966).

6.5 Summary and Discussion

As described in the earlier sections, most of the outstanding equatorial D-, E- and F-region problems can be investigated with the rocket radio propagation experiment. Some of these experiments require that the rocket be launched obliquely. For this reason the ground-based experimental setup should be able to generate both circularly polarized and linearly polarized waves. Moreover the experimental setup should be capable of operating at least on two spot frequencies: one around 2 MHz for nighttime experiments and the other around 3 MHz for daytime experiments in the E-region. For some of these investigations, it might be required to fly some of the following experiments also along with the radio propagation experiment:

(1) Probes for obtaining electron and ion temperatures.

(2) Magnetometer for measuring changes in the magnetic field.

(3) Mass spectrograph for obtaining ion composition.

(4) Sodium cloud release experiment for the measurements of ionospheric drifts.

Thus far there are two equatorial launch sites, one at Thumba, India (Geog. Lat. 8.5°N; Long. 76.9°E) and the other at Natal, Brazil (Geog. Lat. 5.3°S; Long. 35.1°W). For a better investigation of the equatorial ionospheric problems, it is imperative that a good coordination should exist between the experiments conducted at these two launch sites.

REFERENCES

Abdu, M. A., S. S. Degaonkar, and K. R. Ramanathan (1967), Attenuation of galactic radio noise at 25 MHz and 21.3 MHz in the ionosphere over Ahmedabad during 1957-1964, J. Geophys. Res. 72, 1547-1554.

Aikin, A. C. (1965), Formation of the equatorial ionospheric D-region, Proceedings of the Second International Symposium on Equatorial Aeronomy, ed. F. de Mendonca, 1-13.

Appleton, E. V. (1946), Two anomalies in the ionosphere, Nature 157, 691,

Axford, W. J., and C. O. Hines (1961), A unifying theory of high latitude geophysical phenomena and geomagnetic storms, Can. J. Phys. 39, 1433-1464.

Bauer, S. J., and J. E. Jackson (1964), Alouette mid-latitude topside studies, IG Bull., Trans. Am. Geophys. Union 45, 227-231.

Belrose, J. S. (1965), The Ionospheric F-Region in Physics of the Earth's Upper Atmosphere, eds. C. O. Hines, et al., Prentice-Hall, Inc., 73-95.

Berg, R. S., and B. Howland (1962), RF component development for the decon system, Lincoln Laboratory Technical Report No. 275.

Berkner, L. V., and H. W. Wells (1937), Abnormal ionization of the E-region of the ionosphere, Terrest. Magnetism Atmospheric Elec. 42, 73-76.

Beynon, W. J. G., and E. S. O. Jones (1965), Meteorological influences in ionospheric absorption measurements, Proc. Roy. Soc. A288, 558-563.

Rhargava, B. N., and R. V. Subrahmanyan (1964), Geomagnetic disturbances associated'with equatorial electrojet, J. Atmospheric Terrest. Phys. 26, 879-888.

Blumle, L. J., A. C. Aikin, and J. E. Jackson (1965), Rocket observations of the equatorial ionosphere, Proc. of the Second International Conference on Equatorial Aeronomy, ed. F. de Mendonca, 86-87.

Bowhill, S. A. (1964), Origin of field-aligned irregularities in the F2-layer, Presented at AGARD-NATO meeting, Copenhagen.

Bowhill, S. A. (1966), A rocket experiment on the structure of sporadic E, Radio Science 1 (New Series), 187-190.

Bowles, K. L., and R. Cohen (1962), A study of radio wave scattering from sporadic E near the magnetic equator, Ionospheric Sporadic E, eds. Smith, E. K., and S. Matsushita, Macmillan Company, 51-57.

Bowles, K. L., R. Cohen, G. R. Ochs, and B. B. Balsley (1960), Radio echoes from field-aligned ionization above the magnetic equator and their resemblance to auroral echoes, J. Geophys. Res. 65, 1853-1855.

Cahill, L. J. (1959), Equatorial electrojet, J. Geophys. Res. 64, 489-503.

Calvert, W., and C. W. Schmid (1964), Spread F observations by the Alouette topside sounder satellite, J. Geophys. Res. 69, 1839-1852.

Chapman, S. (1951), The equatorial electrojet as deduced from the abnormal electric current distribution above Huancayo, Peru and elsewhere, Arch. Meteoro. Geophys. u. Bioklimatol A4, 368.

Chapman, S. (1956), The electrical conductivity of the ionosphere--a review, Nuova Cimento 4, Ser. 10, No. 4, 1385-1412.

Chapman, S., and J. Bartles (1940), Geomagnetism, Clarendon Press, Oxford.

Chilton, C. J., and S. M. Radicella (1965), Differences between transequatorial and middle latitude VLF propagation, Proc. of the Second International Symposium on Equatorial Aeronomy, ed. F. de Mendonca, 34-39.

Dagg, M. (1957a), The origin of the ionospheric irregularities responsible for radio-star scintillations and spread F--I. Review of existing theories, J. Atmospheric Terrest. Phys. 11, 133-138.

Dagg, M. (1957b), The origin of the ionospheric irregularities responsible for radio-star scintillations and spread F--II. Turbulent motion in the dynamo region, J. Atmospheric Terrest. Phys. 11, 139-150.

Davis, T. N., K. Burrows, and J. D. Stolarik (1967), A latitude survey of the equatorial electrojet with rocket-borne magnetometers, J. Geophys. Res. 72(7), 1845-1861.

Duncan, R. A. (1960), The equatorial F-region of the ionosphere, J. Atmospheric Terrest. Phys. 18, 88-100.

Farley, D. T. (1963), A plasma instability resulting in field-aligned irregularities in the ionosphere, J. Geophys. Res. 68, 6083-6097.

Flügel, M. D. (1962), On the geographical distribution of ionospheric absorption, Ionosph. Res. 10, 5-13.

Goldberg, R. A. (1965), The effect of a variable electron temperature on the equatorial electron density distribution in the upper ionosphere, J. Geophys. Res. 70, 655-665.

Goldberg, R. A., P. C. Kendall, and E. R. Schmerling (1964), Geomagnetic control of the electron density in the F-region of the ionosphere, J. Geophys. Res. 69, 417-427.

Goldberg, R. A., and E. R. Schmerling (1963), The effect of diffusion on the equilibrium electron density distribution in the F-region near the magnetic equator, J. Geophys. Res. 69, 1927-1936.

Gooch, J., H. Krone, and D. Skaperdas (1966), Results of sixteen differential absorption and Faraday rotation measurements with Nike-Apache rockets, Co-ordinated Sciences Laboratory, University of Illinois, Urbana, Illinois, Report No. R-324.

Hanson, W. B., and R. J. Moffett (1966), Ionization transport effects in the equatorial F-region, J. Geophys. Res. 71, 5559-5572.

Knecht, R. W., and R. E. McDuffie (1962), On the width of the equatorial Es belt, Ionospheric Sporadic E, eds. Smith, E. K., and S, Matsushita, The Macmillan Company, 215-218.

Knoebel, A., D. Skaperdas, J. Gooch, B. Kirkwood, and H. Krone (1965), High frequency radio frequency measurements of Faraday rotation and differential absorption with rocket probes, Co-ordinated Sciences Laboratory, University of Illinois, Urbana, Illinois, Report No. R-273.

Kotadia, K. M. (1962), The equatorial sporadic E layer and the electrojet, J. Atmospheric Terrest. Phys. 24, 211-218.

Martyn, D. F. (1955), Theory of height and ionization density changes at the maximum of a Chapman-like region, taking account of ion-production, decay, diffusion and total drift, Phys. Soc. London, Proc. Cambridge Conference, 254-259.

Matsushita, S. (1951), Intense Es ionization near the magnetic equator, J. Geomag. Geoelect. 3, 44-46.

Matsushita, S. (1953), Ionospheric variation associated with geomagnetic disturbances, J. Geomag. Geoelect. 5, 109-135.

Matsushita, S. (1962), Inter-relations of sporadic E and ionospheric currents, Ionospheric Sporadic E, eds. Smith, E. K., and S. Matsushita; Macmillan Company, 344-375.

Matsushita, S. (1964), Geomagnetic storms and related phenomena, Research in Geophysics, ed. Odishaw, H. 455-483,

Maynard, N. C., and C. J. Cahill (1965), Preliminary results of measurements of S_q currents and the equatorial electrojet near Peru, J. Geophys. Res. 70, 5975-5977.

Maynard, N. C., C. J. Cahill, and J. S. G. Sastry (1965), Preliminary results of measurements of the equatorial electrojet over India, J. Geophys. Res. 70, 1241-1245.

Mitra, S. K. (1946), Geomagnetic control of region F2 of the ionosphere, Nature 158, 668-669.

Murthy, B. V. K. (1966), Behavior of topside and bottomside spread F at equatorial latitudes, J. Geophys. Res. 71, 4527-4533.

Nicolet, M., and A. C. Aikin (1960), The formation of the D-region, J. Geophys. Res. 65, 1469-1483.

Ogbuehi, P. O., and D. G. Osborne (1965), Summary of low latitude current system including the electrojet and magnetic variations, Proc. of the International Symposium on Equatorial Aeronomy, ed. F. de Mendonca, 445-448.

Olatunji, E. O. (1965), Some features of equatorial ionospheric storms, Proc. of the Second International Symposium on Equatorial Aeronomy, ed. F. de Mendonca, 479-482.

Piggott, W. R. (1965), Some comments on outstanding problems in absorption, Proc. of the Second International Symposium on Equatorial Aeronomy, ed. F. de Mendonca, 75-77.

Piggott, W. R., and K. Rawer (1961), URSI Handbook of Ionogram Interpretation and Reduction, Elsevier Publishing Company, 47.

Rao, M. M., and B. R. Rao (1963), The effect of electrojet on the seasonal variation of sporadic E, J. Atmospheric Terrest. Phys. 25, 571-576.

Rao, M. M., and B. R. Rao (1966), Long term variation in the equatorial sporadic E and the electrojet, Planet. Space Sci. 14, 529-540.

Rastogi, R. G. (1959a), The diurnal development of the anomalous equatorial belt in the E2 region of the ionosphere, J. Geophys. Res. 64, 727-732.

Rastogi, R. G. (1959b), Geomagnetic influence on the F1 and F2 regions of the ionosphere--effect of solar activity, J. Atmospheric Terrest. Phys. 14, 31-40.

Rastogi, R. G. (1959c), Magnetic control on the variations of the critical frequency of the F2 layer of the ionosphere, Canad. J. Phys. 37, 874.

Rastogi, R. G., N. D. Kaushika, and N. B. Trivedi (1965), Solar flare rocket and sudden commencement in H within the electrojet region, J. Atmospheric Terrest. Phys. 27, 663-668.

Rastogi, R. G., and G. Rajaram (1965), Abnormal disturbance daily at Huancayo during IGY-IGC, Proc. of the Second International Symposium on Equatorial Aeronomy ed. F. de Mendonca, 487-490.

Ratcliffe, J. A. (1962), The magnetoionic theory and its applications to the ionosphere, A Monograph, Cambridge University Press.

Schmerling, E. R. (1966), Advances in ionospheric physics in the rocket and satellite era, Review of Geophysics 4, 329-362.

Sen, H. K., and A. A. Wyller (1960), On the generalization of the Appleton-Hartree magnetoionic formulas, J. Geophys. Res. 65, 3931-3950.

Shirke, J. S. (1966), An equatorial and low latitude anomaly in ionospheric absorption. Results of observations on board the USNS Croatan, Presented at the Fall URSI meeting at Palo Alto, California.

Skinner, N. J. (1965), Absorption in the equatorial ionosphere (Review Paper), Proc. of the Second International Symposium on Equatorial Aeronomy, ed. F. de Mendonca, 43-50.

Skinner, N. J., and R. W. Wright (1956), Ionospheric absorption measurements at the equator, J. Atmospheric Terrest. Phys. 9, 103.

Smith, E. K. (1957), World-wide occurrence of sporadic E, NBS Circular No. 582.

Whitehead, J. D. (1966), The enigma of the equatorial electrojet, Planet. Space Sci. 14, 519-522.

APPENDIX

Fastran Computer Program for Investigating the Regions of QL and QT Approximations

```
$     Fastran
$     Go
10    Read Input Tape 7, 1, H, B, CF, ED
1     Format (F 5.0, 3E 11.0)
      X = 0.7034 E-11 * ED
      Y = 0.8269 E+4 * B
      Z = 0.047 E-6 * CF
      F1 = (6.0/Y) * SQRT ((1.0-X) ** 2 + Z ** 2)
      F2 = (2.0/(3.0*Y)) * SQRT ((1.0-X) ** 2 + Z ** 2)
      P1 = -F1/2.0 + SQRT (F1 ** 2.+4.)/2.0
      Q1 = -F2/2.0 + SQRT (F2 ** 2.+4.)/2.0
      P1 = ARCOS (P1)
      Q1 = ARCOS (Q1)
      Theta 1 = 180.0 * P1/3.1416
      Phi 1   = 180.0 * Q1/3.1416
      Write Output Tape 6, 2, H, F1, F2, Theta 1, Phi 1
2     Format (F5.0, 4E 15.6)
      Go To 10
      End
$     Data
```

H(Altitude) B(Magnetic Field) CF(Collision Frequency) ED(Electron Density)